

# Characterisation of the novel postsynaptic scaffold protein MPP2

Inaugural-Dissertation

to obtain the academic degree

Doctor rerum naturalium (Dr. rer. nat.)

submitted to the Department of Biology, Chemistry, Pharmacy  
of Freie Universität Berlin

by

Bettina Schmerl

February, 2021

The experimental work of this thesis was conducted from October 2014 to January 2021 under the supervision of Prof. Dr. Sarah Shoichet at the Neuroscience Research Centre (NWFZ) of the Charité - Universitätsmedizin Berlin.

1<sup>st</sup> Reviewer: Prof. Dr. Sarah Shoichet  
Charité - Universitätsmedizin Berlin

2<sup>nd</sup> Reviewer: Prof. Dr. Markus Wahl  
Freie Universität Berlin

Date of disputation: June 7, 2021

**Affidavit**

I declare that my dissertation entitled 'Characterisation of the novel postsynaptic scaffold protein MPP2' has been written independently and with no other sources and aides than quoted.

Berlin,

Bettina Schmerl

# Contents

<b>Acknowledgements</b>	<b>7</b>
<b>Synopsis</b>	<b>8</b>
<b>Zusammenfassung</b>	<b>9</b>
<b>List of figures</b>	<b>10</b>
<b>List of tables</b>	<b>11</b>
<b>1 Introduction</b>	<b>12</b>
1.1 Synapses . . . . .	12
1.2 Components of the postsynapse . . . . .	12
1.2.1 Transmembrane proteins . . . . .	12
1.2.2 Cytosolic proteins . . . . .	15
1.3 Membrane-associated guanylate kinases (MAGUKs) . . . . .	17
1.4 MPP family proteins . . . . .	18
1.5 Aim . . . . .	22
<b>2 Material and Methods</b>	<b>23</b>
2.1 Material . . . . .	23
2.1.1 Vectors . . . . .	23
2.1.2 Oligonucleotides . . . . .	24
2.1.3 DNA constructs . . . . .	27
2.1.4 Antibodies . . . . .	28
2.1.5 Chemicals and Consumables . . . . .	32
2.1.6 Compositions . . . . .	37
2.1.7 Software . . . . .	41
2.1.8 Devices . . . . .	42
2.2 Methods . . . . .	43
2.2.1 Molecular Biology . . . . .	43
2.2.2 Cell Biological Techniques . . . . .	47
2.2.3 Biochemical Techniques . . . . .	49
2.2.4 Imaging . . . . .	55
2.2.5 Image Analysis . . . . .	58
<b>3 Results</b>	<b>63</b>
3.1 MPP2 is a novel postsynaptic scaffold protein . . . . .	63
3.1.1 Neuronal expression of MPP2 . . . . .	63
3.1.2 MPP2 is a novel postsynaptic scaffold protein . . . . .	65
3.1.2.1 MPP2 is expressed in neurons at postsynaptic sites . . . . .	65

3.1.2.2	The sub-synaptic positioning of MPP2 is peripheral to PSD-95 . . . . .	65
3.1.2.3	MPP2 is expressed at high levels in a subset of excitatory neurons . . . . .	68
3.1.3	MPP2 is associated with AMPA receptor complexes . . . . .	69
3.1.4	MPP2 interacts with multiple synaptic scaffold proteins . . . . .	70
3.1.4.1	MPP2 interacts with PSD-95 . . . . .	70
3.1.4.2	MPP2 interacts with GKAP . . . . .	72
3.1.4.3	MPP2 interacts with Lin7b . . . . .	74
3.1.4.4	MPP2 homomultimerises . . . . .	75
3.2	Novel MPP2 PDZ domain ligands . . . . .	76
3.2.1	Identification of putative interactors with a yeast-two-hybrid screen	76
3.2.2	MPP2 binds multiple synaptic cell adhesion molecule C-termini .	78
3.2.3	Synaptic cell adhesion molecule SynCAM1 . . . . .	79
3.2.3.1	MPP2 binds the C-terminus of SynCAM1 . . . . .	79
3.2.3.2	MPP2 co-localises with endogenous SynCAM1 at dendritic spines . . . . .	80
3.2.3.3	SynCAM1 binding is mediated by the PDZ domain of MPP2 . . . . .	82
3.2.3.4	MPP2 binds the SynCAM1 C-terminus with high affinity	83
3.2.4	MPP2 and SynCAM1 are located at the border of the postsynaptic density . . . . .	84
3.2.4.1	The sub-synaptic positioning of MPP2 is peripheral to PSD-95 . . . . .	84
3.2.4.2	Quantitative super-resolution imaging and analysis of synaptic proteins and MPP2 . . . . .	86
3.2.4.3	Clusters of MPP2 and SynCAM1 are distinctly localised to the PSD periphery . . . . .	90
3.3	Interactions of the MPP2 SH3GK tandem domain . . . . .	91
3.3.1	Differential interactomes of MPP2 and PSD-95 . . . . .	91
3.3.2	Novel specific interactors for the MPP2 SH3GK tandem domain	95
3.4	MPP2 interacts with GABA <sub>A</sub> receptors at excitatory synapses . . . . .	99
3.4.1	MPP2 binds multiple GABA <sub>A</sub> R subunits . . . . .	99
3.4.2	MPP2 co-localises with GABA <sub>A</sub> Rs at excitatory synapses . . . . .	100
3.4.3	MPP2 and GABA <sub>A</sub> Rs co-localise at the PSD periphery . . . . .	104
<b>4</b>	<b>Discussion</b>	<b>107</b>
4.1	MPP2 is a novel component of postsynaptic protein complexes . . . . .	108
4.2	Linking peripheral and central structural elements of the postsynapse .	109
4.3	MPP2 is engaged in regulatory interaction networks . . . . .	111
4.4	MPP2 links elements of excitatory and inhibitory transmission . . . . .	112

<b>5 Conclusion and Outlook</b>	<b>114</b>
<b>References</b>	<b>117</b>
<b>Appendix</b>	<b>137</b>
Validation of commercial antibodies . . . . .	137
Knock-down of endogenous MPP2 . . . . .	140

## Acknowledgements

I would like to express my sincere gratitude to all the people who have supported and inspired me during my PhD and contributed to this work.

First of all, I would like to thank my supervisor Prof. Sarah Shoichet, who gave me the opportunity to work in her lab and develop this exiting project. I am grateful for her mentoring, motivation and enthusiasm and the constant support I received.

I want to thank Prof. Markus Wahl for accepting to be the second reviewer of this thesis.

My sincere gratitude goes to all members of my lab, for being always open and supportive and creating such a friendly work atmosphere. My special thanks go to Dr. Nils Rademacher for his supervision, great ideas, excellent support and impressive memory for the literature. I want to thank Dr. Stella-Amrei Kunde for her immense help, constant support, the great and precious discussions and the guidance she provided. My thanks also go to current and previous members of the lab, Hanna Zieger, Judith von Sivers, Melanie Fuchs and Sabine Hahn, for their help, lots of fun and snacks and their great company during my PhD. I would also like to thank our students who helped me become a better teacher.

I owe special thanks to Dr. Niclas Gimber not only for his great contributions to my project, but also for eliciting my interest in image analysis and inspiring me to pursue this. Thanks to his friendly and supportive attitude and his expertise, I really enjoyed this collaboration. Moreover, I would like to thank Dr. Jan Schmoranzler and the Advanced Medical BioImaging Core Facility (AMBIO) for the support.

I would also like to thank Dr. Benno Kuroпка and Prof. Christian Freund for the collaboration that provided an unexpected, yet exciting direction to my project. Many thanks go also to Dr. Alexander Stumpf and Prof. Dietmar Schmitz for their motivation and help. I would also like to thank Jakob Rentsch and Prof. Helge Ewers for the nice collaboration. Thanks to Bettina Brokowski, Thorsten Trimbuch and the Viral Core Facility for their help and service.

Many thanks go to the many people who helped, inspired and accompanied me in my activities and responsibilities outside of the lab, making them joyful and valuable experiences and who helped me to keep sane and carry on.

Last, but most importantly, I would like to express my deepest gratitude to my friends and my family, who were always at my side, supported me not just morally and were always patient and encouraging.

## Synopsis

Proper cellular function requires precise and dynamic assembly of multiple structural, regulatory and signalling molecules. Scaffold proteins serve exactly this purpose by functioning as protein-interaction hubs and providing interaction surfaces to a broad variety of proteins. Especially in polarised cells and at cell-cell contact sites, scaffold proteins are indispensable for the positioning and anchoring of diverse classes of proteins. A very particular type of cell-cell contact in highly polarised cells are chemical synapses, where different scaffold proteins, like the prototypical PSD-95, are critical for the proper recruitment and membrane localisation of transmembrane proteins, receptors and ion channels. Scaffold proteins assemble them together with regulatory and additional scaffold proteins into large multiprotein complexes that are responsible for synapse formation, maintenance and plasticity. MPP2 belongs to the MPP subfamily of membrane-associated guanylate kinase (MAGUK) scaffold proteins, which has primarily been studied for its importance at epithelial cell-contact sites.

The present thesis describes MPP2 as a novel scaffold protein at the postsynapse of central neurons. It is demonstrated to be associated with core components of AMPA receptor complexes and directly interacting with the abundant postsynaptic scaffold proteins PSD-95 and GKAP. MPP2 was found at postsynapses of hippocampal neurons, where it co-localises with the transmembrane cell adhesion protein SynCAM1 that was identified as a specific ligand to the MPP2 PDZ domain. SynCAM1 is an important synaptic cell adhesion protein with functions for the formation and maintenance of stable synaptic contacts. Taking advantage of diverse super-resolution imaging approaches, MPP2 and SynCAM1 were found in a particular spatial arrangement at the border of the postsynaptic density (PSD). Distinct nanoclusters of both proteins are positioned juxtaposed and almost alternating, forming a bracelet-like structure surrounding the PSD border. MPP2 being positioned at the PSD border together with SynCAM1 as synapse-stabilising protein, suggests an important role for MPP2 in the formation and maintenance of glutamatergic synapses. Subsequent comparative investigations of the protein complexes, which are organised by the PSD-95 and MPP2 SH3GK tandem domain, revealed an unexpected association of MPP2 with multiple proteins, which are important for inhibitory synaptic transmission, foremost seven different GABA<sub>A</sub> receptor subunits. A direct interaction between MPP2 and the GABA<sub>A</sub>R subunits  $\alpha 1$ ,  $\alpha 2$  and  $\beta 3$  was confirmed. Moreover, MPP2 co-localises with multiple GABA<sub>A</sub>R subunits in a subset of dendritic spines of excitatory glutamatergic, but not inhibitory synapses.

In summary, this dissertation provides evidence that the novel postsynaptic scaffold protein MPP2 sits at the PSD periphery of glutamatergic synapses, where it serves as a link between central protein complexes of excitatory synapses and peripheral elements for the inhibitory regulation of synaptic transmission. These results provide further insights into the postsynaptic architecture and a new perspective for studying its functional regulation.

## Zusammenfassung

Zellfunktionen werden durch das präzise und dynamische Zusammenspiel verschiedenster struktureller und regulatorischer Elemente und Signalmoleküle bestimmt. Gerüstproteine sind hierbei zentrale Elemente, die vielfältige Protein-Interaktionen, insbesondere in polar organisierten Zellen und an Zellkontakten, ermöglichen und die für die Anordnung und Verankerung verschiedenster Klassen von Proteinen von Bedeutung sind. Chemische Synapsen, die Kontaktpunkte zwischen Nervenzellen, sind eine besondere Form von Zellkontakten. Hier sind Gerüstproteine, wie PSD-95, essentiell für die Rekrutierung vielfältiger Proteine, wie Transmembranproteine, Rezeptoren und Ionenkanäle an die synaptische Membran, sowie deren korrekter Positionierung. Darüber hinaus stellen diese Gerüstproteine eine Verbindung zu anderen regulatorisch und strukturell wichtigen Elementen her und organisieren dadurch die großen Multiproteinkomplexe, welche die Bildung, Stabilität und auch Plastizität von Synapsen erst ermöglichen. MPP2 gehört der MPP Unterfamilie der Membran-assoziierten Guanylatkinasen (MAGUK) an und wurde bisher vor allem wegen seiner Funktion an Epithelzellkontakten untersucht.

Die vorliegende Arbeit beschreibt MPP2 erstmals an der postsynaptischen Dichte (PSD) zentraler Neurone. Es wird gezeigt, dass MPP2 mit zentralen Elementen AMPA-Rezeptor-assoziiierter Proteinkomplexe verbunden ist und mit wichtigen Proteinen wie PSD-95 und GKAP direkt interagiert. MPP2 co-lokalisiert in Postsynapsen hippocampaler Neurone mit SynCAM1, welches als spezifischer PDZ-Ligand von MPP2 identifiziert wurde. SynCAM1 ist ein transsynaptisches Zelladhäsionsprotein mit Bedeutung für die Bildung und Stabilisierung von Synapsen. Mithilfe supraauflösender Mikroskopieverfahren konnte gezeigt werden, dass MPP2 und SynCAM1 auf besondere Weise zusammen am Rand der PSD arrangiert sind: Nanocluster beider Proteine liegen fast abwechselnd unmittelbar nebeneinander und bilden dadurch eine Struktur ähnlich einem Armband, das die PSD umgibt. Analyse und Vergleich der Proteinkomplexe, die jeweils durch die SH3GK Tandemdomänen von MPP2 und PSD-95 organisiert werden, ergab eine unerwartete Verbindung von MPP2 zu mehreren Proteinen, die für inhibitorische Signalübertragung verantwortlich sind, allen voran sieben GABA<sub>A</sub>-Rezeptoruntereinheiten. Zwischen MPP2 und den Rezeptoruntereinheiten  $\alpha 1$ ,  $\alpha 2$  und  $\beta 3$  konnte eine direkte Interaktion und darüber hinaus eine Co-Lokalisation von MPP2 mit einigen Untereinheiten gezeigt werden. Diese Co-Lokalisation zeigte sich in einer Subpopulation dendritischer Spines an erregenden glutamatergen, jedoch nicht inhibitorischen Synapsen.

Zusammenfassend zeigt die vorliegende Arbeit, dass MPP2 ein neues postsynaptisches Gerüstprotein ist, welches sich am Rande der PSD exzitatorischer Synapsen befindet und dadurch eine physische Verbindung zwischen zentralen Proteinkomplexen glutamaterger Synapsen und peripheren Elementen der inhibitorischen Regulation synaptischer Signalübertragung herstellt. Diese Ergebnisse erweitern das Verständnis über die Architektur der Postsynapse und bieten eine weitere Perspektive für die Erforschung ihrer funktionellen Regulation.

## List of Figures

1	Scaffold proteins organise protein complexes at excitatory synapses . . .	13
2	Domain structure of selected MAGUK family scaffold proteins . . . . .	21
3	Prevalence of synaptic bracelet-like SynCAM1 and MPP2 cluster arrangements . . . . .	60
4	Neuronal expression of MPP2 . . . . .	64
5	MPP2 localises to postsynaptic sites peripheral to the PSD . . . . .	67
6	MPP2 is expressed in a subset of primary hippocampal neurons . . . . .	68
7	MPP2 is a component of postsynaptic receptor complexes . . . . .	69
8	MPP2 interacts with the postsynaptic density protein PSD-95 . . . . .	71
9	The MPP2 GK domain mediates the interaction with GKAP . . . . .	73
10	MPP2 interacts with additional scaffold proteins and homo-multimerises	75
11	MPP2 binds the C-terminus of the transmembrane cell adhesion protein SynCAM1 . . . . .	81
12	The MPP2-SynCAM1 interaction is PDZ domain-dependent . . . . .	82
13	Binding affinity of MPP2 and the C-terminus of SynCAM1 . . . . .	84
14	Nanoclusters of SynCAM1 and MPP2 surround the postsynaptic density	85
15	Clusters of MPP2 and SynCAM1 form bracelet-like arrangements at the PSD edge . . . . .	88
16	Quantitative analysis of MPP2 and SynCAM1 positioning at the PSD periphery . . . . .	89
17	Identification of interactors that differentially bind to the C-terminal SH3GK modules of MPP2 and PSD-95 . . . . .	94
18	GABA <sub>A</sub> R $\alpha$ 1 differentially binds with higher affinity to MPP2 than PSD-95	95
19	Validation of novel interaction partners by co-IP . . . . .	96
20	Multiple GABA <sub>A</sub> receptor subunits directly interact with MPP2 . . . . .	99
21	GABA <sub>A</sub> R $\alpha$ 1 co-localises with MPP2 in a subset of dendritic spines . . .	101
22	Endogenous MPP2 co-localises with GABA <sub>A</sub> receptors, but not at inhibitory synapses . . . . .	103
23	MPP2 and GABA <sub>A</sub> R $\alpha$ 1 form highly overlapping nanoclusters . . . . .	106
24	Summary of MPP2 and novel interaction partners at glutamatergic synapses . . . . .	108
A1	Validation of commercially available antibodies targeting endogenous MPP2 . . . . .	139
A2	Knock-down of endogenous MPP2 . . . . .	141

## List of Tables

2.1	Vector backbones used for the generation of expression constructs . . . .	23
2.2	Oligonucleotides . . . . .	24
2.3	List of primary and secondary antibodies used throughout this study . .	28
2.4	List of supplies for cloning and molecular biology . . . . .	32
2.5	List of kits for DNA and plasmid purification . . . . .	32
2.6	List of enzymes used for cloning . . . . .	33
2.7	List of supplies for cell culture applications . . . . .	34
2.8	List of compounds for biochemical experiments . . . . .	35
2.9	Compositions of solutions and media for cell culture applications . . . .	37
2.10	Compositions of solutions for biochemical applications . . . . .	38
2.11	List of software and applications . . . . .	41
2.12	List of technical devices and equipment . . . . .	42
2.13	cDNA synthesis reaction mix . . . . .	44
2.14	Cycle protocol for cDNA synthesis . . . . .	44
2.15	PCR reaction mix for cloning from cDNA . . . . .	44
2.16	PCR reaction mix for cloning from plasmid template . . . . .	44
2.17	Cloning PCR cycle . . . . .	45
2.18	Annealing of shRNA oligonucleotides . . . . .	46
2.19	SDS PAGE gel . . . . .	50
3.1	Selected yeast-two-hybrid screen results . . . . .	77
3.2	Overview of validated novel interaction partners for MPP2 . . . . .	98

# 1 Introduction

## 1.1 Synapses

The mammalian brain is a fascinating organ of mesmerising complexity. It computes sensory input from a vast variety of receptive cells and organs into meaningful responses with consequences for the whole organism. Not only does it orchestrate release and contraction of various muscle fibres to create movement, but it also filters countless sensory inputs and converts these experiences into stored memories, which eventually make up our self.

All this complexity of the brain's actions is realised by billions of neurons and their innumerable connections to other neurons cells (Herculano-Houzel, 2009). The contact sites between neurons are called synapses. Although there are different kinds of synapses throughout the body (symmetrical synapses, electrical synapses, neuro-muscular junctions), the brain mainly contains asymmetrical contacts between neurons, which are referred to as chemical synapses. Those are typically characterised by an asymmetric arrangement of structural and functional elements between pre- and postsynaptic sites. They consist of a presynaptic terminal, which releases a chemical compound upon receiving an electrical stimulus. This compound, called a neurotransmitter, diffuses through a physical gap of few nanometres width, known as the synaptic cleft, until it reaches a structure called dendritic spine.

## 1.2 Components of the postsynapse

Postsynaptic protrusions from a neuronal dendrite, also referred to as dendritic spines, are highly dynamic structures. They typically consist of a thin stalk or neck and a terminal spine head of varying size, leading to filamentous, stubby or mushroom-like morphologies, which are associated with different developmental stages (Yuste and Bonhoeffer, 2004) as well as functional specialisations (for review see Sheng and Hoogenraad, 2007; Berry and Nedivi, 2017). Manifold proteins are present at postsynaptic sites and the dynamics and interactions between them require sensible orchestration to provide a stable and simultaneously dynamic basis for synaptic function. Dendritic spines are specific arrangements of more than a thousand proteins, including transmembrane proteins, different classes of receptors, ion channels, structural proteins, cytoskeletal components and regulatory molecules (Figure 1; for review see Sheng and Hoogenraad, 2007).

### 1.2.1 Transmembrane proteins

At the postsynapse, receptive elements for the presynaptically released neurotransmitter are central for signal transmission and synaptic functioning. The predominant neurotransmitters in the central nervous system are glutamate for excitatory and

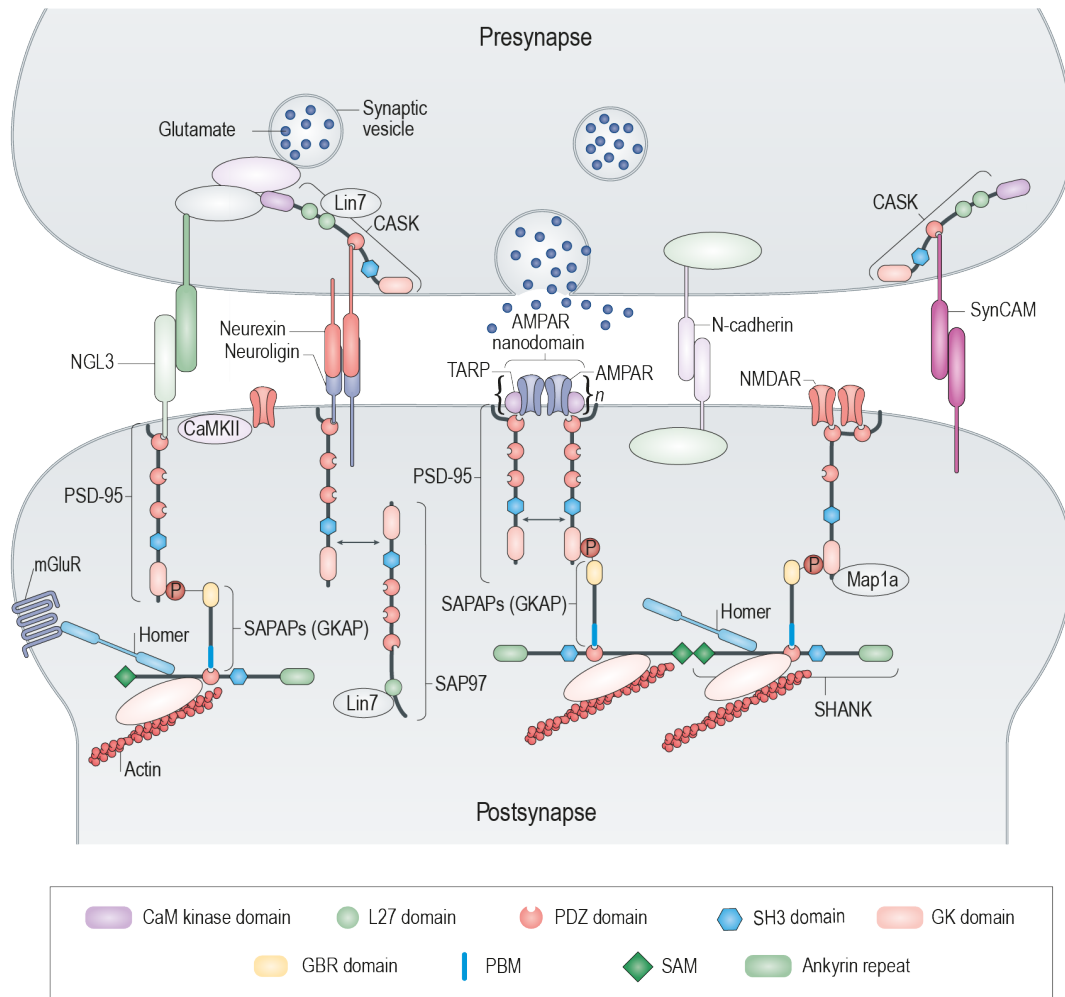


**Figure 1: Scaffold proteins organise protein complexes at excitatory synapses.** Schematic glutamatergic synapse highlighting selected proteins important for synaptic structure and function. Scaffold proteins that are relevant in the present thesis, in particular of the MAGUK family, are drawn with their domains. Double-headed arrows indicate multimerisation of MAGUK family proteins (membrane-associated guanylate kinases), which may contribute to local clustering of AMPA receptors. Such clusters, referred to as nanodomain, are aligned with presynaptic vesicle release sites. Figure modified from Zhu et al. (2016).

$\gamma$ -aminobutyric acid (GABA) for inhibitory signalling. Neurotransmitter receptors are typically transmembrane proteins assembled from several receptor subunits. They can be classified into metabotropic receptors, which are G protein-coupled receptors with a broad range of down-stream effector cascades (reviewed in Reiner and Levitz, 2018), or ionotropic receptors, which provide selective ion permeability upon transmitter binding and thereby allow for changes in membrane potential and also trigger further down-stream signalling.

Ionotropic glutamate receptors can be further sub-classified based on their specific agonist into kainate,  $\alpha$ -amino-3-hydroxy-5-methyl-4-isoxazolepropionic acid (AMPA) and N-methyl-D-aspartate (NMDA) receptors (reviewed in Reiner and Levitz, 2018). While all bind glutamate, they clearly differ in their structures, molecular kinetics, downstream effects and their selective ion permeability e.g. NMDARs are additionally

permeable for  $\text{Ca}^{2+}$ , what allows for effects on calcium-sensitive and/or dependent downstream signalling processes (reviewed in Wollmuth and Sobolevsky, 2004).

The postsynaptic receptor composition is rather dynamic in that it changes upon maturation of a synapse (e.g. the NMDAR/AMPA ‘switch’; Petralia et al., 2005), and is adjusted to regulate synaptic transmission in response to activity (for review see Choquet and Triller, 2013). Therefore, postsynaptic neurotransmitter receptor number and clustering are considered indicators of synaptic strength, as they increase proportionally with spine size and enclosed PSD volume (Schikorski and Stevens, 1997).

Receptors, in particular AMPA receptors, are additionally equipped with several transmembrane auxiliary subunits (TARPs, e.g. Stargazin; for review see Straub and Tomita, 2012), which facilitate proper localisation and clustering of receptors and modulate their trafficking and gating properties (e.g. L. Chen et al., 2000; Elias et al., 2006; Milstein et al., 2007).

Cell adhesion molecules (CAMs) are typically transmembrane proteins, which contribute to the interaction of a cell with its surrounding substrate and/or neighbouring cells. They not only act as molecular anchors for cells, but also mediate downstream signalling effects and help determine cell polarity and guide the formation of various cell junction complexes (Cavallaro and Dejana, 2011). Neurons express several specific sets of CAMs, which may further contribute to the specialisations of synaptic contacts and their regulation (Ullrich et al., 1995; Chubykin et al., 2007; for review see Missler et al., 2012).

Different synaptic CAMs have been identified to facilitate their trans-cellular and trans-synaptic role via diverse modes of protein interactions. The ‘prototypical’ synaptic cell adhesion proteins Neurexin and Neuroligin interact via LNS-domains (Laminin/Neurexin/sex hormone-binding globulin-domains) with three intercalated EGF-like domains at their N-terminus (reviewed in Sudhof, 2008), while SynCAM1 (also referred to as TSLC1/CADM1/Nectin-like 2) and Nectin proteins contain N-terminal IgG-like domains, residing in the extracellular space, which facilitate their trans-synaptic activity. Together with other proteins like SALM, NGLs and N-Cadherins, this class of proteins is critical for neuronal function (for reviews see Missler et al., 2012; Sudhof, 2008).

In neurons, CAMs have been found to be able to initiate synapse formation (Biederer et al., 2002; Scheiffele et al., 2000) and as critical signalling factors for the conversion of initial inter-neuronal contacts into functioning synapses, as e.g. knock-out of SynCAM1 causes memory deficits (Robbins et al., 2010) while Neuroligin defects are associated with autism (Tabuchi et al., 2007) and knock-out of all three Neuroligin isoforms was even found to be lethal (Varoqueaux et al., 2006).

After an initial contact between two neurons has been established, synaptogenesis involves the recruitment of vesicle release and recycling machinery components to the

presynaptic terminal, while postsynaptic assembly requires trafficking and anchoring of transmembrane receptors and assembly of cytosolic signalling complexes (for review see Biederer and Stagi, 2008). Transmembrane CAMs guide the assembly of additional and downstream synaptic proteins and thereby also influence the functional specification of a synapse (reviewed in Missler et al., 2012). Moreover, CAMs are not only developmentally important, but also contribute to synaptic stabilisation and maintenance (Chubykin et al., 2007; Korber and Stein, 2016). They have been shown to delineate PSD boundaries and are further thought to contribute to sub-cellular compartmentalisation and also to determine the width of the synaptic cleft (for review see Missler et al., 2012) as well as the edge of the postsynaptic density (Perez de Arce et al., 2015).

Of course, due to their relevance in stabilising the cell-cell contact and their role in recruiting specific synaptic proteins, CAMs are highly relevant in processes of synaptic plasticity, which require re-organisation of postsynaptic sites. Consequently, their loss has been associated with memory deficits (Robbins et al., 2010), autism (Jamain et al., 2008; Fujita et al., 2012) and epileptic seizures (Penagarikano et al., 2011; for review also see Sudhof, 2008). Remarkably, most of the synaptic cell adhesion molecules contain distinct recognition motifs at their C-terminus, which are bound specifically by PDZ-domains of several postsynaptic scaffold proteins. It is well established that the C-terminus of e.g. Neuroligin is bound by the membrane-associated protein PSD-95, and this interaction is characterised in detail (Irie et al., 1997). Interestingly, despite their importance for synaptic development and function, when the present study was initiated, no postsynaptic PDZ-binding partner for SynCAM proteins had been identified.

### 1.2.2 Cytosolic proteins

Right below the synaptic membrane, large multi-domain scaffold proteins serve as interaction hubs providing surfaces for multiple protein-protein interactions and thereby mediating synaptic function. They enable recruitment and anchoring as well as dynamic movement of transmembrane proteins, receptors, ion channels, structural and regulatory proteins as well as elements of the cytoskeleton (for review see Choquet and Triller, 2013; for a more general review see Good et al., 2011). In this role, they are also critical for the regulation of signalling processes that eventually mediate synaptic structure and function (for review see Won et al., 2017). Scaffold proteins also confer signalling processes from the synaptic membrane into deeper synaptic layers by connecting the involved signalling components (Hayashi et al., 2009).

A very peculiar element of excitatory synapses is the postsynaptic density (PSD): an electron-dense array formed by multiple scaffold proteins and regulatory molecules that cooperate in order to regulate glutamatergic synaptic transmission and plasticity. The PSD is a structure of ~360 nm diameter and accounts to a mass of ~1500 MDa, mainly contributed by the  $\text{Ca}^{2+}$ /calmodulin-dependent protein kinase II (CamKII), which is

the most abundant protein in neurons and critical in modulating synaptic function (X. Chen et al., 2005; Lisman, 2017). The predominant scaffold protein in the PSD, however, is the membrane-associated guanylate-kinase (MAGUK) protein PSD-95 (X. Chen et al., 2005; for review see Sheng and Hoogenraad, 2007). The scaffold proteins of the PSD can grossly be assigned to three different groups that even have distinct localisations within dendrites: PSD-95 family proteins sit just below the membrane and interact with multiple transmembrane proteins and cytosolic scaffold proteins. Deeper into the spine (Dani et al., 2010), GKAP family proteins (GK-associated protein, also SAPAPs; Takeuchi, 1997; E. Kim et al., 1997), connect those membrane-associated scaffolds with the third group of cytoskeleton-associated scaffold molecules: SHANK (SH3 and multiple Ankyrin repeat domains protein) and Homer family scaffold molecules, which are closely associated with the actin cytoskeleton (Hayashi et al., 2009; for review see Sheng and Hoogenraad, 2007).

PSD-95 family proteins have been found to mediate NMDA receptor clustering by directly binding receptor subunit C-termini (Kornau et al., 1995) and influence AMPA receptor accumulation indirectly, by interacting not with the receptors but their transmembrane auxiliary subunits (TARPs) such as Stargazin/TARP $\gamma$ 2 (Bats et al., 2007).

Recent developments in super-resolution imaging techniques have revealed that these scaffold proteins, in particular PSD-95, are not only concentrated at postsynaptic membranes. Instead, they are further organised as nanodomains within the PSD (Dani et al., 2010), which are thought to assist in clustering neurotransmitter receptors with consequences for synaptic transmission (El-Husseini et al., 2000b; MacGillavry et al., 2013; Nair et al., 2013).

PSD-95 family proteins, like SAP102, PSD-93, and SAP97, have been shown to be critically important for the recruitment of synaptic proteins during development and the dynamic processes of synaptic plasticity at mature stages (Kornau et al., 1995; Schnell et al., 2002; Dakoji et al., 2003; Opazo et al., 2012; for review see Elias and Nicoll, 2007; Choquet and Triller, 2013). The importance of PSD-95 family proteins for synaptic transmission is also apparent from their frequent implication in neurodevelopmental defects such as autism and intellectual disability (for review see Coley and Gao, 2018).

Moreover, the postsynaptic PSD-95 family proteins are also able to confer retrograde effects towards the presynaptic terminal, as they also interact directly with transmembrane cell adhesion molecules like Neuroligin (Irie et al., 1997; Futai et al., 2007), which mediates alignment of pre- and postsynaptic membrane by interacting with e.g. Neurexin family proteins (for review see Missler et al., 2012).

The connection between ion channels and cytoskeletal elements that is provided by this network of scaffold proteins is critical for the dynamic regulation of synaptic structure and function. Two basic principles of synaptic plasticity are the up-scaling of synaptic strength in form of long-term potentiation (LTP) and downscaling in form of long-term

depression (LTD) (reviewed in Malenka and Bear, 2004; Kasai et al., 2010). These plasticity processes are realised e.g. by changes in protein activity, protein-protein interaction affinities (mediated e.g. via protein phosphorylation by PIP-kinases, MAP kinases; for reviews see H. K. Lee, 2006; Yokoi et al., 2012) or alterations in protein diffusion and cycling, in particular of receptor proteins (reviewed in Choquet and Triller, 2013). Beyond these effects, synaptic plasticity also involves morphological changes of the dendrite, which requires intense remodelling of the spines' actin-cytoskeleton (for review see Hotulainen and Hoogenraad, 2010). Mediated by the dense protein interaction network that is the PSD, synaptic activity can be translated into cytoskeleton-dynamics: Neurotransmitter binds to respective receptors, which may cause entry of extracellular  $\text{Ca}^{2+}$  to the cell (e.g. via ionotropic NMDA receptors, which exhibit a certain calcium conductivity; reviewed in Reiner and Levitz, 2018) or from internal stores (e.g. via metabotropic glutamate receptors mediated by activity of the downstream signalling cascade involving phospholipase C generating the second messenger inositol tris-phosphate; reviewed in Niswender and Conn, 2010). This increase in  $\text{Ca}^{2+}$  then is able to cause release of CaMKII from F-actin, thereby unbundling those actin filaments which become accessible to actin-binding proteins like Cofilin,  $\alpha$ -actinin, Profilin and Drebrin, which then facilitate re-assembly and stabilisation of the cytoskeleton, e.g. via links to scaffold proteins (reviewed in Borovac et al., 2018; Hotulainen and Hoogenraad, 2010).

### 1.3 Membrane-associated guanylate kinases (MAGUKs)

A large family of scaffold proteins are membrane-associated guanylate-kinases (MAGUKs). These proteins are characterised by their common 'MAGUK core' domains, consisting of a PDZ domain connected via a linker region to an SH3 and GK tandem domain with distinct interaction dynamics (McGee et al., 2001; Li et al., 2014; Rademacher et al., 2019). As illustrated in Figure 2a for a selection of important MAGUK proteins, this is most often complemented by a variety of additional protein-protein-interaction domains e.g. L27 domains which form hetero-dimers with other L27 domains (Li et al., 2004; W. Feng et al., 2005; Petrosky et al., 2005; Zhu et al., 2016). Moreover, the N-terminal domains may also vary, depending on alternative splicing, as is known from e.g. PSD-95 family MAGUKs, which may contain either L27 domains or a palmitoylation site that is necessary for their positioning and function at the membrane (Chetkovich et al., 2002).

Several hundred proteins containing PDZ (PSD-95, Dlg, Zonula Occludens-1) domains are encoded in the human genome ([http://smart.embl.de/smart/do\\_annotation.p1?DOMAIN=SM00228](http://smart.embl.de/smart/do_annotation.p1?DOMAIN=SM00228)). Many of them are MAGUK family proteins that can be found at various types of cell-cell contacts, including tight-, adherens- and septate junctions, as well as neurons (for review see Funke et al., 2005). PDZ domains form a binding pocket that is able to interact with a specific sequence of the four amino acids at a

proteins' C-terminus, also referred to as PDZ domain-binding motif (PBM). Based on the -2 position of the PBM and the respective binding preferences, PDZ domains are typically classified into canonical class I or II PDZ domains (for reviews see H. J. Lee and Zheng, 2010; Ernst et al., 2014), however, much narrower specificity classes exist (Tonikian et al., 2008) and contribute to the importance of PDZ domain-mediated interactions. These differences in PBM specificity are also reflected by the very amino acids that form the PDZ domain ligand binding groove (Songyang et al., 1997; Tonikian et al., 2008; H. J. Lee and Zheng, 2010) and greatly contribute to the organisation of protein complexes by scaffold proteins, especially at synapses (for review see E. Kim and Sheng, 2004).

Interestingly, the former guanylate kinase domain of MAGUKs is no longer catalytically active or binding nucleotides. Instead, it has evolved into another protein-protein interaction domain (Olsen and Brecht, 2003; Zhu et al., 2011) in conjunction with the SH3 domain, which is also altered in that it no longer binds specific proline-rich PXXP motifs (McGee et al., 2001). MAGUKs have been identified as critical players in the formation and maintenance of protein complexes critical for e.g. epithelial contacts, tight and adherens junctions and, in particular, synapses (Gonzalez-Mariscal et al., 2000; Assemat et al., 2008; Fanning and Anderson, 2009). The importance of this family of proteins is impressively demonstrated at glutamatergic synapses of central neurons, where MAGUKs, in particular of the PSD-95 subfamily at the postsynapse (Elias et al., 2006) and CASK at the presynapse (Butz et al., 1998), are critical for synaptic assembly, maintenance and plasticity.

The human MAGUK protein family is homologue to the *Drosophila* tumour suppressor discs-large (DLG). DLG also exhibits the prototypical domain structure of the 'MAGUK core' PSG module and was found to be localised to septate junctions of epithelial tissues as well as neuronal cells (Woods and Bryant, 1991). Hence, MAGUKs are also referred to as *discs-large* (DLG) proteins (Lue et al., 1994), e.g. SAP102 being known as DLG1 or PSD-95 as DGL4.

#### 1.4 MPP family proteins

The focus of the present thesis is the protein MPP2, which belongs to a different subfamily of MAGUKs called membrane proteins, palmitoylated (MPP). In mammals, this subfamily contains seven members with a remarkably conserved domain structure: In addition to the 'MAGUK core' PSG module all but one MPP proteins contain an N-terminal L27 domain tandem (see also Figure 2a). In contrast, MPP1 also referred to as p55, which was eponymous for the subfamily (Alloisio et al., 1993), does not have L27 domains, but instead contains palmitoylation sites at the N-terminus that are critical for its function in erythrocyte lateral membrane integrity (Lach et al., 2012; Biernatowska et al., 2013). Prototypically for MPP family proteins, MPP1 binds the C-terminus of a transmembrane protein, glycophorin C, to form membrane-

associated complexes involving additional cytosolic proteins, e.g. protein 4.1 (Marfatia et al., 1994). Consequently to the description of two additional structurally well conserved proteins, DLG2/MPP2 and DLG3/MPP3, Smith et al., 1996 have proposed to consider MPP proteins as a novel protein family, which couples cytoskeleton elements with the cell membrane. MPP proteins are not only structurally, but also evolutionary well preserved, as homologues of MPP proteins are also found in zebrafish (MPP5: *nagie oko*, *nok*) or *Drosophila* (MPP5: *stardust*; MPP6: *varicose*).

The MPP protein family has to date been best characterised regarding the importance of MPP1 in red blood cells for the role of multiple MPP proteins in epithelia. A big body of literature is available regarding MPP5, also known as Pals1, which shares the domain structure with MPP2 (reviewed in Assemat et al., 2008).

MPP5 is an MPP family MAGUK that is crucial for cell polarity determination as well as the assembly and maintenance of tight junctions (for reviews see Margolis and Borg, 2005; Assemat et al., 2008; Gosens et al., 2008). It binds the C-terminus of the apical transmembrane protein Crumbs (Fogg et al., 2005) with its PDZ domain (Ivanova et al., 2015) and is further connected to the tight junction stabilising proteins Claudin and JAM proteins via PATJ (Makarova et al., 2002; Roh et al., 2002; Michel et al., 2005). Moreover, the multiple interactions of MPP5 allow for a connection of these apical membrane proteins with actin cytoskeletal components via the Par6 complex (Hurd et al., 2003; Q. Wang et al., 2004; for review see Margolis and Borg, 2005; Assemat et al. 2008; Gosens et al., 2008) Cytosolic interactions of MPP proteins also include a different mode of interaction, e.g. protein 4.1 super family proteins where FERM domains interact with the Hook-GK region of MPP family MAGUKs (Gosens et al., 2007a).

Studies investigating MPPs in retinal epithelia have demonstrated that various MPP proteins are able to specifically dimerise with each other in a manner likely involving the SH3GK tandem domains (Kantardzhieva et al., 2005; Kantardzhieva et al., 2006; Gosens et al., 2007a; Stucke et al., 2007). Additionally, in various cellular contexts MPP family proteins were frequently found to interact with other scaffold proteins, in particular Lin7/Veli/Mals, CASK/Pals3 and SAP97/DLG1, via their L27 and SH3GK domains (Kamberov et al., 2000; Karnak et al., 2002; Stohr et al., 2005; Mburu et al., 2006; Bohl et al., 2007; Stucke et al., 2007; J. Yang et al., 2007; X. Yang et al., 2010; Kamijo et al., 2015).

The importance of MPP proteins in maintenance of epithelial integrity is impressively demonstrated in studies interfering with MPP protein expression causing e.g. retinal degeneration, cell polarity inadequacies and developmental defects (Straight et al., 2004; Gosens et al., 2007b; Dudok et al., 2013a; Mroczkowski et al., 2014; Park et al., 2015). In line with the important role of MPP proteins in the establishment and maintenance of cell-cell contacts, in various types of cancer and cancer cell lines the expression of MPP proteins is altered and associated with differences in malignancy (Seo et al., 2009; Guerreiro et al., 2011; X. Feng et al., 2012; Ibrahim et al., 2012; T. Cai et al., 2013; Ma et al., 2014; New et al., 2019).

In cancer cells MPP proteins have also been found to interact in a PDZ domain-dependent fashion with various transmembrane cell adhesion proteins, most importantly CADM1/TSCL1/SynCAM1/Nectin-like 2 and Nectins, which seem to recruit MPP proteins specifically to cell-cell contact sites (Shingai et al., 2003; Sakurai-Yageta et al., 2009; Murakami et al., 2014).

Tight junctions, where MPP proteins are critical elements for assembly and maintenance, share certain features with synapses: Both establish connections of transmembrane cell adhesion systems, which are tightly linked to actin cytoskeletal structures, which are realised by several MAGUK protein interactions (reviewed in Gosens et al., 2008).

Given that many of the interacting proteins, like SAP97 and SynCAM1 are also relevant for synaptic function, it is particularly interesting that some MPPs have been associated with nervous tissue already. There is evidence suggesting a direct or indirect role of MPP proteins in regulating neuronal function: MPP5, for example, was found to bind to the GAT1 GABA-transporter and increase cellular GABA uptake upon co-expression in heterologous cells (McHugh et al., 2004). Additionally, there is already evidence illuminating a functional, rather than only structural, role of MPP3: the protein was found to bind to serotonin receptors and is further able to prevent its desensitisation (Gavarini et al., 2006).

Apart from these studies there are several reports indicating that MPP family proteins are indeed essential proteins with importance in brain development and function. The most striking evidence might be a conditional MPP5 knockout, which is lacking the entire neocortex, indicating a critical neurodevelopmental role of MPP5 (S. Kim et al., 2010). A less severe phenotype was observed in MPP3 knockout experiments, leading to cellular disorganisation at the ventricular (neurogenic) zone in the developing cortex (Dudok et al., 2013b). Furthermore, the authors observed an influence on the localisation of MPP5 upon loss of MPP3, indicating complex scaffolding interactions among MPP subfamily members, similar to the PSD-95 subfamily. Moreover, an interaction between MPP and PSD-95 family proteins has been described and was found to mediate protein complex assembly at retinal synapses (Aartsen et al., 2006).

In line with the idea that MPP family proteins have important functions at synapses, MPP1 and MPP6/Pals2 have been isolated from brain lysates, where they are associated with the well-established synaptic MAGUKs PSD-95, SAP97 and CASK (Kamijo et al., 2015) as well as other scaffold molecules, like GKAP (Jing-Ping et al., 2005), or functional elements, such as Kir2.2 potassium channels (Leonoudakis et al., 2004a; Leonoudakis et al., 2004b).



## 1.5 Aim

Prior to the work described here, MPP2 has only been investigated in conjunction with other MPP family proteins in cancer cell lines (Fukuhara et al., 2003; Shingai et al., 2003; Sakurai-Yageta et al., 2009) and epithelial cells (Baumgartner et al., 2009). However, recently several studies investigating protein complexes associated with glutamate receptors have isolated MPP2 by multi-epitope immunoaffinity purification and LC-MS (Schwenk et al., 2012; Shanks et al., 2012).

Since the well-established synaptic scaffold proteins of the PSD-95 family are crucial for the function of excitatory synapses, the isolation of the structurally remarkably similar MPP2 from glutamate receptor complexes prompted further investigations to characterise the role that MPP proteins, and MPP2 in particular, have at synapses.

The first aim of this project was to confirm the expression of MPP2 in neurons and to investigate its expression and localisation at synaptic sites.

The second aim was to search and validate proteins that interact with the different protein-protein interaction domains of MPP2 in synaptic context. This would reveal protein complexes and regulatory mechanisms that involve MPP2 as a novel structural component and thus deepen the current understanding of synaptic architecture and functional regulation.

As a final aim, manipulations of the MPP2 protein and investigation of their consequences should enable a better understanding of the role of MPP2 in neuronal function.

## 2 Material and Methods

### 2.1 Material

#### 2.1.1 Vectors

Table 2.1: Vector backbones used for the generation of expression constructs

Name	Source	Catalogue number
pEGFP-C1	Clontech	6084-1
pCMV-2A	Stratagene	211172
pCMV-3A	Stratagene	211173
pGEX-6P-1	GE Healthcare	28-9546-48
pGW1-NoTag	Dr. Nils Rademacher	Custom
pCMV-HSTKV-mCherry	Dr. Nils Rademacher	Custom, based on pCMV
pSUPER.neo+GFP	Oligoengine	VEC-PBS-0005/0006
BL100-f(syn)w	Viral Core Facility, Charité - Universitäts- medizin Berlin	f(syn)w
BL-360 f(U6)s0w	Viral Core Facility, Charité - Universitäts- medizin Berlin	BL360

**Table 2.2: Oligonucleotides**

Name	Sequence 5'→3'	Construct
CMV_for	CGCAAATGGGCGGTAGGCGTG	
T7_rev	AATACGACTCACTATAG	
MPP1_BamHI_for	AAGGATCCAACGCTCAAGTCGAGCGAAGG	pCMV-V5a-MPP1
MPP1_SalI_rev	TTGTCGACTTAGTAAACCCAGGAGACAGGC	
EGFP-MPP2_XhoI_noStart_for	AACTCGAGTGCCGGTTGCTGCC	pEGFP-C1-mMPP2
EGFP-MPP2_EcoRI_stop_rev	TTGAATTCTCAGTACACCCAGC	
mMPP2-H174F-V177T_for	CTGCAGGAGAATTCCTGGGTACGACATTC	pEGFP-C1-mMPP2-H150V153T
mMPP2-H174F-V177T_rev	GTCGTACCCAGGAATTCTCCTGCAGTC	
MPP2 PSG GEX for	AGGAATTCCTCCCAAGCCCAGGCCTG	pGEX-mMPP2-PSG
MPP2 SH3GK GEX for	AGGAATTCAGGAACCCACCTGCC	pGEX-mMPP2-SH3-GK
MPP2-PDZ_XhoI_rev	TTCTCGAGTCAGTAGCTGGGCAAGATCTT	pCMV-3a-mMPP2-PDZ
MPP2-PSG_CMV-EcoR1_for	AAGGAATTCCTCCCAAGCCCAGGCCTGGAT	pCMV-Tag3a-mMPP2-PSG
MPP2 SH3-GK_EcoR1_for	AAGAATTCAGGAACCCACCTG	pCMV-3a-mMPP2-SH3GK
MPP2-Hook-GK_EcoR1_for	AAGAATTCACAGCTGTTGGAGGAGAAACGG	pCMV-3a-mMPP2-GK
MPP2-R387A_for	CCCTACACATCAGCGAGGCCCAAGGAC	pCMV-3a-mMPP2-R387A
MPP2-R387A_rev	CCTTGGGCCTCGCTGATGTGTAGGGCACC	
rat_MPP2_BglII_for	AAAGATCTAATGCCGGTTGCTGCCACGAA	pCMV-3a-rMPP2
rat_MPP2_XhoI_rev	TTCTCGAGTCAGTACACCCAGCTCACAGG	
ratMPP2_shRNA1s_GGTCTA- GATCCCACGTTT A	GATCCCCGGTCTAGATCCCACGTTTATTCAA- GAGATAAACGTGGGATCTAGACCTTTTTA	pSUPER-GFP-rMPP2-shRNA1

Name	Sequence 5'→3'	Construct
ratMPP2_shRNA1rc_GGTC-TAGATCCCACGTTTA	AGCTTAAAAAGGTCTAGATCCCACGTT-TATCTCTTGAATAAACGTGGGATCTAGAC-CGGG	
ratMPP2_shRNA2s_GGCACT-GCAGGAACTCCTA	GATCCCCGGCACTGCAGGAACTCCTATTCAA-GAGATAGGAGTTCTGCAGTGCCTTTTTA	pSUPER-GFP-rMPP2-shRNA2
ratMPP2_shRNA2rc_GGCACT-GCAGGAACTCCTA:	AGCTTAAAAAGGCACTGCAGGAACTCC-TATCTCTTGAATAGGAGTTCCTGCAGTGC-CGGG	
ratMPP2_shRNA3s_GAT-GCTGGTTCCCATGCTA:	GATCCCCGATGCTGGTTCCCATGCTATTCAA-GAGATAGCATGGGAACCAGCATCTTTTTA	pSUPER-GFP-rMPP2-shRNA3
ratMPP2_shRNA3rc_GAT-GCTGGTTCCCATGCTA:	AGCTTAAAAAGATGCTGGTTC-CCATGCTATCTCTTGAATAG-CATGGGAACCAGCATCGGG	
rMPP3_EcoRI_fwd	AAGAATTCGCCGGTACTGTCCGAAGAC	pCMV-Tag2a-rMPP3
rMPP3_XhoI_rev	AACTCGAGTTACCTCACCCAGCTGATG	
MPP6_BamHI_for	AAGGATCCACAGCAAGTTTTGGAAAACC	pCMV-2a-MPP6
MPP6_SalI_rev	TTGTCGACTCAGTACACCCAGCTAATTG	
SynCAM-EAFA_rev	TTGTCGACCTAGGCGAAGGC-CTCTTTCTTTTC	pCMV-HA-SynCAM-EAFA
SynCAM1 rev	TTCTCGAGCTAGATGAAG-TACTCTTTCTTTTCTTCGGAGTTTGATC-CGCCGCCACCAGACCCACC	pCMV-HSV-mCherry-SynCAM

Name	Sequence 5'→3'	Construct
mCherry-SynCAM_EAFA_XhoI_rev	TTCTCGAGCTAGGCGAAGGC- CTCTTTCTTTTCTTCGGAGTTTGATCCGC- CGCCACCAGACCCACC	pCMV-HSV-mCherry-SynCAM-EAFA
Cherry-Nectin-1_rev_Primer	TTCTCGAGCCTACACATAACCACTCTTTCTTG- GAAATGAAAGATGATCCGCCGCCACCAGACC- CACC	pCMV-mCherry-Nectin1
Cherry-Nectin-3_rev_Primer	TTCTCGAGTTAGACATAACCACTCCCTCCTG- GAAATTACGGATGATCCGCCGCCACCAGACC- CAC	pCMV-mCherry-Nectin3
Cherry-Cntnap2_rev_Primer	TTCTCGAGTCAAATGAGCCACTC- CTTTTTGCTCTCGTCAATTGATCCGCCGC- CACCAGACCCACC	pCMV-mCherry-Cntnap2

### 2.1.3 DNA constructs

The expression constructs used throughout this thesis were generated by PCR using the primers provided in Table 2.2 on custom-made cDNA reverse-transcribed from rat and mouse brain RNAs as well as a human testis library or based on existing DNA plasmids. Mouse (NM\_016695), rat MPP2 (NM\_053513), mouse MPP1 (NM\_008621.3), rat MPP3 (NM\_053668), mouse MPP6 (NM\_001164734) were cloned into pCMV-2a and -3a using restriction sites as indicated in Table 2.2.

The bacterial expression constructs GST-MPP2-PSG and GST-MPP2-SH3-GK were generated by cloning the fragments encoding amino acids 119-552 (PSG) and 220-552 (SH3GK), respectively, of mouse MPP2 into pGEX-6P-1.

Full-length rat SynCAM1 (NM\_001012201.1) was synthesised with an HA tag introduced after the signal peptide by eurofins and subcloned into pCMV vector with NotI and Sall restriction sites.

FLAG-tagged expression constructs for MPP2 (NM\_016695.3), MPP5 (NM\_001108034), GKAP (NM\_001360665), Arhgef2 (NM\_001012079), Ppp3ca (NM\_017041), Farp1 (NM\_001107287), HA tagged Gnao1 (NM\_017327) and HSVTK-mCherry-constructs with the ten amino acid C-termini of NR2B, GluA2, CKAMP44, Stargazin/TARP $\gamma$ 2, Neuroligin and NGL-1 as well as expression constructs for untagged PSD-95 (NM\_019621) and GST-tagged PSD-95 SH3GK, were generously provided by Dr. Nils Rademacher.

Moreover, the following constructs were obtained from Addgene: GFP-PIPK1-gamma 90 (#22299; <http://n2t.net/addgene:22299>; RRID: Addgene\_22299; Di Paolo et al., 2002), GABA (A) receptor subunit a1SE (#49168; <http://n2t.net/addgene:49168>; RRID: Addgene\_49168; Tretter et al., 2008) and GABA(A) receptor subunit a2SE (Addgene plasmid #49169; <http://n2t.net/addgene:49169>; RRID: Addgene\_49169; Tretter et al., 2008) and GABA(A) receptor subunit B3SE (#49171; <http://n2t.net/addgene:49171>; RRID: Addgene\_49171; Jacob et al., 2005).

Table 2.3: List of primary and secondary antibodies used throughout this study

Target	Clone or Conjugate	Host	Supplier	Catalogue number	Application		
					IP	WB	IF
<i>Endogenous proteins</i>							
GluA2		mouse	NeuroMab	75-002		1:3000	1:200
Homer1 (b+c)		rabbit (poly)	Abcam	ab97593			
Homer1		guinea pig (poly)	Synaptic Systems	160004			
GABA <sub>A</sub> R $\alpha$ 1		mouse (mono)	NeuroMab	75-136	3 $\mu$ g	1:1000	1:200
GABA <sub>A</sub> R $\alpha$ 2		mouse (mono)	NeuroMab	75-384			1:200
GABA <sub>A</sub> R $\alpha$ 4		mouse (mono)	NeuroMab	75-383			1:200
GABA <sub>A</sub> R $\beta$ 1		mouse	Abcam	ab93612			1:200
GABA <sub>A</sub> R $\beta$ 3		mouse	Abcam	ab98968			1:200
Gephyrin	Clone L106/93	mouse (mono)	NeuroMab	75-444			1:200
Gephyrin	Clone L106/83	mouse (mono)	NeuroMab	75-443			1:200
MAP2		guinea pig (poly)	Synaptic Systems	188004			1:500
MAP2		rabbit (poly)	Millipore/Chemicon	AB5622			1:500
MAP2	Clone 5F9	Mouse (mono)	Millipore/Chemicon	05-346			1:500
MAP2		chicken (poly)	Synaptic Systems	188 006			1:500
MPP2		mouse (poly)	Sigma	SAB1400169		1:100	1:10
MPP2		rabbit	Abcam	ab97290	2 $\mu$ g	1:5000	1:250-1:500
MPP2		rabbit (mono)	Abcam	ab156874		1:1000	
PSD-95		mouse	NeuroMab	75-028	3 $\mu$ g	1:5000	1:500
PSD-95		guinea p (poly)	Synaptic Systems	124014			
PSD-95		rabbit	Abcam	ab76115		1:5000	

Target	Clone or Conjugate	Host	Supplier	Catalogue number	Application		
					IP	WB	IF
PSD-95	Biotin	mouse	NeuroMab	75-028	2 µg	1:5000	1:250-1:500
SynCAM		chicken	MBL	CM004-6	3 µg		
SynCAM		chicken	MBL	CM004-3		1:5000	1:500
Stargazin		mouse	NeuroMab	73-242	2 µg	1:5000	
Stargazin		rabbit	Cell Signalling	2503S		1:3000	
Tubulin		rat	Abcam	ab6160		1:20000	
Veli1/2/3		goat (poly)	Santa Cruz	sc-11499			
vGlut1		mouse	NeuroMab	75-066			
Tags							
αFLAG	Clone M2	mouse (mono)	Sigma	F1804	2 µg	1:5000	1:500
αFlag-HRP	HRP	mouse	Sigma	A8592		1:5000	
αDDDK		chicken (poly)	Abcam	ab1170		1:5000	
αHA		mouse	Covance	MMS-101r		1:5000	1:500
αHA		rabbit	Sigma	H6928		1:5000	1:500
αMYC		mouse	Clontech	631206	2 µg	1:5000	1:500
αMYC		rabbit	Cell Signalling	2272S		1:5000	1:500
αHSV		rabbit	Abcam	ab3414		1:5000	
αGFP		chicken (poly)	Abcam	ab13970		1:50000	1:5000
αGFP	Atto 488	Nanobody	Chromotek	gba488-10			1:200

Target	Clone or Conjugate	Host	Supplier	Catalogue number	Application		
					IP	WB	IF
Normal immunoglobuline							
normal IgG		mouse	Santa Cruz	sc-2025	2 µg		
normal IgG		rabbit	Santa Cruz	sc-2027	2 µg		
normal IgY		chicken	Santa Cruz	sc-2718	2 µg		
Secondary antibodies							
αMouse-HRP	HRP		Dianova	115-035-003		1:5000	
αRabbit-HRP	HRP		Dianova	111-035-003		1:10000	
αRat-HRP	HRP		Santa Cruz	sc-2032		1:10000	
αMouse	Alexa Fluor 405	goat	Invitrogen	A-31553			1:1000
αMouse	Alexa Fluor 488	chicken	Invitrogen	A-21200			1:1000
αMouse	Alexa Fluor 568	goat	Life Technologies	A-11031			1:1000
αMouse	Alexa Fluor 647	goat	Jackson Immuno	715-605-150			1:1000
αRabbit	Alexa Fluor 405	goat	Invitrogen	A-31556			1:1000
αRabbit		goat	Jackson Immuno	111-007-008			
αRabbit		goat	AffiniPure	111-005-003			
αRabbit	Alexa Fluor 488	donkey	Invitrogen	A-21206			1:1000
αRabbit	Alexa Fluor 568	goat	Life Technologies	A-11036			1:1000
αRabbit	Cy3b		Custom (AG Ewers)				1:10
αRabbit	Alexa Fluor 647	donkey	Abcam	ab150075			1:1000
αRabbit	CF 680		Custom (AMBIO)				1:100

Target	Clone or Conjugate	Host	Supplier	Catalogue number	Application		
					IP	WB	IF
$\alpha$ Guinea pig		goat	Jackson Immuno	106-007-008			
$\alpha$ Guinea pig	Alexa Fluor 405	goat	Abcam	ab175678			1:1000
$\alpha$ Guinea pig	DyeLight <sup>®</sup> 405	donkey	Dianova	706-475-148			1:1000
$\alpha$ Guinea pig	Alexa Fluor 568	goat	ThermoFisher	A-11075			1:1000
$\alpha$ Guinea pig	Alexa Fluor 647	goat	ThermoFisher	A-21450			1:1000
$\alpha$ Guinea pig	CF 568		Custom (AMBIO)				1:100
$\alpha$ Chicken	Alexa Fluor 405	goat	Abcam	ab175675			1:1000
$\alpha$ Chicken	Alexa Fluor 488	donkey	Jackson Immuno	703-545-155			1:1000

## 2.1.5 Chemicals and Consumables

### 2.1.5.1 Molecular biology

**Table 2.4: List of supplies for cloning and molecular biology**

Name	Source	Catalogue number
Agar-Agar	Roth	5210.1
Agarose	Serva	11404.07
Ampicillin Na-Salt	Roth	K029.1
Competent E.coli OneShot Top10	Invitrogen	C4040-03
DTT Solution 1 M	AppliChem	A3668
Hexamer random pdN6 primer	Amersham Pharmacia	27-2166-01
Hyperladder I	Bioline	bio-33026
Kanamycin (-sulfate)	Roth	T832.1
Nuclease Free Water	Life Technologies	AM9937
Oligo dT Primer (12-18)	Invitrogen	18418012
RNAse Inhibitor	Fermentas	N8080119
RNAse Zap	Ambion	AM9780
Yeast extract	Roth	2363.2

**Table 2.5: List of kits for DNA and plasmid purification**

Name	Source	Catalogue number
Qiagen Maxi Kit	Qiagen	12163
QIAprep Spin Mini Kit	Qiagen	QIA27106
QIAquick Gel Extraction Kit	Qiagen	QIA28704
QIAquick PCR Purification Kit	Qiagen	QIA28106

**Table 2.6: List of enzymes used for cloning**

Name	Source	Catalogue number
RE Bsp1407 I (BsrG I)	Fermentas	ER0931
RE FastDigest Afl II	Fermentas	FD0834
RE FastDigest Age I (BSHT I)	Fermentas	FD1464
RE FastDigest BamHI	Fermentas	FD0055
RE FastDigest Bgl I	Fermentas	FD0074
RE FastDigest Bgl II	Fermentas	FD0084
RE FastDigest BLP I (BPU1102I)	Fermentas	FD0094
RE FastDigest Bsp1407I (BsrGI)	Fermentas	FD0933
RE FastDigest EcoNI (Xag I)	Fermentas	FD1304
RE FastDigest EcoRI	Fermentas	FD0275
RE FastDigest EcoRV (Eco321)	Fermentas	FD0303
RE FastDigest Hind III	Fermentas	FD0504
RE FastDigest Kpn I	Fermentas	FD0524
RE FastDigest Nde I	Fermentas	FD0584
RE FastDigest Nhe I	Fermentas	FD0974
RE FastDigest Not I	Fermentas	FD0594
RE FastDigest Pac I	Fermentas	FD2204
RE FastDigest Sac I	Fermentas	FD1134
RE FastDigest Sal I	Fermentas	FD0644
RE FastDigest Sca I	Fermentas	FD0434
RE FastDigest Xba I	Fermentas	FD0685
RE FastDigest Xho I	Fermentas	FD0695
RE Fse I	NEB	R0588S
T4 DNA Ligase	MBI	EL0014
DNA Polymerase Phusion High-Fidelity	NEB	M0530L
DNA Polymerase Mango Taq	Bioline	bio-21083
Superscript III RT Polymerase	Invitrogen	18080-093
Alkanine Phosphatase Fast AP	Fermentas	EF0651

### 2.1.5.2 Cell culture

**Table 2.7: List of supplies for cell culture applications**

Name	Source	Catalogue number
B27 Supplement 50x	Gibco	17504-044
Cell Culture Flask 75 cm <sup>2</sup>	TPP	P 90075
Cell Culture Plate 12-well	TPP	TPP92012
Cell Culture Plate 6-well	TPP	TPP92006
Cell Scraper 24 cm	TPP	TPP99002
Collagen I	Corning	354236
Coverslips high precision 22x22 mm	Roth	LH24.1
Coverslips high precision Ø 22 mm	VWR	631-0172
Coverslips Ø18 mm	VWR	631-1580
DMEM Low Glucose	Sigma	D5546-24X500ML
DPBS	Lonza	17-512F
FBS Superior	Biochrom	S0615
Laminine	Sigma	L2020
L-Glutamine 200 mM	Lonza	BE 17-605E
Lipofectamine2000	ThermoFisher	116680-19
Neurobasal Medium	Gibco	21103-049
Opti-MEM	Gibco	51985-026
Penicillin-Streptomycin (10.000 U)	Lonza	17-602F
Poly-D-Lysine	Sigma	P7886
Trypsin EDTA	Lonza	17-161E
Trypsin-EDTA Mixture	Lonza	17-161F
Water for Cell Culture	Lonza	17-724F

### 2.1.5.3 Biochemistry

Table 2.8: List of compounds for biochemical experiments

Name	Source	Catalogue number
Acetic Acid	Merck	1.000.63
Acetone	Roth	9372.1
Ammonium persulfate (APS)	Biomol	50404-1
$\beta$ -Mercaptoethanol	Roth	4227.2
Bis-Tris free base	Sigma	B9754
Blotting Paper 707, 7x10cm	VWR	732-0594
Bovine Serum Albumin	Sigma	A3912
Bromphenolblue	Merck	11746
Complete mini, EDTA free	Roche	1836170
DAPI-Fluoromount-G	Southern Biotech	0100-20
Ethanol denatured	Roth	K928.4
Ethanol p.a.	Merck	107017
Ethidium bromide (1%)	Roth	2218.2
Fluoromount-G	Southern Biotech	0100-01
Formaldehyde 37%	Merck	1.104.003
Glycine (for analysis)	Merck/Millipore	1042011000
Hydrochloric acid (HCL 37%)	Merck	100317
Kaleidoscope Protein Marker	BioRad	161-0375
Magnesium chloride (MgCl <sub>2</sub> )	Roth	2189.1
Mangan chloride	Sigma	M3634
Methanol p.a.	J.T. Baker	JB8402.2500
Paraformaldehyde (PFA)	Merck	104005
Protein G Agarose	Roche	1243233
PVDF Membrane	Roche/Sigma	3010040001
Restore™ PLUS Western Blot Stripping Buffer	Thermo Scientific	46430
Rotiphorese Gel 30%	Roth	3029.1
SDS Pellets	Roth	CN30.3
Sodium azide	Serva	30175.01
Sodium chloride (NaCl)	Merck	1.064.041.000

---

Name	Source	Catalogue number
Sodium hydroxide pellets (NaOH)	Roth	6771.1
Syn-PER Synaptic Protein Extraction Reagent	Life Technologies	87793
TEMED	Roth	2367.3
Titriplex III (EDTA)	Merck	108418
Tris	Merck	108382
Triton-X 100	Sigma	9002-93-1
Tween20	Sigma	P9416
Vectashield	Vector Laboratories	H-1000

---

## 2.1.6 Compositions

### 2.1.6.1 Cell culture

**Table 2.9: Compositions of solutions and media for cell culture applications**

Component	Stock concentration	Volume / Amount
<i>CHL V79 and HEK293T Culture Medium</i>		
DMEM LOW Glucose	1x	500 ml
Fetal Bovine Serum (FBS)	1x	55 ml
L-Glutamine	200 mM	5 ml
Penicillin/Streptomycin	1000 U/ml	5 ml
<i>Neuron Culture Medium</i>		
Neurobasal Medium	1x	500 ml
B27	50x	10 ml
L-Glutamine	200 mM	1.25 ml
<i>Neuron Culture Coating Solution</i>		
PBS	1x	
Poly-D-Lysine	10 mg/ml	1:50
Laminin	1 mg/ml	1:500
<i>Trypsin Digest Stopping Medium</i>		
DMEM Low Glucose	1x	20 ml
FBS	1x	2 ml
<i>Cell Line Culture Collagen Coating Medium</i>		
Acetic Acid	0.02N	
Collagen I	3.36 mg/ml	1:66

### 2.1.6.2 Biochemistry

Table 2.10: Compositions of solutions for biochemical applications

Component	Stock concentration	Volume or Amount	
<i>10x PBS, pH 7.4</i>		1 l	5 l
NaCl		80 g	400 g
KCl		2 g	10 g
KH <sub>2</sub> PO <sub>4</sub>		2.4 g	12 g
Na <sub>2</sub> HPO <sub>4</sub> x 7 H <sub>2</sub> O		26.8 g	134 g
<i>or</i>			
Na <sub>2</sub> HPO <sub>4</sub> x 2 H <sub>2</sub> O		14.4 g	72 g
ddH <sub>2</sub> O		<i>ad</i> 1000 ml	<i>ad</i> 5000 ml
 <i>PBST</i>			
PBS	1x	1 l	
Tween 20	0.1%	1 ml	
 <i>50x TAE</i>			
Tris		1 l	
EDTA	0.5 M	242 g	
Acetic Acid	100%	100 ml	
ddH <sub>2</sub> O		57.1 ml	
		<i>ad</i> 1000 ml	
 <i>10x DNA Loading Buffer</i>			
Xylene Cyanol		20 ml	
Bromphenolblue		0.25 g	
SDS	10%	0.25 g	
Glycerin		1.25 ml	
ddH <sub>2</sub> O		12.5 ml	
		6.25 ml	
 <i>LB Medium</i>			
Trypton		1 l	
NaCl		10 g	
Yeast Extract		10 g	
ddH <sub>2</sub> O		5 g	
		<i>ad</i> 1000 ml	
 <i>autoclave, then optionally</i>			
Ampicillin	100 mg / ml	1 ml	
Kanamycin	50 mg / ml	1 ml	

Component	Stock concentration	Volume or Amount	
<i>LB Agar Plates</i>		1 l	
Trypton		10 g	
NaCl		10 g	
Yeast Extract		5 g	
AgarAgar		15 g	
ddH <sub>2</sub> O		<i>ad</i> 1000 ml	
<i>autoclave, then optionally</i>			
Ampicillin	100 mg / ml	1 ml	
Kanamycin	50 mg / ml	1 ml	
<i>SDS Stacking Gel Buffer, pH 6.8</i>		200 ml	
Tris pH 6.8		0.5 M	
SDS		0.4%	
<i>SDS Separation Gel Buffer</i>		500 ml	
Tris pH 8.8		1.5 M	
SDS		0.4%	
<i>10x Laemmli Running Buffer</i>		1 l	5 l
Tris		30.3 g	151.5 g
Glycin		144.1 g	720.5 g
SDS pellets		10 g	50 g
<i>or</i>			
SDS Solution	10%	100 ml	500 ml
ddH <sub>2</sub> O		<i>ad</i> 1000 ml	<i>ad</i> 5000 ml
<i>Protein Sample Buffer (4x)</i>			
SDS		8%	
Glycerol		40%	
Tris pH 6.8		0.25 M	
β-Mercaptoethanol		20%	
<i>10x Blotting Buffer</i>		1 l	
Tris		250 mM	
Glycin		1.92 M	
ddH <sub>2</sub> O		<i>ad</i> 1000 ml	

Component	Stock concentration	Volume or Amount
<i>Immunoprecipitation Buffer</i>		
Tris pH 7.4		50 mM
NaCl		100 mM
EDTA pH 8		1 mM
Triton-X		1%
<i>or</i>		
NP-40		0.1%
<i>Bacterial Protein Resuspension Buffer</i>		
Tris pH 7.5		20 mM
NaCl		200 mM
DTT		2 mM
Lysozyme		10 mg/l
DNase I		5 mg/ml
<i>Bacterial Protein Washing Buffer</i>		
Tris pH 7.5		20 mM
NaCl		200 mM
Imidazole		20 mM
DTT		2 mM
<i>Bacterial Protein Elution Buffer</i>		
Tris pH 7.5		20 mM
NaCl		200 mM
DTT		2 mM
Imidazole		400 mM
<i>ITC Buffer</i>		
Tris-HCl pH 7.5		20 mM
NaCl		200 mM
DTT		1 mM
<i>GLOX Buffer</i>		
Tris-HCl pH 8.8		150 mM
Glucose Oxidase		0.25 mg/ml
Glucose		0.5% (v/w)
$\beta$ -Mercaptoethanol		1.5%
Catalase		20 $\mu$ g/ml

Component	Stock concentration	Volume or Amount
<i>dSTORM Buffer</i>		
Glucose	in PBS	10% (v/w)
Glucose Oxidase		0.5 mg/ml
$\beta$ -Mercaptoethanol		100 mM
Catalase		40 mg/ml

## 2.1.7 Software

**Table 2.11: List of software and applications**

Name	Source or reference
Anaconda (Python, R, Jupyter)	Open-Source Distribution <a href="http://www.anaconda.com/">www.anaconda.com/</a>
Arivis Vision 4D	Arivis AG, Munich, Germany
DNA Star Lasergene Suite 12-15	DNASTAR, Inc., Madison, USA
Fiji / ImageJ	Schindelin et al. (2012) Schneider et al. (2012) <a href="http://fiji.sc/Fiji">http://fiji.sc/Fiji</a>
GraphPad Prism	GraphPad Software, Inc., San Diego, USA
L <sup>A</sup> T <sub>E</sub> X	T <sub>E</sub> XLive CTAN <a href="https://ctan.org/">https://ctan.org/</a>
Microsoft Office (Word, Excel, PowerPoint)	Microsoft Corporation, Redmond, USA
Nikon NIS Elements	Nikon Corporation, Tokio, Japan
Python 2.7	Python Software Foundation, USA <a href="http://www.python.org">www.python.org</a>
R 3.1.3	R Development Core Team, R Foundation for Statistical Computing <a href="https://CRAN.R-project.org/">https://CRAN.R-project.org/</a>
ScientiFig (FIJI plugin)	Aigouy and Mirouse (2013) <a href="https://grr.gred-clermont.fr/labmirouse/software">https://grr.gred-clermont.fr/labmirouse/software</a>
ThunderSTORM	Ovesny et al. (2014)

## 2.1.8 Devices

**Table 2.12: List of technical devices and equipment**

Device	Name	Company
Gel Chamber	CRHU15 Midi standard horizontal unit	Bio-Rad
Heated stirring plate	Heat-stirr CB 162	Stuart
Horizontal shaker	Shaker DOS-20S	NeoLab
ImageQuant	LAS4000 Mini	GE
LED Power light source	ZLED CLS 9000	Zett Optics
Multistep Pipet	Multipette <sup>®</sup> stream	Eppendorf
Nanodrop	Spectrophotometer ND-1000	Eppendorf
PCR Machine	Mastercycler gradient	Eppendorf
PCR Machine	PTC-200	MJ Research
pH Meter	Hi 2211 pH/ORP Meter	Hanna instruments
Platform shaker	Polymax 1040	Heidolph
Power supply unit	PowerPac Basic	Bio-Rad
Roller mixer	BTR5-12V	Ratek
SDS PAGE System	Mini-Protean <sup>®</sup> Tetra System	Bio-Rad
Semi-Dry Blot Chamber	Trans-Blot SD Semi-dry transfer cell	Bio-Rad
Speedvac	Concentrator 5301	Eppendorf
Stereo Microscope	SZ2 Series	Olympus
Tabletop centrifuge	Centrifuge 5418 R	Eppendorf
Tabletop centrifuge	Centrifuge 5702 R	Eppendorf
Tabletop centrifuge	Heraeus BioFuge Primo R	Thermo Scientific
Thermo Mixer	ThermoMixer C	Eppendorf
Thermo Mixer	ThermoMixer Compact	Eppendorf
Ultrasonic Processor	UP100H	Hielscher Ultrasound technology
UV Table	UV-Transilluminator Series USDT	Biostep
Vortex	Vortex Genie 2 <sup>™</sup>	Bender & Hobein SG
Water bath	WNB 14	Memmert

## 2.2 Methods

### 2.2.1 Molecular Biology

#### 2.2.1.1 Yeast-Two-Hybrid

A yeast-two-hybrid screen (Hybrigenics ULTimate Y2H) was performed taking advantage of Hybrigenics services (Paris, France). The screen was conducted for the MPP2 PSG module (aa 119-552), as an N-LexA-PSG-C fusion protein, performed on a rat hippocampus library (screen reference number: RHC\_RP1\_hgx4192v1\_pB27). The results presented in Table 3.1 are ordered according to the Predicted Biological Score as assigned by the company and explained in the guide for interpretation provided alongside the results as follows: ‘This score represents the probability of an interaction to be non-specific: it is a value primarily based on the comparison between the number of independent prey fragments found for an interaction and the chance of finding them at random (background noise). The value varies between 0 and 1. Several thresholds have been arbitrarily defined in order to rank the results in 4 categories from A (the highest confidence rank) to D. PBS D generally represents interactions identified through one unique prey fragment or multiple identical ones. It can be interactions hardly detectable by the Y2H technique (low representation of the mRNA in the library, prey folding, prey toxicity in yeast...)’

#### 2.2.1.2 Molecular cloning

Cloning strategies were designed based on plasmid vectors and backbones provided in Table 2.1 on page 23. Primers were designed with desired restriction sites, genetically encoded peptide tags and/or mutations (see Table 2.2 for details) and synthesised by BioTeZ (Berlin, Germany). Utilised template DNAs were either custom generated mouse or rat brain cDNA, human testis library or already existing DNA constructs. The appropriate template-DNA was amplified by PCR with respective primers. Resulting PCR-products and the target vector plasmid were digested with appropriate restriction enzymes and purified using gel electrophoresis and gel extraction kits (Quiagen). Following ligation, chemically competent *E. coli* were transformed and grown on agar plates supplemented with a selection antibiotic. Potential clones were picked and grown as 5 ml cultures, followed by DNA extraction, test digest and sequence validation, eventually. Sequencing was performed by LGC Genomics (Berlin, Germany).

#### 2.2.1.3 Synthesis of custom cDNA

For the cloning of target constructs cDNA was generated from adult mouse and rat brain RNA extracts, which were prepared with Trizol RNA extraction reagent and stored at -80 °C until use. Desired cDNAs were synthesised with Superscript reverse transcriptase and Oligo-dT and pdN6 oligo primers separately according to the protocol below.

**Table 2.13: cDNA synthesis reaction mix**

Component	Volume
Oligo dT primer <i>or</i> pdN6 oligos	1 $\mu$ l
dNTP-Mix (10 mM each)	1 $\mu$ l
RNA	1 $\mu$ l
ddH <sub>2</sub> O	10 $\mu$ l
Incubate at 65 °C for 5 min	
Place on ice and add	
5x first strand buffer	4 $\mu$ l
0.1 M DTT	1 $\mu$ l
RNAse Inhibitor	1 $\mu$ l
Superscript RT III (200 U/ $\mu$ l)	1 $\mu$ l

**Table 2.14: Cycle protocol for cDNA synthesis**

Time	Temperature
5 min	Room temperature
60 min	50 °C
15 min	70 °C
Store at -20 °C	

#### 2.2.1.4 Cloning of target constructs

Polymerase chain reaction was used to amplify DNA fragments from cDNA in order to clone target proteins and to introduce targeted point mutations, genetically encoded peptide tags, and/or insert desired restriction sites using appropriate primer sequences. All constructs were amplified with Phusion<sup>®</sup> High Fidelity DNA Polymerase (New England Biolabs), except for Lin7b constructs, which were cloned with Mango Taq<sup>™</sup> DNA Polymerase (Bioline).

**Table 2.15: PCR reaction mix for cloning from cDNA**

Component	Volume
5x Phusion HF-Buffer <i>or</i> 5x Mango Buffer	10 $\mu$ l
MgCl <sub>2</sub>	1-1.5 $\mu$ l
DMSO	2.5 $\mu$ l
dNTP-Mix (10 $\mu$ M each)	2 $\mu$ l
forward primer (10 $\mu$ M)	2 $\mu$ l
reverse primer (10 $\mu$ M)	2 $\mu$ l
cDNA (oligo dT amplicon)	4 $\mu$ l
cDNA (pdN6 amplicon)	4 $\mu$ l
Phusion Polymerase <i>or</i> Mango Taq Polymerase	0.5 $\mu$ l
ddH <sub>2</sub> O	22.5 $\mu$ l

**Table 2.16: PCR reaction mix for cloning from plasmid template**

Component	Volume
5x Phusion HF-Buffer	10 $\mu$ l
MgCl <sub>2</sub>	1-1.5 $\mu$ l
DMSO	2.5 $\mu$ l
dNTP-Mix (10 $\mu$ M each)	2 $\mu$ l
forward primer (10 $\mu$ M)	2 $\mu$ l
reverse primer (10 $\mu$ M)	2 $\mu$ l
Template DNA (0.05 $\mu$ g/ $\mu$ l)	1 $\mu$ l
Phusion Polymerase	0.5 $\mu$ l
ddH <sub>2</sub> O	32.5 $\mu$ l

**Table 2.17: Cloning PCR cycle**

Stage	Temperature	Time	Cycles
Denaturation	98 °C	30 sec	1
Denaturation	98 °C	10 sec	
Annealing	55-68 °C (primer-dependent)	30 sec	18
Elongation	72 °C	2 min	
Elongation	72 °C	10 min	1
Short term storage	16 °C	∞	

### 2.2.1.5 Agarose gel electrophoresis

PCR products as well as digested amplicons, vectors and plasmids were purified with agarose gel electrophoresis. For a large gel 1-1.5 g agarose were boiled in 1x TAE buffer until entirely dissolved, let cool and poured after addition of 5-10 µl ethidium-bromide, using appropriate combs to create sample pockets. The solid gel was transferred to an electrophoresis chamber filled with 1x TAE buffer. Samples were mixed with DNA loading buffer and run next to a Hyperladder size marker at 120 V until fragments were sufficiently separated, usually for 60-90 min. Separation was checked using a UV-light table.

### 2.2.1.6 Agarose gel DNA extraction

Agarose gels, containing ethidium-bromide to visualise DNA, were placed on a UV-light table and appropriately sized DNA bands were identified in relation to Hyperladder size marker and cut out using a clean scalpel. DNA fragments were then isolated using the Qiagen Gel Extraction kit according to the manufacturer's recommendation. DNA was eluted with 50 µl nuclease-free water and for further cloning steps concentrated for 17 min at 45 °C in a vacuum centrifuge.

### 2.2.1.7 Design and cloning of RNAi vectors

For the generation of an effective and specific shRNA-mediated knock-down of MPP2, multiple candidate RNAi sequences were designed according to the sequence of rat MPP2 (NM\_053513). Taking advantage of several online computational RNAi prediction tools that were freely available at the time (Oligoengine; Dharmacon, now HorizonDiscovery; <http://sirna.wi.mit.edu/>; <https://portals.broadinstitute.org/gpp/public/seq/search>) target sequences that were suggested by at least two tools, each of which relying on a different algorithm, were designed according to the manufacturer's recommendation of the pSUPER RNAi vector system (Oligoengine, see Table 2.2 for selected sequences) with additional BamHI and PacI restriction sites to allow easy transfer into a lentiviral backbone. These oligonucleotides, synthesised by BioTez (Berlin), were then annealed according to the manufacturers' protocol and

cloned into pSUPER vectors. The shRNA sequence that was most efficient in preventing MPP2 expression (see shRNA1 in Table 2.2) was then transferred into a lentiviral vector provided by the Viral Core Facility (VCF, Charité - Universitätsmedizin Berlin) to knock-down endogenous MPP2 in rat hippocampal neurons.

**Table 2.18: Annealing of shRNA oligonucleotides**

Temperature	Time
90 °C	4 min
70 °C	10 min
Step-cool to RT	30 min
Use immediately or store at -20 °C	

#### 2.2.1.8 Restriction digest

Either 1 µg of purified plasmid DNA in 20 µl nuclease-free water or 20 µl of concentrated agarose gel-extraction of PCR product were digested with 2 µl 10x FastDigest Buffer (Thermo Scientific™) using 0.7 µl of the desired FastDigest restriction enzymes at 37 °C for 1 hour. Subsequent agarose gel electrophoresis and gel extraction was used to isolate resulting DNA fragments of the desired size.

#### 2.2.1.9 Ligation

To ligate appropriately digested inserts of interest with desired backbones, 2 µl vector were mixed with 15 µl insert, 2 µl 10x T4-Ligation buffer and 1 U T4-Ligase. Ligation mix was incubated over night at 16 °C and eventually transformed into chemically competent *E. coli* TOP10 cells.

#### 2.2.1.10 Chemically competent *E. coli*

To generate chemically competent bacteria for cloning and plasmid replication, 5 µl *E. coli* were diluted in 1 ml LB medium. Of this dilution 15-20 µl were streaked out on an LB agar plate without any antibiotic and grown over night at 37 °C. A single colony was picked and grown as starter culture over night. Then, 4 ml of this starter culture were used to inoculate 200 ml LB medium. This was grown at 37 °C in a shaking incubator for approximately 3 hrs until an optical density (OD) of 0.4-0.6 was reached. Working in a cold room the culture was then divided among four tubes and centrifuged for 15 min at 4000 rpm (~2600 rcf) and 4 °C. The resulting pellets were resuspended in 20 ml sterile 100 mM CaCl<sub>2</sub> each. After the resuspensions were pooled into two tubes, they were centrifuged again for 15 min at 4000 rpm (~2600 rcf) and 4 °C. The two resulting pellets were resuspended in 25 ml sterile 100 mM CaCl<sub>2</sub> each

and incubated on ice for 1 hr. Finally, the suspension was pelleted again for 15 min at 4000 rpm (~2600 rcf) and 4 °C and cell pellets were resuspended in a total volume of 13 ml sterile 85 mM CaCl<sub>2</sub> with 15% Glycerol. The final mixture was aliquoted into pre-chilled reaction tubes and snap frozen in liquid nitrogen. Chemically competent cells were stored at -80 °C until use.

#### **2.2.1.11 Transformation of chemically competent *E. coli***

Either 1 µg purified plasmid DNA or 20 µl ligation mixture after incubation was added to 50 µl chemically competent *E. coli* TOP10 cells. The cells were then incubated on ice for at least 20 min. Cells were transformed with a 90 sec heat shock at 42 °C, followed by addition of 1 ml LB medium and incubation at 37 °C for one hour. Transformed ligations were centrifuged for 3 min at 2000 rpm (~1300 rcf) and the pellet resuspended in 20 µl LB medium, which was subsequently streaked onto LB agar plates containing the appropriate selective antibiotic to select for successfully transformed bacteria, and grown over night at 37 °C.

#### **2.2.1.12 Plasmid purification**

Chemically competent *E. coli* TOP10 cells were transformed as described above and grown over night. A single colony was then picked and grown in LB medium (either 5 ml overnight for cloning or 5 ml for six hours as starter culture for a 200 ml culture over night). Bacteria cultures were pelleted by centrifugation (4000 rpm/~2600 rcf, 15 min, 4 °C) and stored at -20 °C until plasmid purification. Plasmids were isolated using Qiagen Plasmid Prep Mini and Maxi kits, respectively, according to the manufacturer's recommendation. The DNA pellets were resuspended in sterile, nucleic-free H<sub>2</sub>O and the concentration determined using a Nanodrop spectrophotometer (ND-1000, Eppendorf).

### **2.2.2 Cell Biological Techniques**

#### **2.2.2.1 Preparation of coverslips**

In order to grow different types of cells on glass coverslips to subject them to later immunofluorescence analysis, these coverslips need to be prepared. For confocal microscopy, Ø 18 mm class coverslips were dipped in 100% ethanol absolute and flame sterilised before being placed in 12-well plates. For super-resolution applications, high precision coverslips (22x22 mm and Ø 25 mm) were cleaned in 1 M HCl for one hour, followed by three washes with ddH<sub>2</sub>O, one hour in 100% acetone and three washes with ddH<sub>2</sub>O prior to one hour each in 70% and 100% ethanol. All steps were performed at room temperature. To cultivate primary neurons, coverslips were coated with a Laminin (final concentration 2 µg/ml) and Poly-D-Lysine (final concentration 0.2 mg/ml) in PBS over night at 4 °C. For heterologous cells coverslips were coated with

50 µg/ml Collagen-I solution in 0.02 N acetic acid for two hours at room temperature, followed by three washes with sterile PBS prior to plating.

### **2.2.2.2 Cell culture and protein expression**

CHL V79 and HEK293T cells were maintained in DMEM (Lonza/Sigma) supplemented with 10% FBS (Sigma), 2 mM L-glutamine and 1% penicillin/streptomycin at 37 °C with 5% CO<sub>2</sub>. Cells were passaged (CHL V79 1:10-1:40 and HEK293T 1:5-1:20) after 7 min trypsin digest (2.5% Trypsin-EDTA, LONZA) and seeded at 5x10<sup>4</sup>/6-well, 2.5x10<sup>4</sup>/12-well, or 10<sup>6</sup>/75 cm<sup>2</sup> flask (T75, TPP) as determined using a Millipore cell sceptor with a 60 µm sensor tip. Transient transfection was performed with Lipofectamine 2000<sup>TM</sup> (Invitrogen) according to manufacturer's recommendation. In brief, required amounts of DNA and 1 µl/12-well or 14 µl/T75 were pre-diluted in 100 µl/12-well or 750 µl/T75 in serum-free Opti-MEM (Lonza), incubated for 5 min and mixed, followed by 20 min incubation at room temperature. The culture medium volume was adjusted to 400 µl/12-well or 4 ml/T75 before adding the DNA/Lipofectamine mix. Transfected cells were either fixed or harvested 18-24 hours after transfection and subjected to further experiments.

### **2.2.2.3 Primary rat hippocampal neuronal cultures**

All animal protocols were approved by the 'Landesamt für Gesundheit und Soziales' (LaGeSo; Regional Office for Health and Social Affairs) and animals reported permit number T0280/10).

Adult wild-type Wistar rats at embryonic stage E18 were subjected to anaesthesia with isoflurane (Forene<sup>®</sup>) and sacrificed by decapitation. The uterus was removed and placed in sterile PBS (Lonza). Embryos were removed from uterus, freed of amniotic membranes and the heads cut off with fine scissors. In a separate dish with sterile PBS, the heads were briefly washed off blood and drained before transfer to a sterile dish. While the head was held firmly with fine ridged tweezers, the skull was opened by puncture with sharp tweezers approximately posterior of the Lambda point. The skull was then opened and the brain carefully extracted and placed in a drop of ice-cold DMEM (Lonza/Sigma). Using fine tweezers and a micro-scalpel, the two brain hemispheres were separated. With gentle separation of cortex and midbrain, the hippocampal formation is exposed and extracted using tweezers and a micro-scalpel. After careful removal of any remaining meninges, the hippocampi were collected in ice-cold DMEM. The collected hippocampi were centrifuged (3 min, 300 rpm/10 rcf, RT) and supernatant removed. Tissue digest was performed by adding 5 ml 2.5% Trypsin-EDTA Solution and incubation in a 37 °C water bath for 4:30 min and periodic shaking. Tissue digest was stopped with the addition of 20 ml cold DMEM (Lonza/Sigma) with 10% FBS (Biochrom). Hippocampi were then washed twice with cold DMEM and centrifugation. Next, the hippocampi were taken up in 2 ml pre-warmed, pH-adjusted neuron culture medium (Neurobasal, supplemented with B27 and 0.5 mM L-glutamine).

With firm pressure towards the tube, slowly pipetting the solution three to five strokes created shear-forces to dissociate the tissue to yield a cell suspension. Depending on the amount of prepped hippocampi, the volume was then adjusted to 15-20 ml with pre-warmed and pH-adjusted neuron culture medium and cell density was counted with 1:10 dilution in PBS, using a Millipore Cell Counter Sceptre and 60 µm sensor tips. Neurons were plated at desired density ( $1.5\text{-}2.5 \times 10^5$  cells per well) in pre-warmed and pH-adjusted neuron culture medium onto wells and coverslips previously coated with 1:50 Poly-D-Lysine (10 mg/ml, Sigma) and 1:500 Laminin (1 mg/ml, Sigma) in PBS. Except for infections and live cell imaging purposes, the neurons were left undisturbed typically until 21-22 *days in vitro* (DIV 21-22).

#### **2.2.2.4 Lentivirus-mediated knock-down and gene delivery and expression**

Lentivirus-mediated gene transfer and knock-down was realised with lentivirus particles generated by the Viral Core Facility (VCF). The underlying constructs were generated by sub-cloning from mammalian expression vectors into lentiviral backbones provided by the VCF. Cultured hippocampal neurons were infected at DIV 3 and 10 with Knock-down/Scrb1 or expression vectors, respectively, unless indicated otherwise.

### **2.2.3 Biochemical Techniques**

#### **2.2.3.1 Tissue and whole cell lysates**

Adult Wistar rats were anaesthetised with isoflurane and sacrificed by decapitation. Brains were removed, rinsed with ice-cold PBS and dissected into desired brain regions (olfactory bulbs, cortex, hippocampus, cerebellum and brainstem) with a scalpel. Isolated regions were then finely minced and lysed in SDS sample buffer (1 ml per 1 g tissue). Cultured primary neurons and CHL V79 cells were lysed in SDS sample buffer (100 µl per well of a 12-well plate). Lysates were then treated with three ultrasonic pulses (0.7 cycle, 0.7 amplitude), boiled for 5 min and centrifuged (10 min, 14k rpm/20k rcf, RT) before loading the supernatant on an SDS PAGE gel.

#### **2.2.3.2 Crude synaptosomal fraction preparation**

Adult Wistar rats were anaesthetised with isoflurane and sacrificed by decapitation. Brains were removed, rinsed with ice-cold PBS and immediately frozen and stored at -80 °C until use. Tissue was thawed on ice, roughly minced with a scalpel and homogenised in 10 ml/1 g Tissue Syn-PER Synaptic Protein Extraction Reagent (Thermo Science) according to the manufacturer's recommendation. For co-IP experiments, the crude synaptosome fraction was resuspended in 10 ml immunoprecipitation buffer (50 mM Tris pH 7.4; 100 mM NaCl; 1 mM EDTA, 1% Triton-X; supplemented with Complete Mini protease inhibitors (Roche) and cleared by 3x centrifugation at 20k rpm. In GST pull-down experiments the pellet was solubilised in 10 ml 1% Triton-X/PBS.

### 2.2.3.3 Co-immunoprecipitation

CHL V79 and HEK293T cells were plated at  $10^6$  cells/75 cm<sup>2</sup> and transfected as described before. Transiently transfected cells were harvested 18-20 hrs after transfection with a cell scraper and collected in PBS. Following centrifugation (1200 rpm/230 rcf, 7 min, RT) pellets were lysed with 7 strokes using a 30G syringe needle in immunoprecipitation buffer (50 mM Tris pH 7.4; 100 mM NaCl; 1 mM EDTA, 1% Triton-X or 0.1% NP-40; supplemented with Complete Mini protease inhibitors, Roche) and briefly incubated on ice. Lysates were then cleared by three centrifugations (each 10 min, 20k rcf, 4 °C). Supernatants were then incubated under gentle agitation for 3 hrs with 2-3 µg of appropriate antibodies and respective normal IgGs as negative control. Pull-down was performed with 30 µg protein G agarose beads (or streptavidin-coupled beads for biotin-coupled antibodies) slurry (Roche) for 1 hr at 4 °C, followed by three washes with IP buffer prior to analysis by Western blot.

### 2.2.3.4 SDS PAGE

All protein samples were separated by electrophoresis on 10% SDS-polyacrylamide gels using the Mini-Protean<sup>®</sup> Tetra System (BioRad). Separation gels were cast between glass plates with 1 mm spacers and overlaid with isopropanol to ensure an even and bubble-free surface until fully polymerised. Isopropanol was then thoroughly removed with ddH<sub>2</sub>O and remaining water carefully removed with strips of filter paper without disturbing the gel. Next, the stacking gel (optionally stained with bromphenolblue) was cast and, after adding an appropriate comb to create sample pockets, left to polymerise for no more than 10 min. Combs were then removed and pockets rinsed with ddH<sub>2</sub>O and 1x Laemmli-running Buffer to remove any unpolymerised gel. Whole cell lysates were prepared by lysing cells in 200 µl per 12-well or 300 µl per 6-well, followed by sonication (3x, 0.7 cycle, 0.7 amplitude). Samples were boiled in SDS PAGE Sample Buffer for 5 min at 95 °C, followed by centrifugation (1 min, 20k rcf, RT). Samples were loaded next to Kaleidoscope size marker (BioRad) and run at 50 V until all sample entered the collection gel, followed by running 100-130 V until the desired separation, indicated by the coloured size marker, was achieved.

**Table 2.19: SDS PAGE gel**

Component	Collection Gel 5% (2 ml)	Separation Gel 10% (6 ml)
ddH <sub>2</sub> O	1.38 ml	2.46 ml
Rotiphorese 30% Acryl/Bis-acrylamid -Mix	0.34 ml	1.98 ml
Collection Gel Buffer	0.25 ml	-
Separation Gel Buffer	-	1.5 ml
TEMED	2 µl	2.4 µl
APS 10%	20 µl	60 µl

### 2.2.3.5 Western blot

For specific protein detection, SDS PAGE gels were subjected to semi-dry Western blotting. SDS PAGE gels were rinsed with water to remove SDS-running buffer and then incubated in 1x blotting buffer for 5-10 min under gentle agitation. PVDF membrane were briefly rinsed with methanol and then incubated in 1x blotting buffer for 5-10 min under gentle agitation. Thick blotting paper (VWR type 707) was adjusted in size to be slightly smaller than the target PVDF membrane. Blotting paper was soaked in 1x blotting buffer and blot-sandwich assembled (bottom – blotting paper, membrane, SDS PAGE gel, blotting paper – top). The blot-sandwich was then carefully milled to remove any air trapped between gel and membrane and excess buffer removed. Western blots were run at 20 W for 1 hr. After blotting the stained Kaleidoscope, size labels were marked and membranes blocked with 5% milk/PBST for at least 1 hour, prior to incubation with primary antibodies in blocking solution over night at 4 °C under constant agitation. Subsequently, membranes were washed three times with PBST and incubated with secondary horseradish peroxidase-coupled (HRP) antibody in blocking solution for 1 hour at room temperature. HRP-signals were detected using Western Lightning chemiluminescent substrates (Perkin Elmer) with a luminescent image analyser (ImageQuant LAS4000, GE Healthcare).

### 2.2.3.6 Immunofluorescence staining

Heterologous cells were fixed with 4% PFA/PBS for 10 min at room temperature after removal of the cell culture medium. Following fixation, cells were washed once with PBS and stored at 4 °C until staining, not longer than two weeks. Primary rat hippocampal neurons were fixed at DIV 21 with 4% PFA/PBS for 10 min at RT, washed thrice for 10 min with PBS, followed by 45 min quenching at RT with 50 mM NH<sub>4</sub>Cl to reduce auto-fluorescence. After washing with PBS, cells were permeabilised with 0.2% Triton-X/PBS for 5 min and washed with PBS. For *d*STORM microscopy, cells were additionally treated with Image-IT Signal Enhancer (Thermo Fisher) for 30 min at RT and three washes with PBS. Cells were then blocked for at least 1 hour at RT with blocking solution (4% BSA/PBST). Primary antibodies were diluted 1:250 in blocking solution (1:500 for confocal microscopy) and incubated over night at 4 °C, followed by incubation with desired secondary antibodies at 1:1000 dilution in blocking solution for 1 hr at RT and for *d*STORM custom-labelled secondary antibodies at 1 µg/ml (~7 nM) in blocking solution for 20 min, followed by post-fixation and quenching as above. After final washing with PBS, coverslips were mounted with Fluoromount-G (SBA) or Vectashield (H1000, Vector Laboratories) for confocal and 3D-SIM imaging, respectively. For triple-colour *d*STORM imaging, primary hippocampal rat neurons (DIV 21) were stained for the postsynaptic proteins Homer1 as PSD marker, MPP2 and GABA<sub>A</sub>R α1 with respective primary antibodies as described above. Samples were then incubated with appropriate secondary antibody Fab fragments coupled to Alexa Fluor 647 (goat αMouse AF647, A21236, Invitrogen, USA), CF 680

(goat  $\alpha$ Rabbit, custom labelled 111-007-008, Jackson Immuno Research) or CF 568 (goat  $\alpha$ Guinea pig, custom labelled 106-007-008, Jackson Immuno Research) for 1 hour at room temperature, followed by washes and application of fluorescent beads (100 nm, TetraSpeck<sup>TM</sup>, Life Technologies, USA), 1:200 in 0.01% PLL/PBS. Parts of this section of Material and Methods have been published as preprint (Schmerl et al., 2020).

### 2.2.3.7 Custom labelling of primary antibodies

Labelling of secondary antibodies for *d*STORM imaging were performed in collaboration with Jakob Rentsch, AG Ewers (Freie Universität Berlin) and Dr. Niclas Gimber, AG Schmoranzler (AMBIO, Charité - Universitätsmedizin Berlin).

For dual-colour *d*STORM imaging, secondary antibodies (goat  $\alpha$ Rabbit, 111-005-003, AffiniPure or donkey  $\alpha$ Mouse, 715-005-151, AffiniPure) were diluted 1:10 in labelling buffer (0.2 M NaHCO<sub>3</sub>, pH 8.3). Cy3b NHS Ester (PA63101, Life Sciences) was added to the diluted antibodies in 10-fold molar excess. The samples were incubated for 1 hour at room temperature. To stop the reaction, 100 mM Tris pH 8.0 was added. Zebra spin desalting columns (8989, ThermoFisher) were equilibrated with PBS. The samples were added to the column and centrifuged at 1000 rcf for 2 min. The filtrate was added to a second column and centrifuged at 1000 rcf for 2 min. For triple-colour *d*STORM imaging, CF 680 and CF 658 secondary antibodies were generated by incubating 100  $\mu$ g IgG Fab fragments dissolved in NaHCO<sub>3</sub> (50 mM, pH 8.1) with a five-fold excess of succinimidyl esters of fluorescent dye CF 680 or CF 568 dyes (Biotium, USA) in DMSO (10  $\mu$ M) for 1 hour at room temperature under gentle agitation. Unbound dye was removed with Nap-5 Sephadex G 25 columns (GE Healthcare, UK) and labelled antibody eluted from the column with PBS. This section of Material and Methods has been published as preprint (Schmerl et al., 2020).

### 2.2.3.8 Bacterial protein expression and purification

Bacterial protein expression and purification for ITC measurements was performed in collaboration with Jennifer Lardong, AG Wahl (Freie Universität Berlin).

Protein expression was conducted using chemically competent *E. coli* Rosetta cells. The cells were grown in auto-induction ZY medium with kanamycin and chloramphenicol for 5 hrs at 37 °C. The temperature was then decreased to 18 °C and the cells were grown overnight. The cells were harvested by centrifugation and the cell pellet was resuspended in resuspension buffer (200 mM NaCl, 20 mM Tris pH 7.5, 2 mM DTT, 10 mg/l lysozyme, 5 mg/l DNase I) and subsequently lysed by sonication for 15 min. The lysate was cleared at 56k rcf for 45 min and the supernatant was applied to affinity chromatography using a column packed with 2 ml Ni-NTA agarose (NEB). The average incubation time was 1 hour. Two washing steps were then performed using 25 ml washing buffer (200 mM NaCl, 20 mM Tris pH 7.5, 20 mM imidazole, 2 mM DTT) for each step. For elution, the Ni-NTA agarose was incubated with

20 ml elution buffer (200 mM NaCl, 20 mM Tris pH 7.5, 400 mM imidazole, 2 mM DTT) for 15 min. The eluted constructs were purified using a Superdex 75 16/60 column (GE Healthcare). The protein-containing fractions were pooled and concentrated using a 30 kDa molecular-weight cut-off concentrator (Millipore). The progress of protein purification was monitored by SDS-PAGE. Protein concentrations were determined by UV absorption with extinction coefficients  $\epsilon_{\text{MPP2}} = 52830/\text{mol}\cdot\text{cm}$  and  $\epsilon_{\text{mCherry-SynCAM1}} = 35870/\text{mol}\cdot\text{cm}$ , respectively. This section of Material and Methods has been published (Rademacher\*, Schmerl\*, et al., 2016).

### 2.2.3.9 Isothermal titration calorimetry

Isothermal titration calorimetry (ITC) experiments were performed in collaboration with Jennifer Lardong, AG Wahl (Freie Universität Berlin).

ITC experiments were performed on an ITC200 microcalorimeter (Malvern Instruments Ltd., United Kingdom) at 25 °C with constant stirring at 500 rpm and a buffer containing 200 mM NaCl, 20 mM Tris-HCl (pH 7.5) and 1 mM DTT. Each experiment comprised a 0.5  $\mu\text{l}$  initial injection, followed by fifteen 2.5  $\mu\text{l}$  injections every 150 sec. The cell contained 55  $\mu\text{M}$  of the MPP2 PSG module, and 350  $\mu\text{M}$  of mCherry-tagged SynCAM1 peptide or mCherry-tagged mutated SynCAM1 peptide were titrated into the MPP2 PSG solution. Control experiments were carried out titrating mCherry-tagged peptide into ITC buffer under otherwise identical conditions. No heat exchange was detected in the control experiments, confirming that there was appropriate match of buffer conditions with no indication of dilution effects. The thermodynamic parameters were determined using ORIGIN software (v7.0, Microcal) and fitted by nonlinear least square analysis using a single-site binding model. This section of Material and Methods has been published (Rademacher\*, Schmerl\*, et al., 2016).

### 2.2.3.10 GST-pull-down

GST-pull-down experiments were conducted in collaboration with Dr. Nils Rademacher, AG Shoichet (Charité - Universitätsmedizin Berlin).

GST-SH3-GK domain constructs of PSD-95 and MPP2 were expressed in *E. coli* BL21 DE3 and purified according to the manufacturer's manual (GST Gene Fusion System, GE Healthcare). Per pulldown, 30  $\mu\text{l}$  of glutathione agarose (Pierce) was loaded with GST-SH3-GK proteins (PSD-95 and MPP2) and incubated for 3 hrs with protein lysate from crude synaptosomes. The beads were washed three times with PBS/1% Triton-X-100 and eluted from the matrix by incubation with SDS sample buffer for 5 min at 95 °C. This section of Material and Methods has been published as preprint (Schmerl et al., 2020).

### 2.2.3.11 Sample preparation and liquid chromatography-mass spectrometry (LC-MS)

Proteomics experiments and analysis were conducted in collaboration with Dr. Benno Kuroopka, AG Freund (Freie Universität Berlin).

Proteins from two technical replicates were separated by SDS PAGE (10% Tricine SDS PAGE). Coomassie-stained lanes were cut into 12 slices and in-gel protein digestion and  $^{16}\text{O}/^{18}\text{O}$ -labelling was performed as described previously (Kristiansen et al., 2008; Lange et al., 2010). In brief, corresponding samples (PSD-95 and MPP2) were incubated overnight at 37 °C with 50 ng trypsin (sequencing grade modified, Promega) in 25  $\mu\text{l}$  of 50 mM ammonium bicarbonate in the presence of heavy water (Campro Scientific GmbH, 97%  $^{18}\text{O}$ ) and regular  $^{16}\text{O}$ -water, respectively. Isotope-labels were switched between the two replicates. To prevent oxygen back-exchange by residual trypsin activity, samples were heated at 95 °C for 20 min. After cooling down, 50  $\mu\text{l}$  of 0.5% trifluoroacetic acid (TFA) in acetonitrile was added to decrease the pH of the sample from  $\sim\text{pH}$  8 to  $\sim\text{pH}$  2. Afterwards, corresponding heavy- and light-isotope labelled samples were combined and peptides were dried under vacuum. Peptides were reconstituted in 10  $\mu\text{l}$  of 0.05% TFA, 2% acetonitrile in water, and 6.5  $\mu\text{l}$  were analysed by a reversed-phase nano liquid chromatography system (Ultimate 3000, Thermo Scientific) connected to an Orbitrap Velos mass spectrometer (Thermo Scientific). Samples were injected and concentrated on a trap column (PepMap100 C18, 3  $\mu\text{m}$ , 100  $\text{\AA}$ , 75  $\mu\text{m}$  i.d. x 2 cm, Thermo Scientific) equilibrated with 0.05% TFA, 2% acetonitrile in water. After switching the trap column inline, LC separations were performed on a capillary column (Acclaim PepMap100 C18, 2  $\mu\text{m}$ , 100  $\text{\AA}$ , 75  $\mu\text{m}$  i.d. x 25 cm, Thermo Scientific) at an eluent flow rate of 300 nl/min. Mobile phase A contained 0.1% formic acid in water, and mobile phase B contained 0.1% formic acid in acetonitrile. The column was pre-equilibrated with 3% mobile phase B followed by an increase of 3–50% mobile phase B in 50 min. Mass spectra were acquired in a data-dependent mode using a single MS survey scan ( $m/z$  350–1500) with a resolution of 60,000 in the Orbitrap, and MS/MS scans of the 20 most intense precursor ions in the linear trap quadrupole. The dynamic exclusion time was set to 60 sec and automatic gain control was set to  $1 \times 10^6$  and 5,000 for Orbitrap-MS and LTQ-MS/MS scans, respectively. This section of Material and Methods has been published as preprint (Schmerl et al., 2020).

### 2.2.3.12 Proteomic data analysis

Proteomics experiments and analysis were conducted in collaboration with Dr. Benno Kuroopka, AG Freund (Freie Universität Berlin).

Identification and quantification of  $^{16}\text{O}/^{18}\text{O}$ -labelled samples was performed using the Mascot Distiller Quantitation Toolbox (version 2.7.1.0, Matrix Science).

Data were matched against the SwissProt protein sequence database using the taxonomy rattus (August 2017 release with 7996 protein sequences). Sequences of the employed protein constructs and the sequence of the GST tag were manually added to the database. A maximum of two missed cleavages was tolerated and the mass tolerance of precursor and fragment ions was set to 15 ppm and 0.35 Da, respectively. Methionine oxidation, acetylation (protein N-terminus), propionamide (Cysteine), and C-terminal  $^{18}\text{O}_1$ - and  $^{18}\text{O}_2$ -isotope labelling were used as variable modifications. A significance threshold of 0.05 at the peptide level was used based on decoy database searches. At the protein level, a minimum of two quantified peptides was set as a threshold. Protein ratios were calculated from the intensity-weighted average of all corresponding peptide ratios. The protein ratio of GST was used for normalisation of protein ratios. Only proteins that were quantified in both replicates with a geometric standard deviation of  $<2$  were considered. Known contaminants (e.g. keratins) and the bait proteins were removed from the protein output table. This section of Material and Methods has been published as preprint (Schmerl et al., 2020).

## **2.2.4 Imaging**

### **2.2.4.1 Confocal imaging**

Cells were fixed and stained as described above and imaged with a Leica TCS SP5 II confocal laser scanning microscope run with LAS AF X scan software (Leica Microsystems, Wetzlar, Germany). Image stacks were acquired with a 63x oil immersion objective and standard emission filters at 2x zoom for overviews and 5x zoom for details at 2048x2048 px as 5-7 planes with 0.4  $\mu\text{m}$  step size in Z. Image analysis was performed in FiJi/ImageJ (Schindelin et al., 2012; Schneider et al., 2012).

Additionally, cells were fixed and stained as described above and imaged with a Nikon A1Rsi+ confocal laser scanning microscope run with NIS Elements scan software. Image stacks were acquired with a 60x 1.4 N.A. oil immersion objective, an additional 1.5x optovar lens (Nikon) and standard emission filters at 1.8x zoom at 1024x1024 px as 12 planes with 0.175  $\mu\text{m}$  step size in Z. Image analysis was performed in Fiji/ImageJ (Schindelin et al., 2012; Schneider et al., 2012). Four-colour confocal images were maximum projected and subjected to further analysis. Parts of this section of Material and Methods have been published as preprint (Schmerl et al., 2020).

### **2.2.4.2 Structured-illumination microscopy imaging**

SIM imaging was performed in collaboration with Dr. Niclas Gimber, AG Schmoranzer (AMBIO, Charité - Universitätsmedizin Berlin).

Targets were selected based on the SynCAM1 signal. Three-dimensional SIM images were acquired with the OMX V4 Blaze system (GE Healthcare), using the 405 nm, 488 nm, 568 nm and 647 nm laser lines, a 60x 1.42 N.A. oil objective (Olympus), an immersion oil with a refractive index of 1.518 and standard emission filters at 125 nm z-sectioning. Multi-colour registration with an error below 40 nm was done using 100 nm fluorescent beads (TetraSpeck™, T7284, Thermo Scientific). Images were acquired with the DeltaVision OMX acquisition software (GE Healthcare) and images were reconstructed with softWoRx (GE Healthcare). Parameters for the reconstruction can be found in the supplements (File S1) in Schmerl et al. (2020). The quality of 3D-SIM reconstructions was tested with SIMcheck (Ball et al., 2015). The super-resolution channels 642, 568 and 488 show a good signal-to-noise ratio and no signs of hexagonal artefacts. Fast Fourier transformed images uncover a high amount of information below the diffraction limit. Due to the limited brightness and stability of the Alexa Fluor 405 dye, the signal-to-noise ratio and resolution in the 405 nm channel were limited. We thus decided to use this channel only for vGlut1 as a reference for the segmentation of mature synapses and not as a structural super-resolution readout. This section of Material and Methods has been published as preprint (Schmerl et al., 2020).

#### **2.2.4.3 Dual-colour dSTORM imaging**

STORM imaging was performed in collaboration with Jakob Rentsch, AG Ewers (Freie Universität Berlin).

All samples were imaged using a Vutara 352 super-resolution microscope (Bruker) equipped with a Hamamatsu ORCA Flash4.0 sCMOS camera for super-resolution imaging and a 60x oil immersion TIRF objective with a numerical aperture of 1.49 (Olympus). Immersion Oil 23 °C (#1261, Cargille) was used. Samples were mounted onto the microscope in GLOX buffer (1.5%  $\beta$ -mercaptoethanol, 0.5% (v/w) glucose, 0.25 mg/ml glucose oxidase and 20  $\mu$ g/ml catalase, 150 mM Tris-HCl pH 8.8), illumination at a laser-power density of 5.5 kW/cm<sup>2</sup> using a 637 nm laser for Alexa Fluor 647 or a 561 nm laser at a laser-power density of 4.6 kW/cm<sup>2</sup> for Cy3b. Images were collected with 20 ms acquisition time. Per probe (Cy3b or Alexa Fluor 647), 10,000 frames were acquired. Acquired raw data were localised using SRX (Bruker). Localisations were estimated by fitting single emitters to a 3D experimentally determined point spread function (PSF) under optimisation of maximum likelihood. The maximum number of localisation iterations performed before a given non-converging localisation was discarded was set to 40. PSFs were interpolated using the B-spline method. Obtained localisations were filtered according to precision estimates based on the Thompson method (Thompson et al., 2002), i.e. all localisations with localisation precision worse than 20 nm were excluded. Localisations were rendered as Gaussian distri-

butions with a constant width of 20 nm. Alignment of colour channels and drift correction were performed in SRX using Tetraspeck<sup>TM</sup> beads (Thermo Scientific, T7279). In total, *d*STORM images from 2-4 independent experiments (2 for SynCAM1/PSD-95; 3 for MPP2/PSD-95; 4 for SynCAM1/MPP2) were acquired. Individual synapse panels were prepared using the ScientiFig Plugin for Fiji/ImageJ (Aigouy and Mirouse, 2013). This section of Material and Methods has been published as preprint (Schmerl et al., 2020).

#### 2.2.4.4 Triple-colour *d*STORM imaging

STORM imaging was performed in collaboration with Dr. Niclas Gimber, AG Schmoranzler (AMBIO, Charité - Universitätsmedizin Berlin).

Triple-colour *d*STORM images were generated by using two channels acquired in SD-*d*STORM mode (simultaneous excitation at 642 nm of Alexa Fluor 647 (Invitrogen, USA) and CF 680 (Biotium, USA) Lampe et al., 2015; Lehmann et al., 2016) and an additional channel (CF 568 (Biotium, USA)) acquired in conventional *d*STORM mode. The spectral de-mixing (SD-) mode has the advantage of being inherently free of any registration errors. The *d*STORM channel was registered toward the SD-*d*STORM channels using bead-based registration (100 nm, TetraSpeck<sup>TM</sup>, Invitrogen). Samples were imaged with the N-STORM super-resolution setup (Nikon Instruments) controlled by NIS-Elements (Nikon) and equipped with a sCMOS camera (Prime 95B, Photometrics), a 100x oil-immersion objective (NA 1.49; Nikon), an additional 1.5x optovar lens (Nikon) and an emission splitter (OptoSplit III; Cairn Research, UK) in the emission path for the SD-mode. The emission splitter was equipped with a dichroic mirror (700-DCXXR; AHF Analysentechnik, Germany) for spectral demixing of AF 647 and CF 680. An autofocus system (PerfectFocus II; Nikon) was used to prevent focal drift. Lateral drift was minimised by stabilising the temperature at 26 °C with an incubator (Okolab, Italy) and corrected using immobilised beads (100 nm, Tetraspeck<sup>TM</sup>, Invitrogen) as fiduciary marks. Samples were mounted in *d*STORM imaging buffer: 0.5 mg/ml glucose oxidase (Sigma-Aldrich, USA), 40 mg/ml catalase (Roche, Switzerland), 10% (w/v) glucose, 100 mM MEA ( $\beta$ -mercaptoethylamine; Sigma-Aldrich, USA) in PBS. Samples were illuminated with a 642 nm laser diode at about 3.5 kW/cm<sup>2</sup> for the SD-mode and with a 561 nm laser at 1.2 kW/cm<sup>2</sup> for the *d*STORM-mode. Typically, 15,000 frames with an exposure time of 30 ms for all channels were recorded.

## 2.2.5 Image Analysis

### 2.2.5.1 Manual assessment of MPP2-positive neurons in primary cultures

Overview images were acquired with a 20x objective and analysed manually. The frequency of neurons (as DAPI and MAP2 double-positive cells) with Homer1 staining or MPP2 staining, assessable at this low magnification, was determined. For analysis, cell numbers were counted individually for every marker together with DAPI, to exclude background and unspecifically stained structures. At first, cells positive for MAP2 and DAPI were counted, then the displayed channels were changed to DAPI and Homer1 or DAPI and MPP2, respectively, and again double-positive cells were counted. Finally, the fraction of cells positive MAP2 and DAPI, which were also positive for Homer1 and DAPI or MPP2 and DAPI, respectively, was calculated.

### 2.2.5.2 Quantification of MPP2- and GABA<sub>A</sub>R $\alpha$ 1-positive Homer1 spines

Image analysis was performed with a custom written FIJI/ImageJ script available at Github: <https://github.com/BettinaSchmerl/MPP2>). For segmentation and skeletonisation of dendritic branches labelled with MAP2, maximum projections of confocal images were subjected to Otsu's threshold clustering algorithm, followed by Gaussian blur, binarisation and skeletonisation. For analysis of the fraction of Homer1 spines positive for both proteins of interest, MPP2 and GABA<sub>A</sub>R  $\alpha$ 1, channels were filtered (Mean filter, 1.5 radius), punctate structures identified with histogram-based threshold procedures (Otsu's, Yen's and the RenyiEntropy methods), followed by Gaussian blur (sigma = 1.5) and counted with the build-in 'Find Maxima' tool of FIJI/ImageJ. To ensure analysis of only synapses fully enclosed by the image stack, only puncta within a 2  $\mu$ m periphery to a MAP2 dendrite skeleton were considered for further analysis. In order to select spines with immunostaining of MPP2 and GABA<sub>A</sub>R  $\alpha$ 1 proteins, those point selections were enlarged by 0.5  $\mu$ m and checked for co-occurrence of identified puncta within that perimeter, covering an average synaptic spine area. Fractions of Homer1-positive spines per image having also MPP2 and GABA<sub>A</sub>R  $\alpha$ 1 signal were calculated based on the overall count of Homer1-positive spines per image.

### 2.2.5.3 Manual analysis of dual-colour *d*STORM data

To assess the frequency and dimensions of the described bracelet-like arrangement of SynCAM1 and MPP2 clusters at the periphery of PSDs, synapses were matched manually from corresponding widefield and *d*STORM images based on the staining pattern of PSD-95 or MPP2 along a dendrite. Those dendritic spines, which were apparent in images acquired with both techniques, were then individually categorised whether SynCAM1 and/or MPP2 (depending on the marker

combination of the dual-colour stainings) exhibited a bracelet-like arrangement of protein clusters or not. Data was expressed as fraction of all synapses identified in both widefield and *d*STORM image (Figure 3). Analysis was performed for 57 synapses per image in 3-6 images per marker combination. Using the ‘line tool’ in FIJI/ImageJ, three measurements per synapse were taken for both channels (Cy3b and AF 647) independently and were averaged per synapse. Summarised data were acquired from 170-236 synapses in 6-8 images of 2-4 independent experiments.

#### **2.2.5.4 Automated segmentation of SIM images with Arivis Vision 4D**

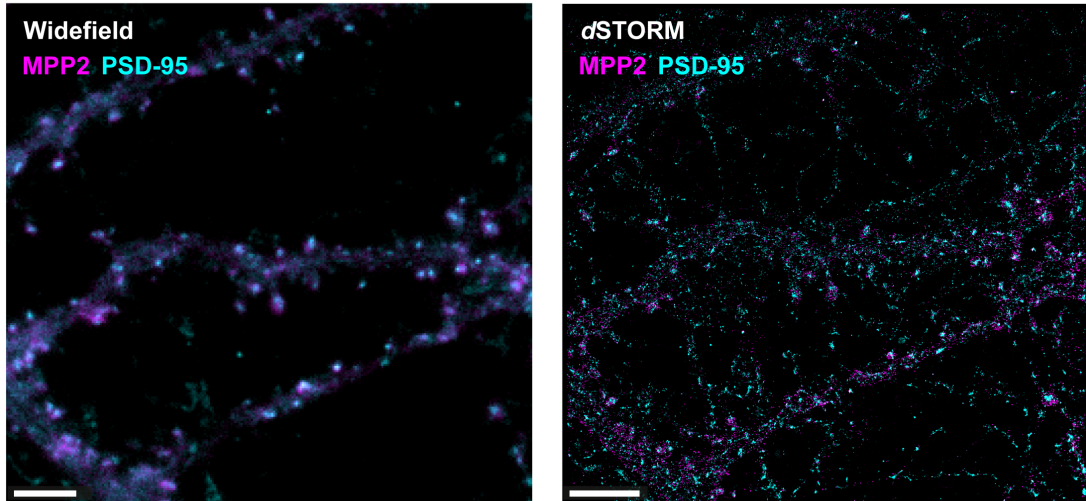
Image segmentation was performed in Arivis Vision 4D (Arivis AG, Munich, Germany). MPP2, SynCAM1 and vGlut1 clusters were identified with histogram-based threshold procedures (Otsu’s and Yen’s method) after Gaussian filtering and background subtraction. PSD-95 clusters and their centres were identified with the built in ‘Blob Finder’ tool, a combination of automatic seed finding and watershed segmentation (watershed level: 6.7, threshold: 4.5, expected blob diameter: 0.5  $\mu\text{m}$ ). Subsequently, such segmented PSD-95 clusters were further filtered for sphericity ( $>0.4$ ) and volume ( $>000.5 \mu\text{m}^3$ ) to exclude unusual segmented clusters that likely only represent background. Further, the co-existence of MPP2, SynCAM1 and vGlut1 staining within the same synapse (2-2.5  $\mu\text{m}$  distance cut-off to the centre of the next PSD-95 cluster) was ensured by applying the built-in co-localisation tool. Only synapses within a manually determined and set range of planes (selected for the best signal intensity for PSD-95) were considered for further analysis. Staining for the presynaptic protein vGlut1 only served as a marker for mature synapses, but was not further included in the analysis due to the limited quality in the 405 channel. The Arivis pipeline is available as XML file in the supplements (File S2) in Schmerl et al. (2020). The segmentation was performed on 50 images of three independent experiments and the whole dataset was subjected for further analysis.

To approximate the frequency with which synapses on our imaged neurons express all three proteins of interest (PSD-95, MPP2 and SynCAM1), using the same segmentation pipeline, we examined 8 images from 2 independent experiments with regard to how the incorporation of co-localisation selectors MPP2 and SynCAM1 affect the total number of segmented synapses. This section of Material and Methods has been published as preprint (Schmerl et al., 2020).

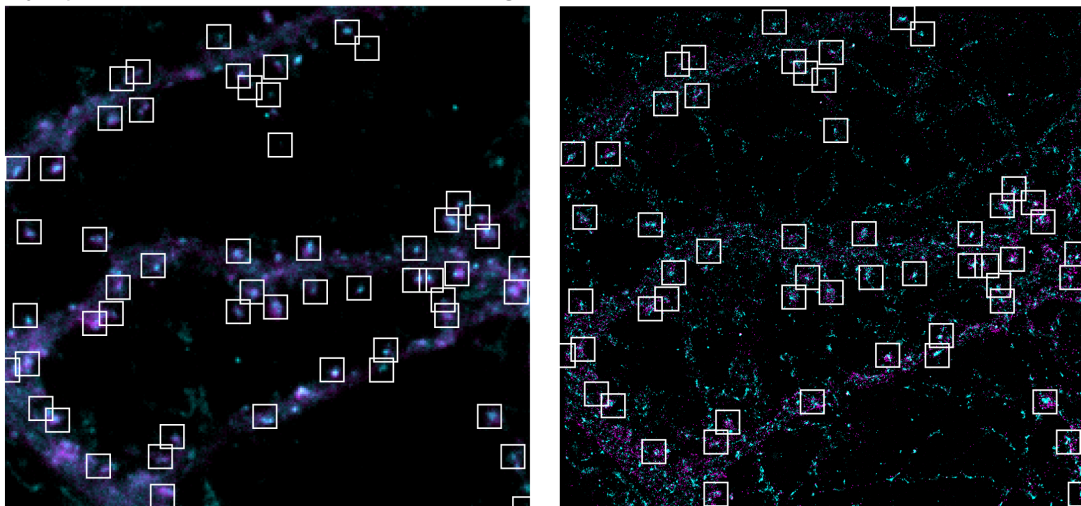
#### **2.2.5.5 Data analysis of Arivis output**

Cluster size histograms (bin size = 15 nm) were generated based on the Arivis cluster segmentation data using a custom-written script implemented in R+ (<https://github.com/BettinaSchmerl/Thesis.git>).

Corresponding widefield and dSTORM images:



Synapses that could be identified in both images:



Synapses that exhibited a ring-/ bracelet-like arrangement of SynCAM1 and/or MPP2 clusters:

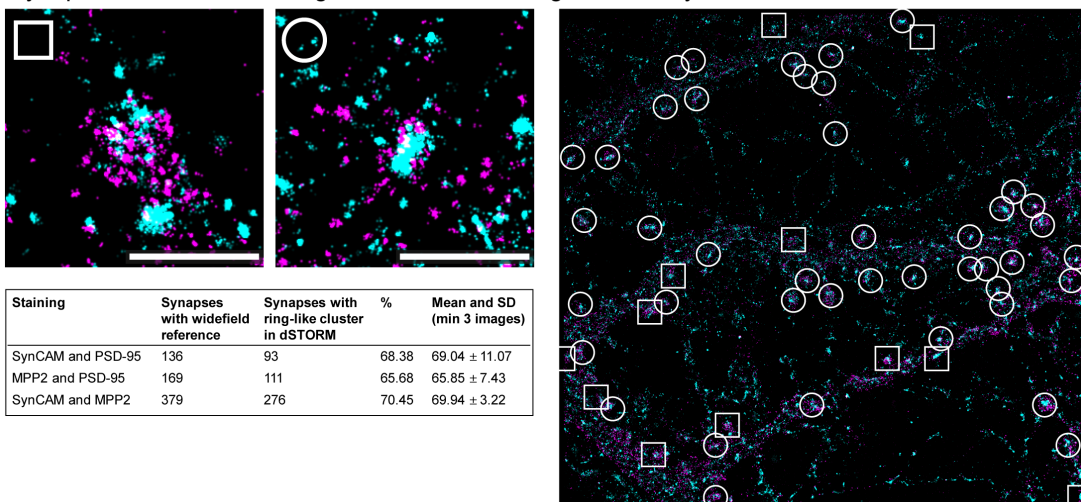


**Figure 3: Prevalence of synaptic bracelet-like SynCAM1 and MPP2 cluster arrangements.**

SynCAM1 and MPP2 clusters are arranged in a bracelet-like manner in the majority of synapses. Exemplary image to illustrate the manual assessment of the frequency of bracelet-like arrangement of SynCAM1 and MPP2 at synapses. In corresponding sections of widefield (left column)

and dual-colour *d*STORM images (right column) synaptic structures that were captured with both techniques were identified (white boxes, second row) and then individually assessed whether SynCAM1 and/or MPP2 (magenta) protein clusters are arranged to form a bracelet-like structure (white circles, third row) around PSD-95 (cyan), if applicable. Table summarising counts of 3-6 images per staining combination (SynCAM1 with PSD-95, MPP2 with PSD-95 and SynCAM1 with MPP2) indicating the number of synapses identified and those with a ring/bracelet-like structure. Scale bars: overview = 5  $\mu\text{m}$ ; detail = 1  $\mu\text{m}$ .

#### **2.2.5.6 Radial profile analysis**

A FiJi/ImageJ macro custom-written by Dr. Niclas Gimber, AG Schmoranzer (AMBIO, Charité - Universitätsmedizin Berlin) (<https://github.com/ngimber/RadialProfile3D>) was used to calculate 3D radial intensity profiles around PSD-95 centres (segmentation from above). Radial intensity profiles were 0-1 normalised and averaged twice (per image and per experiment) using Python before plotting with Prism 7 (GraphPad). This section of Material and Methods has been published as preprint (Schmerl et al., 2020).

#### **2.2.5.7 Nearest neighbour analysis of SIM data**

This analysis was performed in collaboration with Dr. Niclas Gimber, AG Schmoranzer (AMBIO, Charité - Universitätsmedizin Berlin).

Nearest neighbour analysis and randomisations were performed in Python using custom-written scripts. Nearest neighbour distances between PSD-95, MPP2 and SynCAM1 clusters were calculated based on the Arivis segmentations. Random controls were generated by randomly distributing spherical objects, representing PSD-95, MPP2 and SynCAM1 clusters within a simplified spherical postsynapse with a diameter of 0.8  $\mu\text{m}$  (Adrian et al., 2017). Randomised distributions were generated for each image using the object counts and volumes from the corresponding segmentation (10 simulation rounds per synapse, ~40,000 synapses from 50 images). Plotting was done with Prism 7 (GraphPad). This section of Material and Methods has been published as preprint (Schmerl et al., 2020).

#### **2.2.5.8 Image processing and analysis of triple-colour *d*STORM data**

Triple-colour *d*STORM data processing and data analysis was performed by and in collaboration with Dr. Niclas Gimber, AG Schmoranzer (AMBIO, Charité - Universitätsmedizin Berlin).

##### **2.2.5.8.1 Single molecule localisation and drift correction**

The open source Fiji/ImageJ plugin ThunderSTORM1.3 (Ovesny et al., 2014) was used to localise single molecule blinking events. Specifically, the ‘integrated

Gaussian' and the 'weighted least squares' functions of ThunderSTORM with a fitting radius of 4 pixels (292 nm) and an initial sigma of 1.5 pixels (110 nm) were used to localise the events. Further details are provided in the parameter files (see File S3, File S4) in Schmerl et al., 2020. Localisations were rendered as Gaussian distributions (FWHM = 20 nm). TetraSpeck<sup>TM</sup> beads were used for drift-correction and alignment of the 568 channel to the de-mixed 647/680 channels.

#### **2.2.5.8.2 Spectral de-mixing of triple-colour dSTORM data**

The recently published open source software tool SD-Mixer2 (Tadeus et al., 2015:<https://github.com/gtadeus/sdmixer2/>) was used for pairing and colour assignment to Alexa 648/CF 680 localisations. ThunderSTORM localisation files were converted into the SD-Mixer file format (custom Python script available on GitHub: [https://github.com/ngimber/Converter\\_ThunderSTORM\\_SDmixer](https://github.com/ngimber/Converter_ThunderSTORM_SDmixer)). Parameter files and binary masks for colour separation can be found in the supplements (File S3; File S4 and Fig S15) in Schmerl et al. (2020).

#### **2.2.5.8.3 Cluster detection in triple-colour dSTORM datasets**

Clusters were automatically detected with the DBSCAN (Density-based spatial clustering of applications with noise) approach using the Python Package Scikit-learn 0.22.2 (Parameters:  $\epsilon = 20$  nm, min 5 points Pedregosa et al., 2011). Histograms from 26 images (from three independent experiments) were averaged. Plotting was done with Prism 7 (GraphPad).

#### **2.2.5.8.4 Nearest Neighbour Analysis in dSTORM datasets**

Nearest neighbour analysis and randomisation were performed in Python using a custom-written script. Clusters were detected, as described above. Nearest neighbour distances were calculated between MPP2 and GABA<sub>A</sub>R  $\alpha 1$  cluster centres. Random controls were generated for each image by introducing a toroidal shift of 20 nm to the MPP2 channel. Histograms from 26 images (from three independent experiments) were averaged. Plotting was done with Prism 7 (GraphPad).

## 3 Results

Scaffold proteins of the family of membrane-associated guanylate-kinases have been demonstrated to be critical components for the assembly of synaptic structures and the maintenance of neuronal function. In several high-throughput proteomics studies investigating AMPA receptor-associated protein complexes (Schwenk et al., 2012; Shanks et al., 2012), MPP family proteins were identified as novel proteins among well-established components of the postsynaptic density proteome.

The present study aims to shed light on the characteristics of the membrane-protein, palmitoylated 2 (MPP2) and investigate its function at synapses, as MPP2 has not been studied in a neuronal context before.

### 3.1 MPP2 is a novel postsynaptic scaffold protein

#### 3.1.1 Neuronal expression of MPP2

After successful validation of a commercially available antibody (see also appendix, page 139), tissue lysates of several brain regions from adult rat brain were analysed for MPP2 expression. As apparent from Figure 4a, a protein band between 50 and 75 kDa could be detected, in accordance with a calculated molecular weight of full-length murine MPP2 according to its amino acid sequence (~62 kDa). In line with the in-situ hybridisation (ISH) data provided by the Allen Brain Atlas database (<https://mouse.brain-map.org/experiment/show/68798980>), MPP2 protein can be found in lysates of olfactory bulb, cortex, hippocampus and cerebellum. Interestingly, almost no MPP2 could be detected in brain stem lysates.

Additionally, analysing MPP2 expression in lysates from cultured primary hippocampal neurons harvested at DIV 24, commonly considered a mature state, could confirm the expression of MPP2 in mixed hippocampal cultures. Interestingly, in neuron lysates, an additional, faint band below 50 kDa can be detected, which does not occur in untransfected CHL V79 cell lysates (see also appendix, Figure A1a), thus seems specific for neuronal tissue and cells. This additional band is also weakly present in the brain lysates, and might constitute an alternatively spliced isoform of endogenous MPP2.

The currently best-characterised MAGUK proteins in the brain belong to the PSD-95 family. Although they share a well-conserved structure, some have been found to fulfil very different roles at synapses. For example, SAP102 and PSD-95 share a high sequence identity, however, they have different functions

in a developmental context: SAP102 is expressed at higher level early in development, and is thought to recruit and traffic synaptic proteins to their targets (Elias et al., 2006; Murata and Constantine-Paton, 2013). In contrast, PSD-95 expression starts later in development and remains high upon maturity, in line with its role to anchor transmembrane proteins at postsynaptic sites and mediate plasticity (Dakoji et al., 2003).

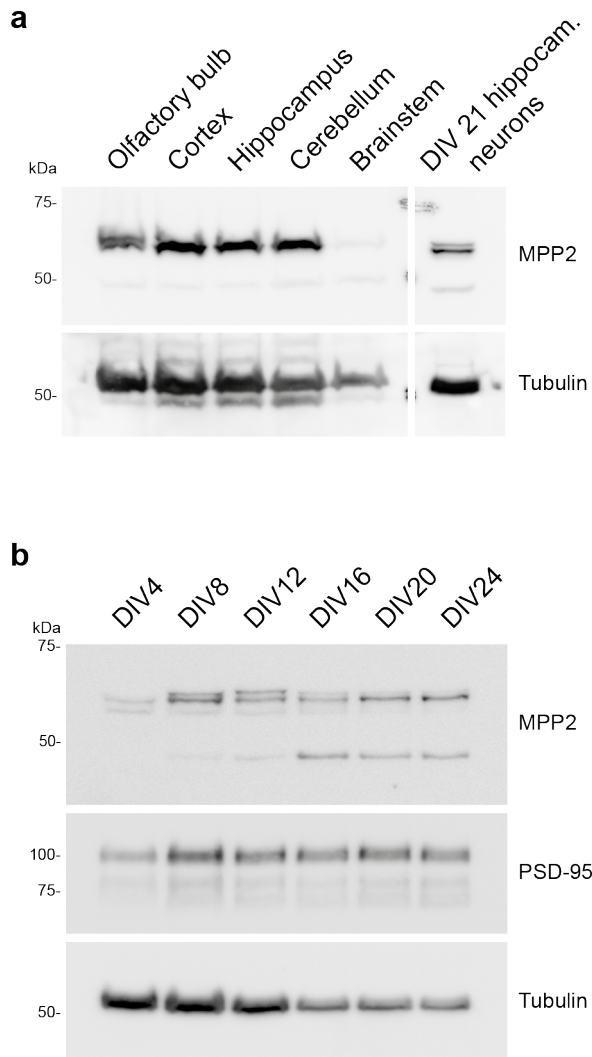


**Figure 4: Neuronal expression of MPP2.**

a) Adult rat whole brains were dissected into the indicated brain regions, minced and lysed in SDS sample buffer. Cultured hippocampal neurons were harvested at DIV 21 in SDS sample buffer and all lysates were separated on an SDS PAGE. Endogenous MPP2 was detected by Western blot with  $\alpha$ MPP2 antibody. Immunoblotting with  $\alpha$ Tubulin served as a loading control. b) Cultured primary hippocampal neurons of different DIV were lysed in SDS sample buffer and analysed by SDS PAGE and Western blot. The expression levels of MPP2 increase with maturity, similar to the established PSD scaffold protein PSD-95, as detected with  $\alpha$ MPP2 and  $\alpha$ PSD-95 antibodies. Immunoblotting with  $\alpha$ Tubulin served as a loading control.

In order to gain a more detailed view on the developmental expression profile of MPP2, whole cell lysates of cultured primary rat hippocampal neurons were harvested every fourth day until DIV 24 (days in vitro), when cultured neurons are considered mature. Western blot analysis with  $\alpha$ MPP2 antibody shows that the protein is expressed at low levels as early as DIV 4 and increases until DIV 8 (Figure 4b). Afterwards, MPP2 seems to be expressed at consistently high levels. Moreover, MPP2 expression levels appear similar to that of PSD-95, which is also considered as maturity marker. Interestingly, while expression levels of MPP2 remain consistently high during later stages, an additional lower band at ~50 kDa that was also observed in brain lysates, increases. The precise identity of this additional band was not determined, however, it might constitute an alternatively spliced isoform of MPP2, which is increasing upon maturation.

### **3.1.2 MPP2 is a novel postsynaptic scaffold protein**

Confirming the presence of MPP2 protein in brain and neuron lysates further supports previous *in vitro* studies, suggesting an association of MPP2 with synaptic AMPA receptor complexes (Schwenk et al., 2012; Shanks et al., 2012). Given the important role of other MAGUK proteins at postsynaptic sites, this study continuously focussed on MPP2 and examined its location in greater detail.

#### **3.1.2.1 MPP2 is expressed in neurons at postsynaptic sites**

In order to investigate the sub-cellular localisation of MPP2, cultured primary hippocampal neurons were immunostained with  $\alpha$ MPP2 antibody together with the dendritic marker MAP2 (microtubule-associated protein 2), the postsynaptic density marker PSD-95 and the presynaptic marker vGlut1 (vesicular glutamate transporter 1). In mixed hippocampal cultures, staining for MPP2 was detected exclusively in cells that were also positive for MAP2, confirming that MPP2 expression is specific for neurons and that MPP2 detected in brain lysates does not originate from e.g. glial cells (Figure 5a, upper panels). As a next step, the sub-cellular localisation of MPP2 was examined by co-staining with established pre- and postsynaptic markers. In line with studies reporting MPP2 in postsynaptic density preparations (Schwenk et al., 2012; Shanks et al., 2012), MPP2 puncta were co-localising with the core PSD protein PSD-95 (Figure 5a, middle panels). Moreover, those puncta were located rather adjacent to vGlut1, a presynaptic marker, further emphasising its localisation at postsynaptic compartments (Figure 5a, lower panels).

#### **3.1.2.2 The sub-synaptic positioning of MPP2 is peripheral to PSD-95**

With confocal imaging, which provides an optical resolution of  $\sim$ 300 nm, endogenous MPP2 protein was observed at the postsynaptic sites of cultured primary neurons, where it co-localised with the established postsynaptic density marker and important scaffold protein PSD-95. Photoactivated localisation microscopy (PALM) super-resolution imaging had revealed that PSD-95 is not just forming a homogenous PSD structure that is observed with confocal microscopy, but instead is organised into sub-synaptic clusters, referred to as nanodomains (MacGillavry et al., 2013; Nair et al., 2013).

To investigate the precise sub-synaptic localisation and clustering of MPP2, a related super-resolution imaging technique, dual-colour *d*STORM (direct stochastic optical reconstruction microscopy), which allows for resolution of up to 20 nm, was applied. In collaboration with the Membrane Biochemistry Research Group (AG Ewers) of the Institute for Biochemistry at Freie Universität Berlin,

cultured primary hippocampal neurons were fixed at DIV 22 and stained for endogenous PSD-95, SynCAM1 and MPP2 with respective antibodies and subjected to *d*STORM imaging (Figure 5b).

Unexpectedly, based on previous confocal imaging of endogenous synaptic MPP2, super-resolution imaging revealed that MPP2 is not simply co-localising with PSD-95. Instead, the protein is present as small clusters, which are surrounding the PSD in a bracelet-like arrangement (Figure 5b) of in average 791 nm diameter (mean  $\pm$  SD 209 nm). Manual assessment and categorisation of synapses identified in corresponding widefield and *d*STORM images into bracelet-like or non-bracelet-like (see also Figure 3 in Material and Methods, page 60) revealed that this novel arrangement of MPP2 protein clusters is found in the majority of synapses (65%) in mature neurons of mixed hippocampal cultures, supporting that this arrangement is representative.

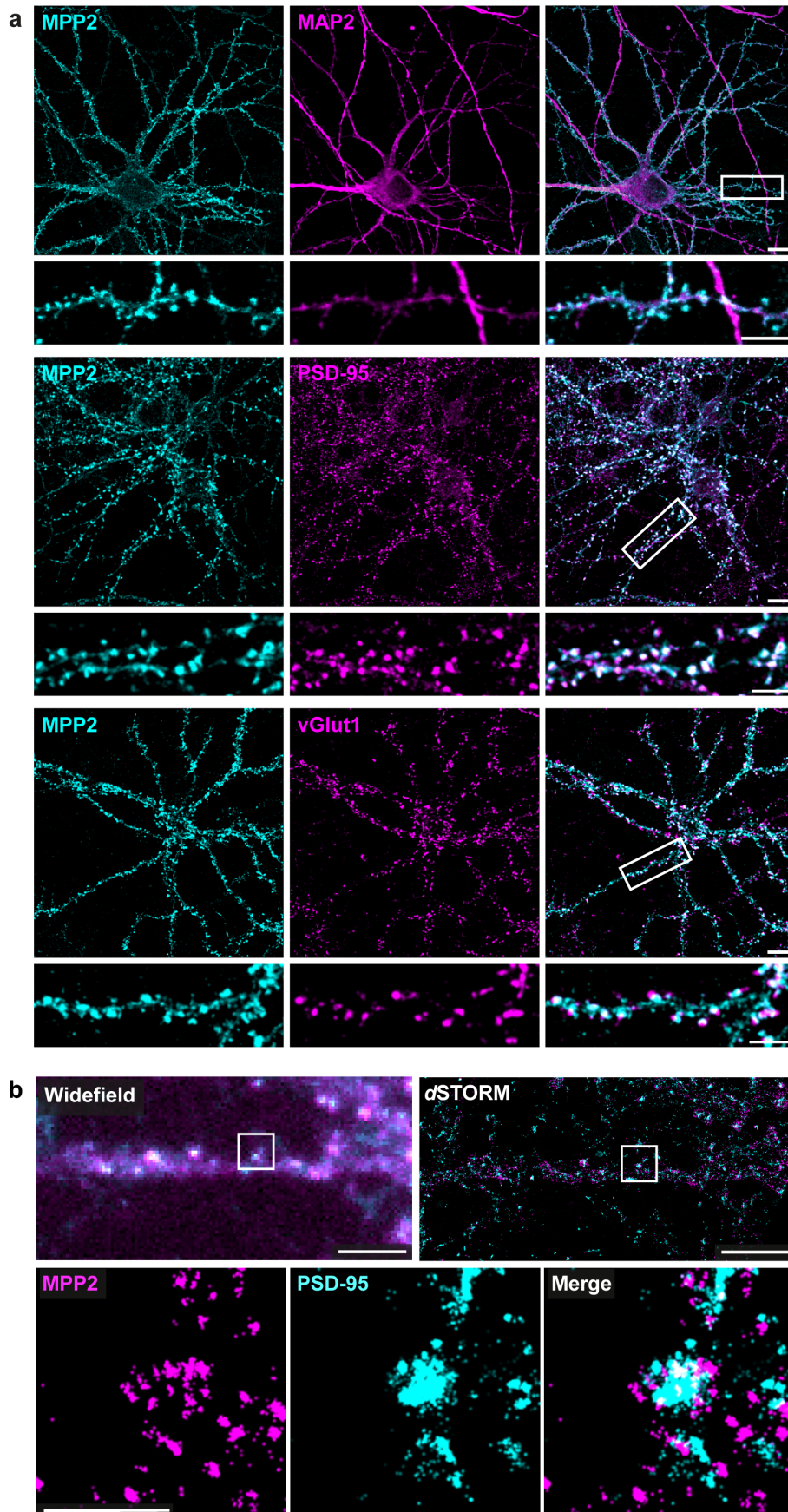


**Figure 5: MPP2 localises to postsynaptic sites peripheral to the PSD.**  
 a) Cultured rat hippocampal neurons (E18) were fixed at DIV 28 and stained for MPP2 (cyan, left panels) together with the microtubule-associated protein 2 (MAP2, dendritic marker), the

postsynaptic density protein 95 (PSD-95, postsynaptic marker) or the vesicular glutamate transporter 1 (vGlut1, presynaptic marker) and respective secondary antibodies and subjected to confocal imaging. Overlapping signals are visible in the merged images on the right, with the indicated regions selected for detailed images. Scale bars: overview = 10  $\mu\text{m}$ , detail = 5  $\mu\text{m}$ . b) Corresponding widefield (left, top) and *d*STORM (left, bottom) images of a dendrite segment stained for endogenous MPP2 and PSD-95. White box indicates location of the synapse shown in the detail view (right panel). Clusters of endogenous MPP2 (magenta) show a similar bracelet-like arrangement at the periphery of the PSD (PSD-95, cyan). Scale bars: overview = 5  $\mu\text{m}$ , detail = 1  $\mu\text{m}$ . This data and legend have been published in Rademacher\*, Schmerl\*, et al. (2016) and Schmerl et al. (2020).

### 3.1.2.3 MPP2 is expressed at high levels in a subset of excitatory neurons

Immunofluorescence experiments revealed that not every neuron seemed to express MPP2 at high levels. Some MAP2-positive cells in primary rat hippocampal cultures did not exhibit a strong staining with the  $\alpha$ MPP2 antibody. Since mixed hippocampal cultures consist of several cell types, e.g. pyramidal neurons, interneurons as well as glial cells, MPP2 may be expressed only in a sub-population of neuronal cells.

To shed light on the prevalence of MPP2 signal in primary neuronal cultures, neurons were fixed at DIV 21-22 and stained for the nuclear marker DAPI together with the neuronal dendrite marker MAP2 in combination with either MPP2 or the PSD marker Homer1 and subjected to analysis with confocal imaging.

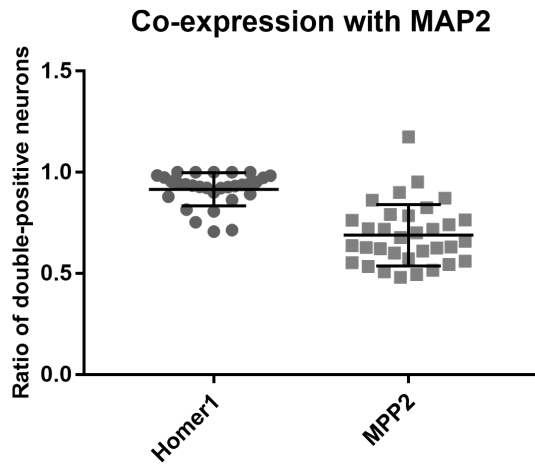


**Figure 6: MPP2 is expressed in a subset of primary hippocampal neurons.**

Primary neurons were fixed at DIV 21 and stained for DAPI, a nuclear marker, and the dendritic marker MAP2 together with either the PSD marker Homer1 or the protein of interest, MPP2. Confocal images acquired with 20x objective were assessed manually and neurons were marked positive for each channel individually. Data represent double positive cells as a fraction of all MAP2-positive neurons. Mean  $\pm$  SD, analysis of 32 images of 3 independent experiments.

In mixed hippocampal cultures most (~92%) of the MAP2-positive cells were also expressing the postsynaptic marker Homer1 (Figure 6). This is in line with the idea that most neurons in hippocampal cultures have excitatory glutamatergic synapses. The identity of the remaining fraction of cells, which could comprise inhibitory interneurons that make up a small percentage in mixed cultures (Craig et al., 1996), was not determined. The same analysis for MPP2-positive cells revealed, that ~69% of all MAP2-positive cells express MPP2 at levels observable by immunofluorescence

staining and confocal microscopy at low magnification with a 20x objective. This data is particularly relevant when analysing MPP2 and manipulations thereof on a single cell level, in order to ensure (either by appropriate controls or by appropriate increase in sample size) that any potential result is not masked by analysis of MPP2-negative neurons.

### 3.1.3 MPP2 is associated with AMPA receptor complexes

Following establishment of MPP2 as a postsynaptically located protein in neurons, the next aim was to verify the previously reported identification of MPP2 within AMPA receptor complexes. Adult rat brain crude synaptosomal preparations were subjected to immunoprecipitation experiments, where the well-established AMPA receptor-auxiliary subunit Stargazin/TARP $\gamma$ 2 was pulled down using a monoclonal antibody, followed by SDS PAGE and Western blot analysis. As expected, the most prevalent AMPA receptor subunit GluA2 was detected in the precipitate, similar to the established postsynaptic scaffold protein PSD-95, both of which are known as directly binding interaction partners of Stargazin/TARP $\gamma$ 2 (Schnell et al., 2002). Most importantly, MPP2 was also present in the precipitate (Figure 7), further supporting the idea that MPP2 is associated with AMPA receptor complexes, which are crucial for excitatory synaptic transmission.

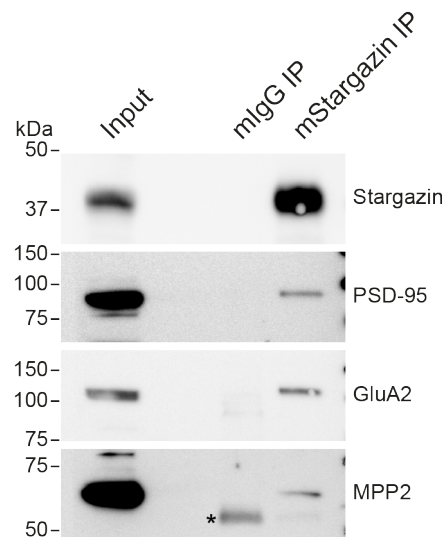


**Figure 7: MPP2 is a component of postsynaptic receptor complexes.**

The AMPA receptor auxiliary subunit Stargazin/TARP $\gamma$ 2 was immunoprecipitated from crude synaptosomal preparations of adult rat brain with a monoclonal mouse antibody and precipitates were analysed by Western blot, with antibodies to synaptic proteins, as indicated. A pull-down with mouse IgGs (mIgG IP) was performed as negative control (a nonspecific IgG background band is marked with an asterisk). This figure and legend have been published (Rademacher\*, Schmerl\*, et al., 2016). The data as shown was generated by Dr. Nils Rademacher and is shown with permission.

### **3.1.4 MPP2 interacts with multiple synaptic scaffold proteins**

As the association of MPP2 with AMPA receptor complexes has been confirmed, the interactions that mediate this association remained unclear. These AMPA receptor-associated protein complexes, however, comprise of multiple other classes of proteins including various scaffold proteins, which contribute critically to the complexes' structure and function.

#### **3.1.4.1 MPP2 interacts with PSD-95**

The scaffold protein PSD-95 is among the most frequent proteins that form the postsynaptic density (X. Chen et al., 2005; for review see Sheng and Hoogenraad, 2007) and, like other MAGUK proteins, it is known to multimerise with structurally related MAGUK proteins (C. Cai et al., 2006; Rademacher et al., 2013; for review see Funke et al., 2005). In the preceding experiments, MPP2 and PSD-95 were found together at postsynaptic sites in cultured hippocampal neurons and to co-purify together with AMPA receptor complexes (see again Figure 5 and Figure 7), hence this potential interaction was explored further.

Indeed, upon pull-down of endogenous MPP2 from adult rat brain crude synaptosome preparations, PSD-95 co-precipitates (Figure 8a). To test whether this is a direct interaction of the two proteins, they were overexpressed together in heterologous cells. Upon overexpression of untagged PSD-95 together with MYC-MPP2 in CHL V79 cells (an epithelial cell line, which does not express synaptic proteins), followed by co-immunoprecipitation with  $\alpha$ PSD-95 antibody and Western blot analysis, MYC-tagged MPP2 was present in the precipitate (Figure 8c). This demonstrates that the two MAGUK scaffold protein PSD-95 and MPP2 are able to directly interact, thus likely mediating the association of MPP2 with AMPA receptor complexes, of which PSD-95 is a critical structural component.

#### **Interaction of MPP2 and PSD-95 is mediated via the GK domains**

MAGUK family proteins contain multiple protein-protein interaction domains, which allow these scaffold proteins to act as protein interaction hubs in multiple cellular contexts. Interestingly, the modes of interaction differ a lot, e.g. in terms of affinity and specificity, depending on the domains that are involved in these interactions.

In order to characterise the novel interaction between MPP2 and PSD-95 in greater detail and to identify the domains relevant for this interaction, several truncation constructs of MPP2 were generated. These constructs were incrementally devoid of N-terminal domains (i.e. lacking the two L27 domains or the L27 and PDZ domains) or consisted of only an isolated domain (PDZ or GK) of the

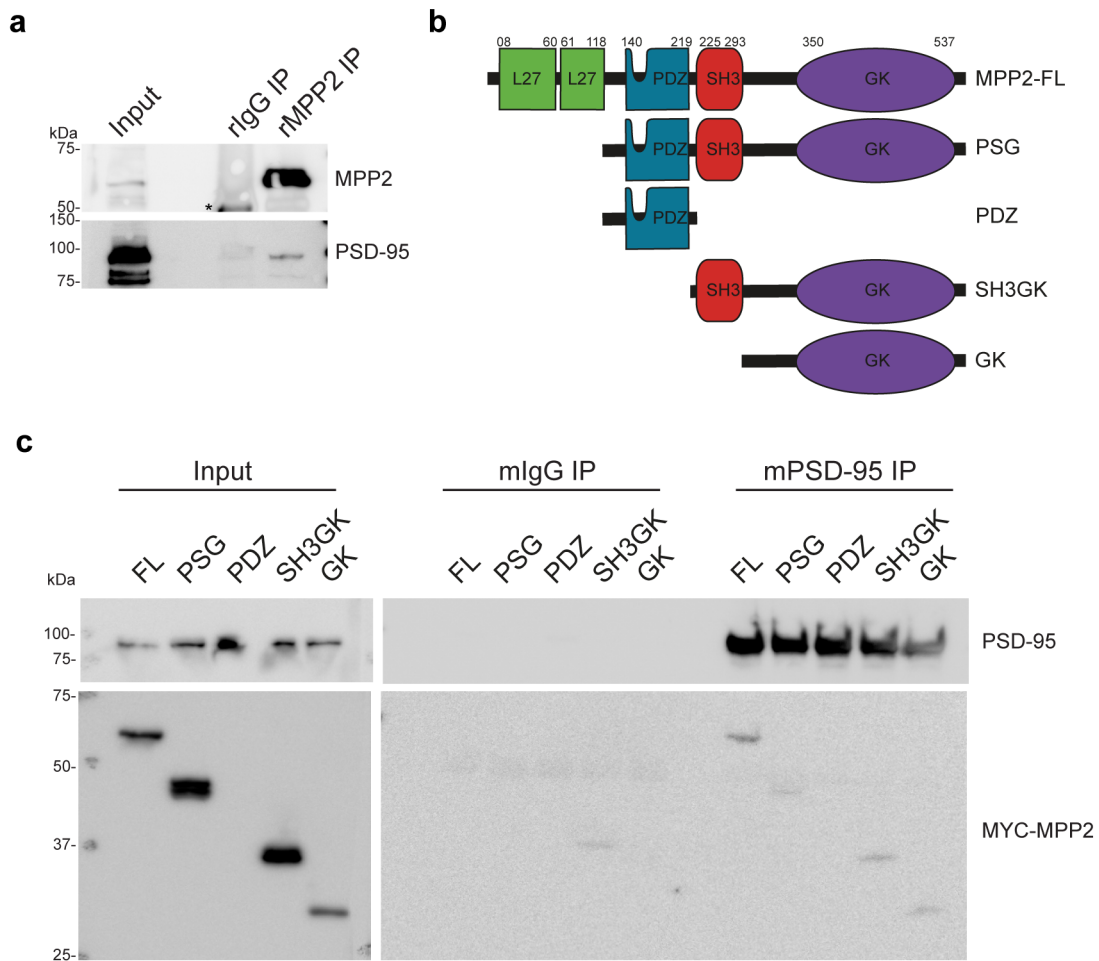


**Figure 8: MPP2 interacts with the postsynaptic density protein PSD-95.**

a) Immunoprecipitation of MPP2 (using a rabbit polyclonal MPP2 antibody or rabbit IgGs as a negative control) from a crude synaptosome preparation of adult rat brain co precipitates PSD-95, as detected by Western blot with antibodies to PSD-95 (co-IP) or MPP2 (IP control). A background IgG signal is marked with an asterisk. This data as shown was generated by Dr. Nils Rademacher and is shown with permission. This figure and legend have been published (Rademacher\*, Schmerl\*, et al., 2016). b) Domain structure overview of full-length MPP2 (MPP2-FL, top) and the truncation constructs used in b. Number on top indicate first and last amino acids of the respective domains: L27 tandem domain (green), PDZ domain (petrol) and a tandem domain formed by SH3 (red) and GK (violet). c) Untagged PSD-95 was overexpressed in CHL V79 cells together with MYC-tagged MPP2 full length and several truncated versions. Upon pull-down of PSD-95 using  $\alpha$ PSD-95 antibodies or normal mouse IgG as negative control, all MPP2 constructs containing the C-terminal GK domain were co-precipitated as detected by Western blot using  $\alpha$ MYC antibodies. Please note that the isolated MPP2-PDZ domain construct was not expressed at comparable levels.

protein (for overview see Figure 8b). Those constructs were overexpressed together with untagged PSD-95 and upon immunoprecipitation with an  $\alpha$ PSD-95 antibody full-length MPP2 and the SH3GK and GK constructs co-precipitated with comparative efficiency, suggesting that the GK domain alone is sufficient to mediate the PSD-95-MPP2 interaction. Interestingly, the MPP2 ‘MAGUK core’ of PDZ-SH3GK domains did co-purify with lower efficiency despite high protein

content in the input lysate, possibly hinting at a regulatory interplay between the PDZ domain and SH3GK tandem of MPP2, as has been described for PSD-95 (Rademacher et al., 2013; Rademacher et al., 2019).

#### **3.1.4.2 MPP2 interacts with GKAP**

Beside the very important PSD-95 family of synaptic MAGUK scaffold proteins, several other scaffold molecules are critical for synapse structure and function. These proteins feature distinct interactomes and facilitate different interactions, based on their specific interaction domains and protein structure. Moreover, their different interactions also determine different localisations within dendritic spines: MAGUK proteins for example are typically membrane-associated, as many of their interactions involve proteins positioned in the membrane. Other scaffolding proteins, like e.g. SHANK family proteins, lie deeper within synaptic structures, where they are directly or indirectly connecting with cytoskeletal elements (Dani et al., 2010). Yet another family of scaffolding proteins serves at an intermediate position: Guanylate kinase-associated proteins (GKAP). It is an important connector of membrane-associated scaffolds with deeper synaptic structures, like SHANK and Homer, which eventually connect with the cytoskeleton (Petralia et al., 2005; Tao-Cheng et al., 2015).

GKAP is also referred to as DLGAP (DLG-associated protein, DLG being short for disk large protein as alternative name for PSD-95 family MAGUK proteins) or SAPAPs (SAP90/PSD-95-associated proteins). These proteins are well known for their ability to interact with multiple MAGUK protein GK domains including PSD-95 (E. Kim et al., 1997; Takeuchi, 1997).

In order to explore whether MPP2 is integrated in protein scaffold complexes of a similar composition as PSD-95, a putative direct interaction between MPP2 and GKAP was tested. Full-length MYC-MPP2 was overexpressed together with FLAG-tagged GKAP in CHL V79 cells and following MPP2 pull-down using  $\alpha$ MYC antibodies, GKAP was co-purified as detected by Western blot (Figure 9a).

In an additional Y2H screen using the MPP2 PSG module as bait (see section 3.2.1, page 76), multiple clones for GKAP were identified among the prey proteins (see Table 3.1), what further validates this result. The clones covered two different selected interacting domains (SID), which correspond to known GKAP domains that interact with MAGUK protein GK domains (E. Kim et al., 1997; Takeuchi, 1997).

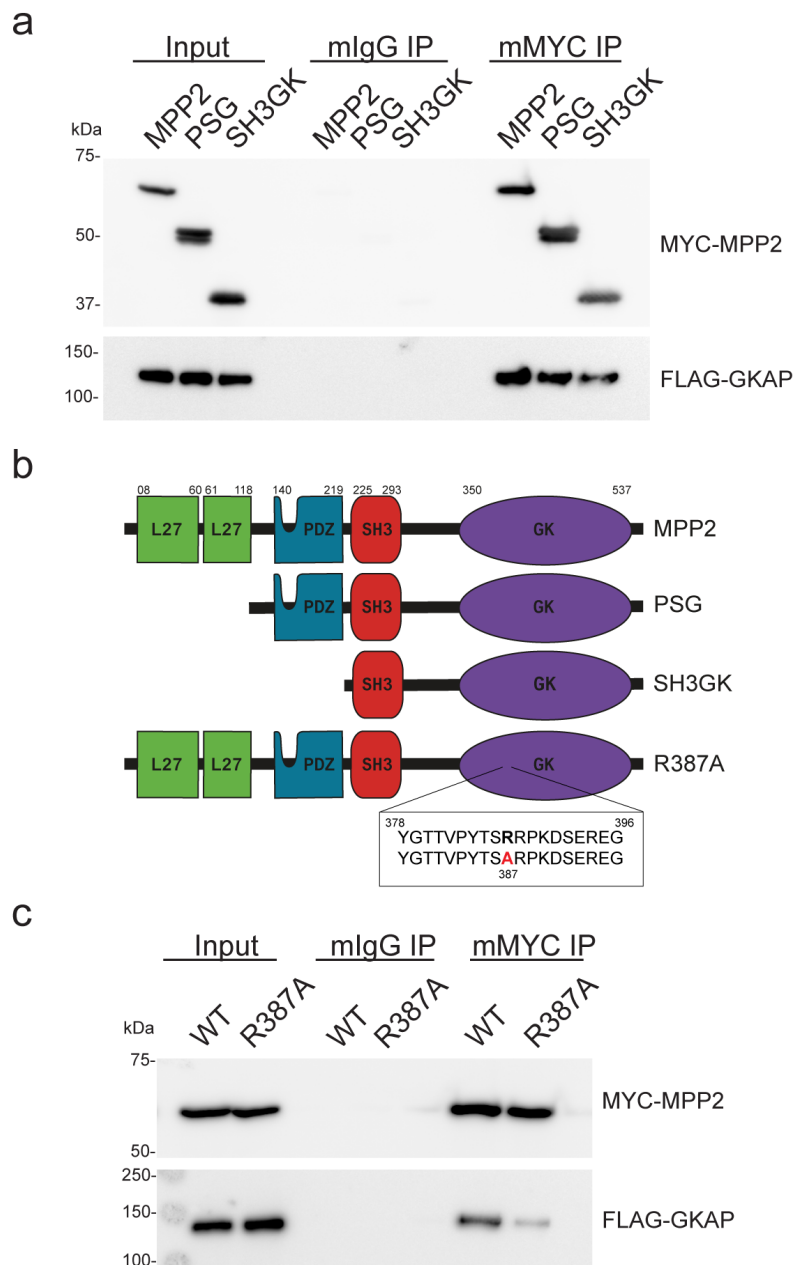


**Figure 9: The MPP2 GK domain mediates the interaction with GKAP.**

a) MYC-tagged MPP2 (MPP2), MYC-tagged MPP2 PDZ-SH3GK (PSG), or MYC-tagged MPP2 SH3GK (SH3GK) were co-expressed with FLAG-tagged recombinant GKAP in CHL V79 cells and immunoprecipitated with  $\alpha$ MYC antibody (mMYC IP) or with mouse IgGs (mIgG IP) as a negative control. Co-precipitated proteins were analysed by Western blot with  $\alpha$ FLAG antibody, pull-down controls with  $\alpha$ MYC antibody. This figure and legend have been published (Rademacher\*, Schmerl\*, et al., 2016). b) Schematic domain overview of the MPP2 full-length as well as the used truncation constructs and point mutation used to characterise the MPP2-GKAP interaction. Number on top indicate first and last amino acids of the respective domains: L27 tandem domain (green), PDZ domain (petrol) and a tandem domain formed by SH3 (red) and GK (violet). c) MYC-tagged MPP2-WT or -R387A was overexpressed together with FLAG-GKAP in CHL V79 cells. Upon immunoprecipitation using  $\alpha$ MYC antibodies or normal mouse IgG as negative control, GKAP co-purified much more efficiently with wildtype MPP2 than the R387A point mutation.

### **Interaction of MPP2 and GKAP is mediated via the GK domain of MPP2**

GKAP family proteins characteristically interact with multiple GK domains, primarily of MAGUK proteins (E. Kim et al., 1997; Takeuchi, 1997), hence a potential interaction with MPP2 was investigated. Indeed, upon immunoprecipitation of full-length as well as PSG and SH3GK truncation constructs of MPP2 (see Figure 9b for overview), which were overexpressed together with FLAG-GKAP in CHL V79 cells, efficiently co-purified FLAG-GKAP, as analysed by Western blot (Figure 9a).

Moreover, based on previous work and sequence homology with PSD-95 (Rademacher et al., 2013) a mutant MPP2 was generated, carrying an amino acid exchange of the arginine residue at position 387 for an alanine, hereafter referred to as MPP2-R387A (see also Figure 9b). For PSD-95 it was shown that mutating this single homologue amino acid was sufficient to prevent interactions of the PSD-95 GK domain (Reese et al., 2007). Indeed, introducing this mutation to the MPP2 GK domain interferes with the interaction between MPP2 and GKAP, as demonstrated by pull-down of MYC-tagged full-length MPP2-wildtype (WT) or R387A where only the WT construct was able to co-precipitate FLAG-GKAP efficiently (Figure 9c).

Taken together, the isolated SH3GK tandem domain of MPP2 is sufficient to mediate the interaction with GKAP and further introducing a point mutation to the GK domain abolishes this interaction. This is in line with studies on other MAGUK family proteins, which demonstrated that the GK domain is no longer catalytically active, but instead has evolved into an important protein-protein interaction domain (Zhu et al., 2011) that is critical for binding to GKAP scaffold proteins (Takeuchi, 1997).

#### **3.1.4.3 MPP2 interacts with Lin7b**

MPP2 is a typical scaffold protein in that it harbours a variety of protein-protein interaction domains: two L27 domains at the N-terminus, followed by the ‘MAGUK core’ domains (PDZ-SH3GK). According to the EMBL SMART and Pfam databases (<http://smart.embl-heidelberg.de> and <http://pfam.xfam.org/family/PF02828>), L27 domains are present in relatively few proteins. In humans, only 13 different proteins contain L27 domains (all of which also harbour PDZ domains, including MPP2-7 and CASK, as well as certain splicing variants of PSD-95 family proteins). These domains are known to interact between different proteins, forming L27-L27 heterodimers (W. Feng et al., 2004). Lin7 proteins are small scaffold proteins, containing only a single PDZ domain in addition to an L27 domain. They are involved in multiple protein complexes, and known to interact presynaptically with CASK, another MAGUK scaffold

with high similarity to MPP2 (Butz et al., 1998), but are also present in the postsynapse (Misawa et al., 2001). Since MPP2 is among these relatively few synaptic L27 domain-containing proteins, its potential interaction with Lin7 proteins was investigated. N-terminally MYC-tagged Lin7b (one of three synaptic Lin7 isoforms) was overexpressed together with FLAG-MPP2 and upon pull-down with  $\alpha$ MYC antibodies, MPP2 co-precipitates as analysed by Western blot (Figure 10a). In line with other studies on different MPP family proteins (Zhang et al., 2011; Hauri et al., 2013; Stohr et al., 2005). This result confirms Lin7b as a direct interaction partner for the MPP2 L27 domain.

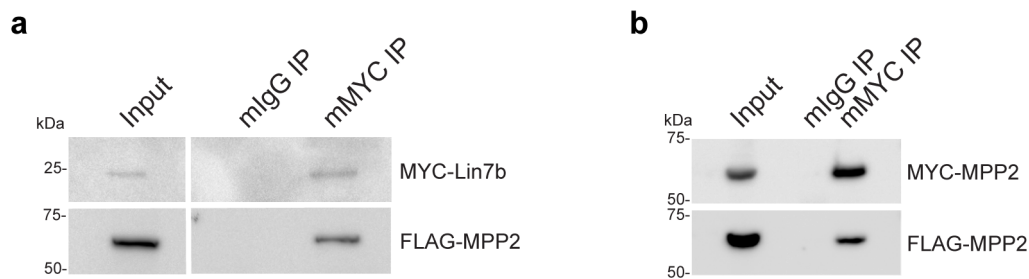


**Figure 10: MPP2 interacts with additional scaffold proteins and homomultimerises.**

a) MYC-tagged Lin7b was overexpressed together with FLAG-MPP2 in CHL V79 cells. Following immunoprecipitation with  $\alpha$ MYC antibodies or normal mouse IgG as negative control, MPP2 was co-purified as detected by Western blot with  $\alpha$ FLAG-HRP antibody. b) FLAG- and MYC-tagged MPP2 proteins were co-expressed in CHL V79 cells. MYC-MPP2 was pulled down with  $\alpha$ MYC antibody (mMYC IP) and co-precipitated FLAG-tagged MPP2 was analysed by Western blot with  $\alpha$ FLAG antibody. Mouse IgGs (mIgG IP) served as a negative control. Parts of this figure and legend have been published (Rademacher\*, Schmerl\*, et al., 2016).

### 3.1.4.4 MPP2 homomultimerises

In addition to the N-terminal L27 domains, MPP2 also harbours the characteristic PDZ-SH3GK domain ‘MAGUK core’. In particular the SH3GK tandem domain, which has developed to a novel type of protein-protein interaction domain (Zhu et al., 2011), was found to be critical for the assembly of MAGUK protein hetero- and homo-multimers (C. Cai et al., 2006; Gosens et al., 2007b), which significantly contribute to the scaffold function of this protein family.

To explore whether MPP2 is similarly able to form homo-multimer protein complexes, differently tagged full-length MPP2 constructs were overexpressed in CHL V79 cells. Indeed, after pull-down of MYC-MPP2 with  $\alpha$ MYC antibodies (thus targeting the peptide-tag), FLAG-MPP2 was found in the precipitate (Figure 10b). This result demonstrates that MPP2 is able to form protein homomultimers by interacting with other MPP2 molecules, similar to many other MAGUK proteins.

Subsequent experiments confirmed that the MPP2 PSG module is sufficient to mediate this interaction with MPP2 (data not shown). This further suggests

that the SH3GK domain is particularly relevant for homo-multimerisation of MPP2. Whether also the isolated L27 domains, that form hetero-dimers with L27 domains of other proteins, would suffice to mediate MPP2-homo-multimerisation was not explored.

## **3.2 Novel MPP2 PDZ domain ligands**

Many protein-protein interactions of MAGUK proteins are mediated by their characteristic ‘MAGUK core’ domains (PDZ-SH3GK). After having identified several interactors for the L27 and SH3GK domains of MPP2 the next aim was to find a ligand for its PDZ domain. PDZ domain-containing scaffold proteins have been found crucial especially for synaptic function (for review see E. Kim and Sheng, 2004). While for other MPP family proteins several PDZ domain-ligand interactions (e.g. between MPP5/Pals1 and its PDZ ligand Crumbs; Ivanova et al., 2015) are already well characterised, prior to this thesis no studies have tried to find a synaptic ligand for the MPP2 PDZ domain.

### **3.2.1 Identification of putative interactors with a yeast-two-hybrid screen**

Having identified MPP2 as a novel postsynaptic scaffold protein that is associated with functionally important protein complexes and interacts with distinct scaffold proteins, further identification of additional synaptic interactors of MPP2 was desirable, as this protein has not been studied in a neuronal context before.

Taking advantage of a commercial service, a yeast-two-hybrid (Y2H) screen was applied in order to identify potential interactors of MPP2. Since only few synaptic proteins carry L27 domains, which form hetero-dimers in a particular and already well-characterised fashion (Petrosky et al., 2005), the screen was focussed on putative interactions of the ‘MAGUK core’ domains, the PSG module of MPP2. Together with Hybrigenics services (France), a Y2H screen was conducted using the murine MPP2 PSG module (amino acids 119-552) in form of an N-LexA-PSG fusion protein as bait in a screen performed on a rat hippocampus cDNA library.

Out of 77 million interactions, a total of 347 positive clones could be sequenced. Analysis revealed a total of only 25 genes were found as prey in the screen. Three of those did not match with the GenBank database, for another three no additional information was available and two more hits were homologues to humane and murine genes. Table 3.1 summarises the highest ranked hits of the Y2H screen, consisting of only 13 different proteins, what indicates a high specificity and therefore relevance of the screen results. Based on the selected interacting domains (SID), two groups of potential interaction partners were found: putative

PDZ-ligands (Table 3.1, white rows), where the SID comprises the C-terminus of the prey protein (likely carrying a PDZ-binding motif H. J. Lee and Zheng, 2010) and potential SH3GK interactors, where the SID comprises a sequence enclosed within the target protein sequence (Table 3.1, blue rows). Indeed, as described before (see page 72) GKAP was confirmed as interaction partner for the MPP2 GK domain, what further validates the quality of the Y2H screen results.

Interestingly, most proteins identified in this screen belong to the group of trans-membrane cell adhesion proteins and are potential PDZ domain ligands, whereas others (e.g. Septin-4 and GKAP/Dlgap1) are scaffold proteins that might rather interact with the SH3GK module of MPP2. Together this suggests an important role of MPP2 in mediating interactions between adhesion proteins, positioned within the synaptic membrane, with deeper synaptic structures, in form of additional scaffold proteins.

**Table 3.1: Selected yeast-two-hybrid screen results**

Y2H screen performed by Hybrigenics services (France) using murine MPP2 amino acids 119-552, corresponding to the PSG module, as bait on a rat hippocampal cDNA library. Results are ordered and clustered according to ‘confidence scores’ assigned by Hybrigenics. White rows indicate putative PDZ interactors, where the selected interaction domain (SID) of the prey proteins comprised the very C-terminal amino acids. Blue rows indicate putative GK interactors, as the SID comprised larger stretches within the prey protein. Proteins are ordered according to Predicted Biological Score (PBS) of the Hybrigenics system. See Material and Methods page 43 for details.

		(SID) AA	Gene ID	Clones detected
<b>Bait: <i>Mus musculus</i> MPP2 PSG Module</b>		119-552	50997	
<hr/>				
<b>PBS</b>	<b>Prey (<i>Rattus norvegicus</i>)</b>			
<hr/>				
	SynCAM1 / CADM1 / TSLC1 / Igsf4 / Necl-2	402-417	363058	24
	SynCAM2 / CADM2 / Igsf4d / Necl-3	418-430	360882	34
A	GKAP / Dlgap1 / SAPAP	245-399	65040	11
	Pvrl1 / Nectin1	472-515	192183	15
	Pvrl3 / Nectin3	480-508	288124	19
	SynCAM3 / CADM3 / TSL1 / Igsf4b / Necl-1	373-395	363058	9
	Cntnap 2 / Caspr4 / Neurexin-like	473-487	360882	37
B	Cntnap5b / Caspr5-2 similar to contactin associated protein-like 5 isoform 1	1267-1292	65040	16
	Septin-4	352-563	287606	5
	Neurexin3	1575-1578	115508	7
	GKAP/Dlgap1/SAPAP	28-237	65040	5
C	Fam124a	443-436	691938	4
	Neurexin2	1709-1715	287606	3

### 3.2.2 MPP2 binds multiple synaptic cell adhesion molecule C-termini

Most of the proteins identified as potential interaction partner of the MPP2 PSG module in the Y2H screen (where the SID spanned the proteins' C-terminus) belong to the group of synaptic transmembrane cell adhesion proteins. They comprise important components for the development and maintenance of physical contact between cells and the C-termini of these proteins often constitute ligands for PDZ domains (for reviews see e.g. Dalva et al., 2007; Missler et al., 2012). The specificity of PDZ domain-ligand interactions is determined by the amino acid sequence at the very C-terminus of the ligand (Tonikian et al., 2008). Although the putative MPP2 PDZ domain ligands belong to different family of cell adhesion proteins (SynCAMs, Nectins, Neurexins and Cntnap family proteins), they share a rather unusual class II PDZ binding motif by harbouring large aromatic residues (see Figure 11a and 11c for comparison with other synaptic PDZ ligands; see also H. J. Lee and Zheng, 2010 for review). Since no synaptic PDZ ligands for MPP2 were known, these proteins constituted promising targets to validate these novel interactions.

SynCAM family proteins were identified as synapse formation-inducing factors during synapse development (Biederer et al., 2002) and have since then been intensely investigated for their function in synaptic differentiation and maintenance (Perez de Arce et al., 2015, Korber and Stein, 2016; for reviews see Biederer and Stagi, 2008 and Biederer et al., 2017). SynCAM proteins, also known as CADMs, are important at epithelial cell-cell contacts, where they interact with MPP family proteins (Sakurai-Yageta et al., 2009; Murakami et al., 2014). Another alternate denotation for SynCAM family proteins is Nectin-like (Necl) proteins.

Nectins belong to a different family of cell adhesion proteins that is structurally very similar to SynCAMs in that they assemble via their extracellular N-terminus that harbours several immunoglobulin-like loops (Momose et al., 2002; for review see Sakisaka and Takai, 2004). Just like SynCAMs, Nectin family proteins have been described to be involved in synapse formation (Mizoguchi et al., 2002). Moreover, in epithelial cell lines, Nectin trafficking and processing were found to be regulated by interaction with MPP3 and -5 (Dudak et al., 2011).

Cntnap proteins belong to the Neurexin superfamily but have been shown to be located at postsynaptic membranes (Horresh et al., 2008), where they seem to be involved in AMPA receptor trafficking (Varea et al., 2015). Alterations in Cntnap family proteins have been associated with neurodevelopmental alterations and e.g. epilepsy (Strauss et al., 2006; Friedman et al., 2008; Penagarikano et al., 2011), making it an interesting putative interaction partner for MPP2.

Neurexins were found in the Y2H screen results too, however, they are well-established cell adhesion proteins positioned in the presynaptic membrane (for

review see Sudhof, 2008) and known to bind to the presynaptic MAGUK CASK (Mukherjee et al., 2008), hence Neurexins were not considered for subsequent experiments.

In order to validate the Y2H screen results, suggesting a binding of MPP2 to the C-termini of SynCAM1, Nectin-1, Nectin-3 and Cntnap2, expression constructs were generated that consisted of the ten C-terminal amino acids of each protein fused to an N-terminal monomeric mCherry and an additional HSV1-tag. Indeed, when co-expressed together with MYC-MPP2 all four candidate PDZ ligands co-purified in an MPP2 pull-down similar to SynCAM1, as analysed by Western blot (Figure 11b).

### **3.2.3 Synaptic cell adhesion molecule SynCAM1**

The importance of SynCAM1, in different cellular contexts also known as CADM1, TSCL1, IGSF4 or Nectin-like 2, in synapse development and maintenance was demonstrated in multiple studies, however no postsynaptic PDZ domain interaction partners had been identified so far. Therefore, subsequent experiments focussed on characterising the interaction between MPP2 and SynCAM1 to investigate its importance for the structure and function of excitatory synapses.

#### **3.2.3.1 MPP2 binds the C-terminus of SynCAM1**

Having confirmed the interaction between MPP2 and multiple of the putative PDZ domain ligands from the Y2H screen, a second strategy was applied to confirm the specificity of these interactions. Since MPP2 was demonstrated as a novel protein present at postsynapses and associated with AMPA receptor complexes (see section 3.1.3), in a targeted approach, several established postsynaptic PDZ domain ligands were tested for binding to MPP2. Multiple mCherry fusion constructs of synaptic PDZ ligands were generated, as described above, containing the last ten amino acid residues, also referred to as C-terminal PDZ binding motives. This targeted approach included the C-termini of transmembrane proteins, which belong to several groups of protein that are especially relevant for excitatory synaptic function: glutamate receptor subunits (NR2B and GluA2), receptor auxiliary subunits (CKAMP44 and Stargazin) and synaptic cell adhesion molecules (Neurologin, NGL1 and SynCAM1). Figure 11c depicts the tested proteins' names and C-terminal amino acid sequences.

Following co-expression of these most abundant synaptic PDZ ligands (for review see E. Kim and Sheng, 2004) and subsequent pull-down of MPP2, no co-precipitation for NR2B, GluA2, CKAMP44, Stargazin, Neurologin or NGL-1

was observed (Figure 11d). Additional co-IP experiments, utilising full-length constructs of the central AMPA receptor complex proteins GluA1 and GluA2 (two different AMPA receptor subunits) as well as Stargazin/TARP $\gamma$ 2 (an AMPA receptor auxiliary subunit), where no co-precipitation with MPP2 was found (data not shown), further support that MPP2 is not directly interacting with glutamate receptors or additional subunits.

However, with this experimental strategy the C-terminus of the synaptic transmembrane cell adhesion protein SynCAM1 could be identified as a specific PDZ ligand for MPP2, as among the PDZ ligands tested, only the SynCAM1 C-terminus co-purified efficiently upon MPP2 pull-down (Figure 11d). Moreover, when the C-terminus was mutated to alanine at positions 0 and -2, the co-precipitation was abolished, further confirming the specificity of this interaction and validating the Y2H screen results.

Among the amino acid sequences of the tested C-termini, SynCAM1 (like Nectin1, -3 and Cntnap2) is remarkably different from the other tested PDZ domain ligands: other than most of these established postsynaptic PDZ ligands, SynCAM1 shows a class II C-terminal PDZ ligand sequence harbouring two large aromatic residues at positions -1 (phenylalanine) and -2 (tyrosine).

Most importantly, this *in vitro* result was confirmed by co-IP of endogenous proteins from rat brain crude synaptosome preparations. Following pull-down with  $\alpha$ SynCAM1 antibody from the lysate, endogenous MPP2 was co-precipitated, as analysed by Western blot (Figure 11e), demonstrating that the previous results reflect a true and specific interaction between MPP2 and SynCAM1.

### **3.2.3.2 MPP2 co-localises with endogenous SynCAM1 at dendritic spines**

Next, to further support the biochemical interaction data, a putative co-localisation of MPP2 and SynCAM1 at postsynaptic sites was examined using immunohistochemical stainings and confocal microscopy. Primary rat hippocampal neurons were fixed at DIV 21 and stained for endogenous MPP2 and SynCAM1 with respective primary and secondary antibodies. In these neurons, signal for both proteins of interest is observable at dendritic spines, where they widely co-localise (Figure 11f), further supporting the idea that MPP2, as a novel postsynaptic scaffold protein is engaged in SynCAM1 binding at postsynapses of glutamatergic neurons.

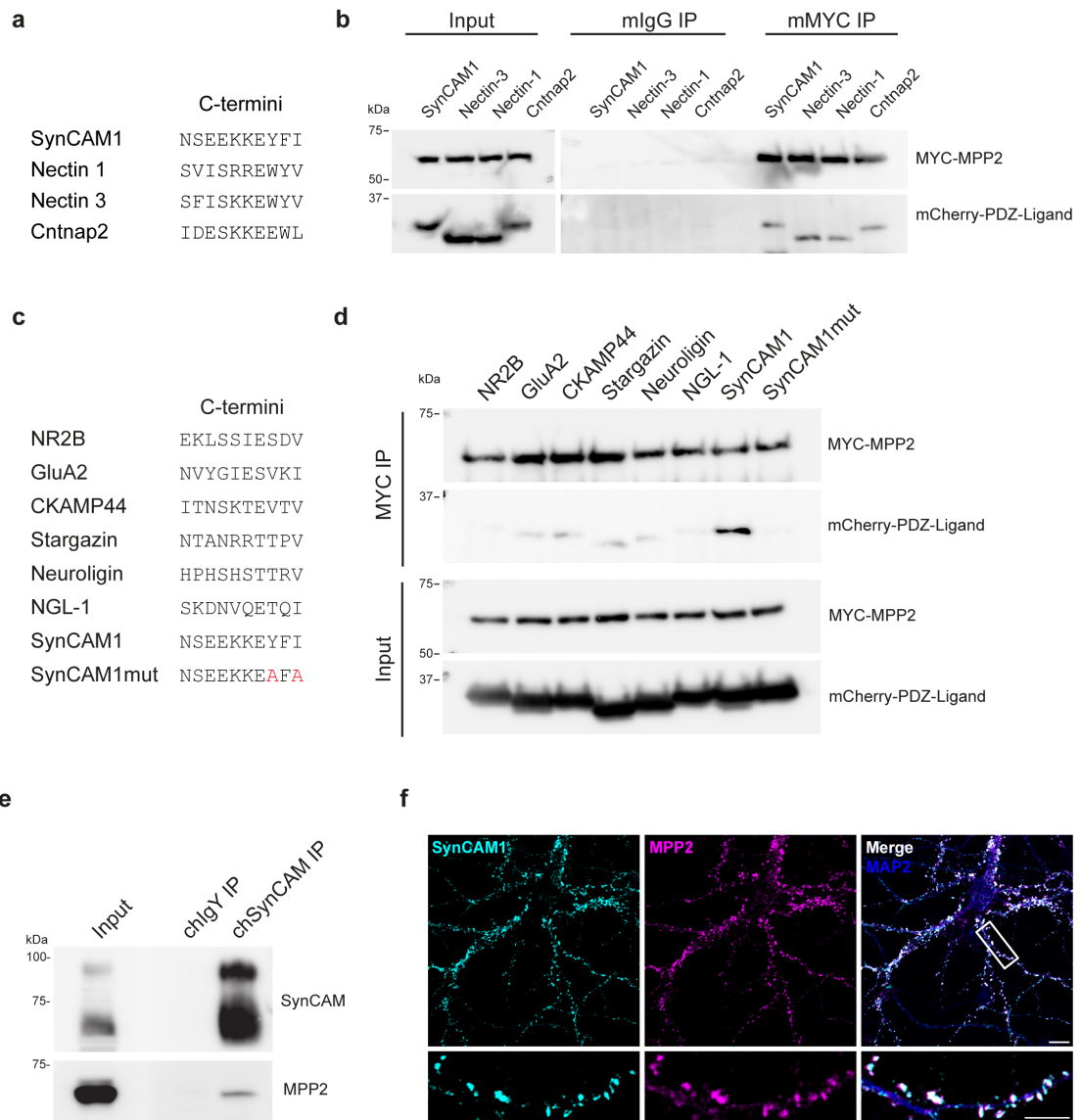


**Figure 11: MPP2 binds the C-terminus of the transmembrane cell adhesion protein SynCAM1.**

Targeted identification of putative MPP2 PDZ domain interactors: a) The ten C-terminal amino acids of the potential MPP2 PDZ domain ligands SynCAM1, Nectin-1, Nectin-3 and Cntnap2, which were identified in a Y2H screen, were fused to the monomeric mCherry tag and tested for interaction with MYC-tagged MPP2 in co-immunoprecipitation experiments. b) Following pull-down with  $\alpha$ MYC antibodies or normal mouse IgG as negative control, all tested ligands co-precipitated as detected by Western blot probed with  $\alpha$ MYC and  $\alpha$ HSVT antibodies. c) The ten C-terminal amino acids of common synaptic PDZ-ligand proteins were fused to the monomeric mCherry tag and d) tested for interaction with MYC-tagged MPP2 in co-immunoprecipitation experiments. Pull-down control (MYC-MPP2) and co-precipitated proteins (mCherry-PDZ-Ligand) were detected by Western blot (upper panels); input controls are shown below. e) Endogenous SynCAM1 was immunoprecipitated (using a chicken  $\alpha$ SynCAM1-Biotin antibody or chicken IgYs as a negative control) from a crude synaptosome preparation of adult rat brain. The co-precipitate contained MPP2, as detected by Western blot with antibodies to MPP2 (co-IP) or SynCAM1 (IP control). f) Cultured rat hippocampal neurons (E18) were fixed at DIV 21 and stained for endogenous SynCAM1, MPP2 and MAP2 (depicted together with merged image on the right). White box indicates the region selected for detailed image. Scale bars: overview = 10  $\mu$ m, detail = 5  $\mu$ m. Parts of this figure have been published (Rademacher\*, Schmerl\*, et al., 2016).

### 3.2.3.3 SynCAM1 binding is mediated by the PDZ domain of MPP2

Different proteins have been described to interact with the C-terminus of SynCAM1. Interestingly, however, these are not PDZ domain-mediated (Cheadle and Biederer, 2012). Thus, the identified interaction between MPP2 and SynCAM1 was further characterised to establish that it is dependent on the PDZ domain of MPP2.

Full-length SynCAM1 constructs with wildtype or mutated C-terminus (see again Figure 11c for C-terminal amino acid sequences) were generated, containing an HA-tag positioned N-terminally immediately after the signalling peptide that is cleaved from the protein upon transport (Biederer et al., 2002). In heterologous cells, wildtype or mutant HA-SynCAM1 were co-expressed together with either wildtype MYC-tagged MPP2 or a truncation construct consisting only of the SH3GK tandem domain, thus lacking the supposedly interacting PDZ domain (see also again Figure 8b, page 71 for construct overview). Following immunoprecipitation of SynCAM1 with  $\alpha$ HA antibodies, only wildtype MPP2 co-purified efficiently. Neither wildtype MPP2 co-precipitated with mutant SynCAM1, nor did the MPP2 SH3GK co-purify with wildtype SynCAM1 (Figure 12a). Using site-directed mutagenesis, a targeted point mutation of MPP2 within the PDZ domain binding pocket was created by exchanging histidine at position 150 for phenylalanine (H150F) and valine at position 170 for threonine (V153T), referred to as HFVT. When overexpressed together with wildtype HA-SynCAM1, this N-terminally EGFP-tagged H150F-V153T-MPP2 did not co-precipitate upon IP with  $\alpha$ HA antibody, in contrast to wildtype MYC- and EGFP-MPP2, which were efficiently co-purified (Figure 12b). In summary, these results clearly demonstrate that the C-terminus of SynCAM1 specifically interacts with the PDZ domain of MPP2.

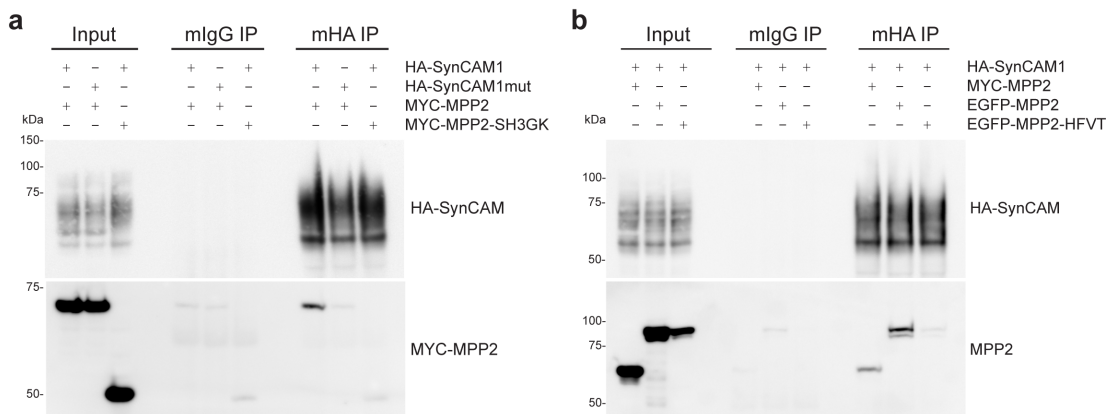


**Figure 12: The MPP2-SynCAM1 interaction is PDZ domain-dependent.**

a) Full-length HA-tagged SynCAM1 (HA-SynCAM1) and MYC-tagged MPP2 (MYC-MPP2), HA-tagged mutant SynCAM1 (HA-SynCAM1mut) and MYC-MPP2, or HA-SynCAM1 and

MYC-tagged MPP2 SH3-GK (MYC-MPP2-SH3GK) were co-expressed in CHL V79 cells and immunoprecipitated with  $\alpha$ HA (mHA IP) or mouse IgGs (mIgG IP) as a negative control. Pull-down controls are shown (HA-SynCAM1); co-precipitated proteins are detected by Western blot with  $\alpha$ MYC antibody below. This figure has been published (Rademacher\*, Schmerl\*, et al., 2016). b) Full-length HA-tagged SynCAM1 was overexpressed together with MYC- or EGFP-tagged full-length wildtype MPP2 or EGFP-tagged MPP2-HFVT double point mutation. Following immunoprecipitation with  $\alpha$ HA antibodies or normal mouse IgG as negative control, wildtype MPP2 was co-purified while HFVT did not co-precipitate as detected by Western blot with  $\alpha$ MPP2 and  $\alpha$ SynCAM1 antibodies.

### 3.2.3.4 MPP2 binds the SynCAM1 C-terminus with high affinity

Next, in collaboration with the Structural Biochemistry Research Group (AG Wahl) of the Institute for Biochemistry at Freie Universität Berlin, this novel interaction was further characterised, using isothermal titration calorimetry (ITC). This experiment is not only suitable to validate the finding of this novel interaction, but additionally provides insight to the binding affinity between the MPP2 PDZ domain and the SynCAM1 C-terminus.

Bacterially expressed MPP2 PDZ-SH3GK ('MAGUK core' PSG module) binds to the mCherry-fused C-terminus of SynCAM1 with a  $K_d$  of 3.1  $\mu$ M, whereas the mutated SynCAM1 (harbouring alanine substitutions at positions 0 and -2) did not bind at all (Figure 13).

Compared with other MAGUKs' PDZ domain ligand interactions (Li et al., 2014; Wei et al., 2015; Zeng et al., 2018), this might be considered a high-affinity binding, further supporting the idea that MPP2 is an important interacting scaffolding protein for the transmembrane cell adhesion molecule SynCAM1.

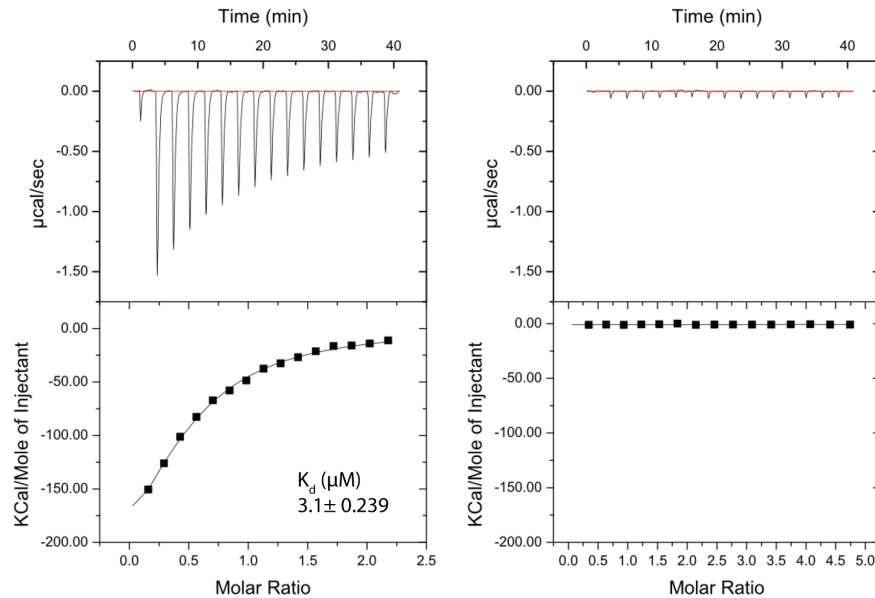


**Figure 13: Binding affinity of MPP2 and the C-terminus of SynCAM1.**

Isothermal titration calorimetry measurements with 350 nM mCherry-SynCAM1 and SynCAM1<sub>mut</sub>, respectively, injected to 55 µM MPP2-PSG module revealed a robust binding of the SynCAM1 C-terminus with a  $K_d$  of  $3.1 \pm 0.239$  µM (left panels). Results for the mutated SynCAM1 C-terminus control are shown on the right. This data was generated by Jennifer Lardong and is shown with permission. This figure and legend have been published (Rademacher\*, Schmerl\*, et al., 2016).

### 3.2.4 MPP2 and SynCAM1 are located at the border of the postsynaptic density

Using confocal imaging, which provides an optical resolution of 300 nm, endogenous MPP2 protein was observed at postsynaptic sites of cultured primary neurons, where it co-localised with its novel PDZ domain-ligand SynCAM1 (see again Figure 11f).

Studies on SynCAM1 at synapses applying super-resolution imaging techniques have found it tightly associated with the postsynaptic density, however, also mapped its localisation in form of clusters towards the periphery of the PSD, where it is potentially defining PSD size (Perez de Arce et al., 2015). Taken together with SynCAM1 binding to the MPP2 PDZ domain, this leads to the hypothesis that at synapses the scaffold protein MPP2 might be the structural element linking peripheral SynCAM1 with central components within the postsynaptic density.

#### 3.2.4.1 The sub-synaptic positioning of MPP2 is peripheral to PSD-95

To investigate how MPP2 might link peripheral SynCAM1 with central PSD-95, the localisation of these proteins within dendritic spines was analysed in collaboration with the Membrane Biochemistry Research Group (AG Ewers)

of the Institute for Biochemistry at Freie Universität Berlin, taking advantage of super-resolution imaging by using dual-colour *d*STORM imaging. Cultured primary hippocampal neurons were fixed at DIV 22 and stained for endogenous PSD-95, SynCAM1 and MPP2 with respective antibodies and subjected to *d*STORM imaging (Figure 14).

In line with previous studies (Perez de Arce et al., 2015), SynCAM1 clusters were observed positioned around a central postsynaptic density, as marked by staining for PSD-95. The analysed postsynaptic densities (mean diameter 448 nm  $\pm$  SD 105 nm) were surrounded by clusters of SynCAM1 protein that appeared like beads of a bracelet (Figure 14a), similar to what has been observed for MPP2 before (see again Figure 5b on page 67). These bracelet-like arrangements had an average diameter of 894 nm (mean  $\pm$  SD 162 nm) and delineated the edge of the PSD as determined by PSD-95, what is in line with published data (Perez de Arce et al., 2015). Manual analysis categorising synapses that were apparent in corresponding widefield and *d*STORM images revealed that 68% of all synapses exhibited such a bracelet-like arrangement of SynCAM1 clusters surrounding a PSD.

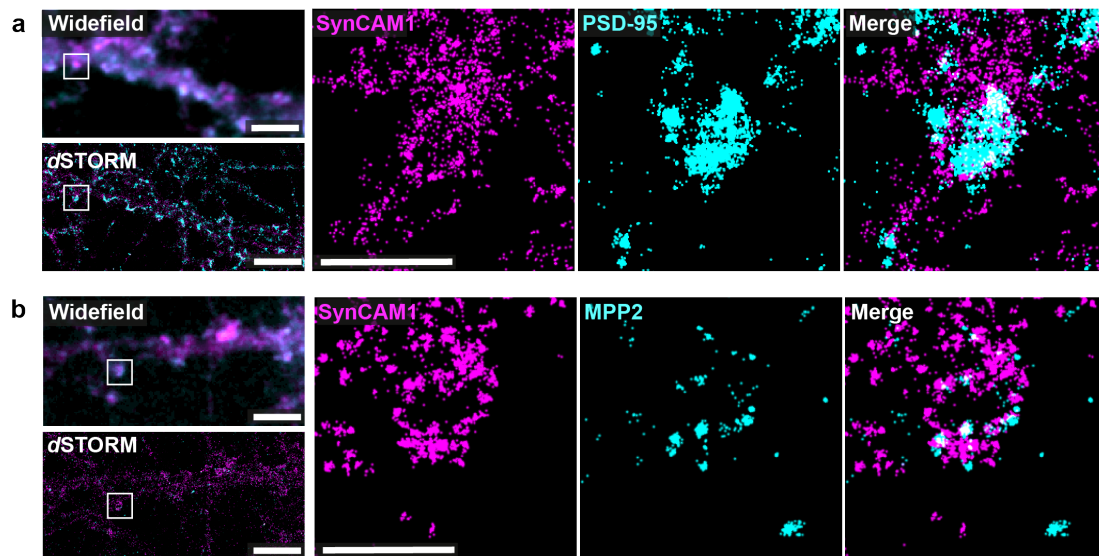


**Figure 14: Nanoclusters of SynCAM1 and MPP2 surround the postsynaptic density**

E18 rat hippocampal neurons were fixed at DIV 21 and subjected to immunostaining for endogenous SynCAM1, PSD-95 and/or MPP2 proteins followed by dual-colour *d*STORM imaging. Localisations were filtered according to precision estimates based on the Thompson method (Thompson et al., 2002), i.e. all localisations with localisation precision worse than 20 nm were excluded. Localisations were rendered as Gaussian distributions with a constant width of 20 nm. a) Corresponding widefield (left, top) and *d*STORM (left, bottom) images of a neuronal dendrite stained for endogenous SynCAM1 and PSD-95. White box indicates location of the detail view of the individual synapse enlarged in the right panels. Clusters of SynCAM1 (magenta) are arranged in a bracelet-like fashion surrounding postsynaptic densities marked

by PSD-95 (cyan). b) Corresponding widefield (left, top) and *d*STORM (left, bottom) images of a neuronal dendrite stained for endogenous SynCAM1 and MPP2. White box indicates the location of the detail view of the individual synapse enlarged in the right panels. Adjacent protein clusters of SynCAM1 (magenta) and MPP2 (cyan) form a bracelet-like arrangement at post synaptic sites. See again Figure 5b on page 67 for *d*STORM images of MPP2 together with PSD-95). Scale bars: overview = 5  $\mu\text{m}$ ; detail = 1  $\mu\text{m}$ . These data were acquired in collaboration with Jakob Rentsch.

Subsequently, primary neurons were stained for MPP2 and SynCAM1 together to examine how the individually observed nanoclusters are positioned in relation to each other. Examination of endogenous SynCAM1 together with MPP2 shows that at postsynaptic sites multiple small clusters of both proteins are arranged together almost alternating upon forming a bracelet-like structure, however, with only minor overlap with each other (Figure 14b). Unfortunately, by using dual-colour *d*STORM it was not possible to combine the staining of MPP2 and SynCAM1 with an additional marker of the postsynaptic density. However, synapses were identified based on a widefield reference and again manual categorisation of the cluster arrangements into bracelet-like and non-bracelet-like accounted the prevalence of these MPP2 and SynCAM1 bracelets to approximately 70% of all synapses, what is in accordance with the prevalence observed for MPP2 and SynCAM1 in combination with PSD-95.

A major advantage of the used dual-colour *d*STORM imaging is the great spatial resolution of up to 20 nm it provides. However, to examine whether these rather qualitative observations of bracelet-like SynCAM1 and MPP2 cluster arrangements in selected synapses are indeed representative, an efficient quantitative super-resolution approach was necessary.

#### **3.2.4.2 Quantitative super-resolution imaging and analysis of synaptic proteins and MPP2**

Despite providing less spatial resolution compared to dual-colour *d*STORM imaging, structured illumination microscopy (SIM) inherently generates three-dimensional data and allows for easy multi-channel application. To evaluate whether the slightly lower resolution provided by SIM is sufficient to resolve the bracelet-like arrangement of MPP2 and SynCAM1 clusters surrounding PSDs, fixed primary neurons were subjected to four-colour immunostaining and SIM imaging, performed in collaboration with Dr. Niclas Gimber (AG Schmoranzer) and the Advanced Medical Bioimaging Core Facility (AMBIO) at Charité - Universitätsmedizin Berlin.

As shown in Figure 15a, depicting a maximum projection of a dendrite segment (first row) and detail view of a single synapse (second row), SIM proved sufficient

to resolve the observed bracelet-like arrangements of SynCAM1 and MPP2 protein surrounding postsynaptic densities. Clusters of PSD-95 (Figure 15a, blue, second column), the most abundant scaffold protein within the postsynaptic density of glutamatergic synapses, was positioned centrally to a bracelet-like - almost alternating - arrangement of MPP2 and SynCAM1 puncta (Figure 15a, green, third column and red, fourth column, respectively). The three-dimensional imaging data allowed for creation of a 3D rendering, which further indicates that a central postsynaptic density is surrounded by a bracelet-like structure of MPP2 and SynCAM1 clusters in a planar fashion (Figure 15a, third and fourth row). This is in line with the idea that the transmembrane cell adhesion protein SynCAM1 is positioned in the synaptic membrane and located to the periphery of the synaptic cleft, where it might be involved in delineating PSD size (Perez de Arce et al., 2015).

Next, taking advantage of a semi-automatic image segmentation sequence implemented in Arivis Vision 4D software, images were segmented and object counts and sizes, as derived from the segmented volume information, were assessed quantitatively. In accordance with the previous *d*STORM images and published data (Perez de Arce et al., 2015) this analysis revealed PSD-95 cluster radii over a range of expected sizes (Figure 15b, upper graph, blue). Similarly and in line with the previous *d*STORM results, the average cluster sizes for MPP2 and SynCAM1 are much smaller, in average under 100 nm in radius (Figure 15b, middle panel, green and bottom panel, red). Using the same segmentation pipeline demonstrated that most, i.e. more than 90%, of the imaged synapses indeed contain all three proteins of interest.

Following a quantitative assessment of the sub-synaptic protein distribution, the three-dimensional radial intensity profiles of PSD-95, MPP2 and SynCAM1 in relation to PSD-95 clusters were measured. The central coordinate of PSD-95 clusters, as determined by the semi-automated segmentation, served as the starting point for this analysis (see inlet in Figure 16a). PSD-95 as a central postsynaptic scaffold protein is a well-established marker of the PSD and its relative co-localisation with a presynaptic marker (vGlut1 that was used as criterion for the segmentation procedure) is an indicator for mature and functional synapses. Consistent with reported sizes of the PSD and the previously discussed dual-colour *d*STORM data, the 3D radial intensity profile of PSD-95 immunofluorescence is highest at the PSD centre and drops at a radial distance of 250-300 nm (Figure 16a, blue curve).

In contrast, SynCAM1 immunofluorescence is low at the PSD centre and increases to its highest values at the PSD edge as derived from the steep decrease in PSD-95 intensity. This difference in PSD-95 and SynCAM1 distribution is in line with reported data suggesting that SynCAM1 is involved in defining the edge of the PSD (Perez de Arce et al., 2015).

Interestingly, the distribution of MPP2 immunofluorescence reflects that of SynCAM1 in that there is little signal within the postsynaptic density (at radial distances below 250 nm) while the highest values are measured towards the PSD border (Figure 16a, red and green curves).

This quantitative assessment further validates the previous qualitative super-resolution data suggesting that MPP2 and SynCAM1 are distributed together at the periphery of the postsynaptic density.

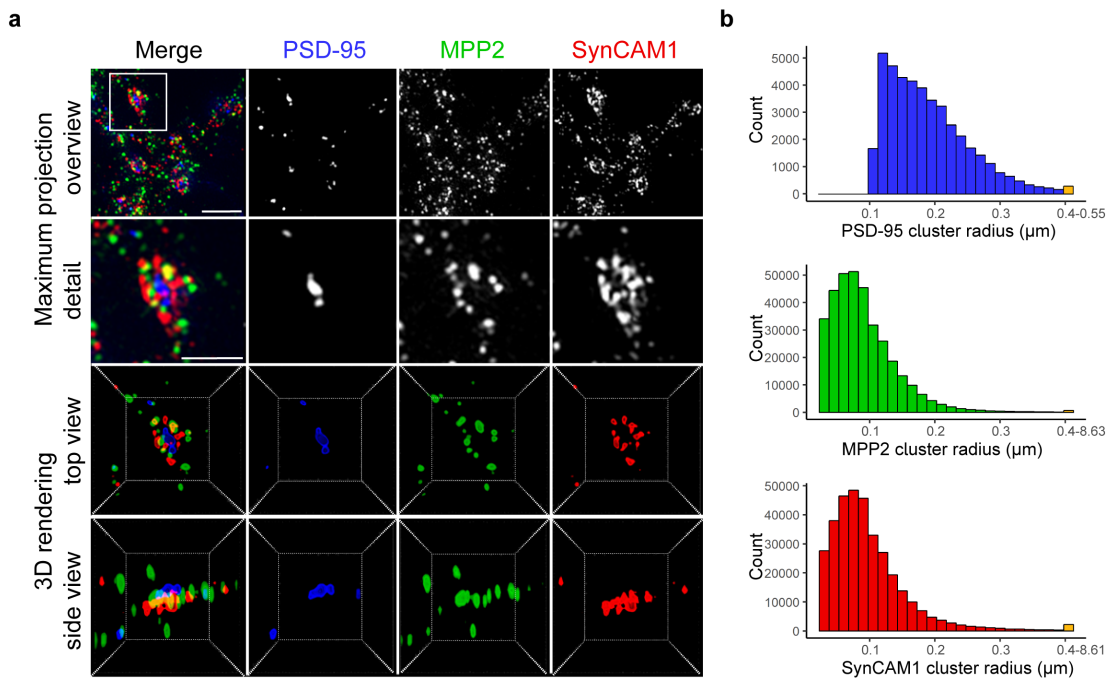


**Figure 15: Clusters of MPP2 and SynCAM1 form bracelet-like arrangements at the PSD edge.**

Mature (DIV 21) primary rat hippocampal neurons immunostained for endogenous PSD-95 (blue, second column), MPP2 (green, third column) and SynCAM1 (red, fourth column) and subjected to 3D structured illumination microscopy (3D SIM). a) More than 90% of the imaged dendritic spines express all three proteins of interest (overview maximum projection, first row). A single synapse detail (second row) depicts the bracelet-like arrangements of MPP2 and SynCAM1 surrounding central PSD-95 puncta. A 3D rendering of that particular synapse in top (third row) and side view (fourth row) reveals that SynCAM1 and MPP2 clusters are arranged in an interlocked, bracelet-like form, surrounding a central cluster of PSD-95. Scale bars: overview = 1  $\mu\text{m}$ ; detail = 1  $\mu\text{m}$ . 3D rendering box size = 2.8  $\mu\text{m}$ . b) Histograms illustrating the distribution of protein cluster sizes for PSD-95 (top, blue), MPP2 (middle, green) and SynCAM1 (bottom, red). Indicated radii were calculated based on extracted cluster volumes, assuming a spherical shape. The final bin in each histogram contains summarised data for cluster sizes greater than 400 nm. Histograms reflect clusters associated with 40,000 synapses (in 50 images from  $N = 3$  independent experiments). This data was generated in collaboration with Dr. Niclas Gimber. These figures and legend have been published as preprint (Schmerl et al., 2020).

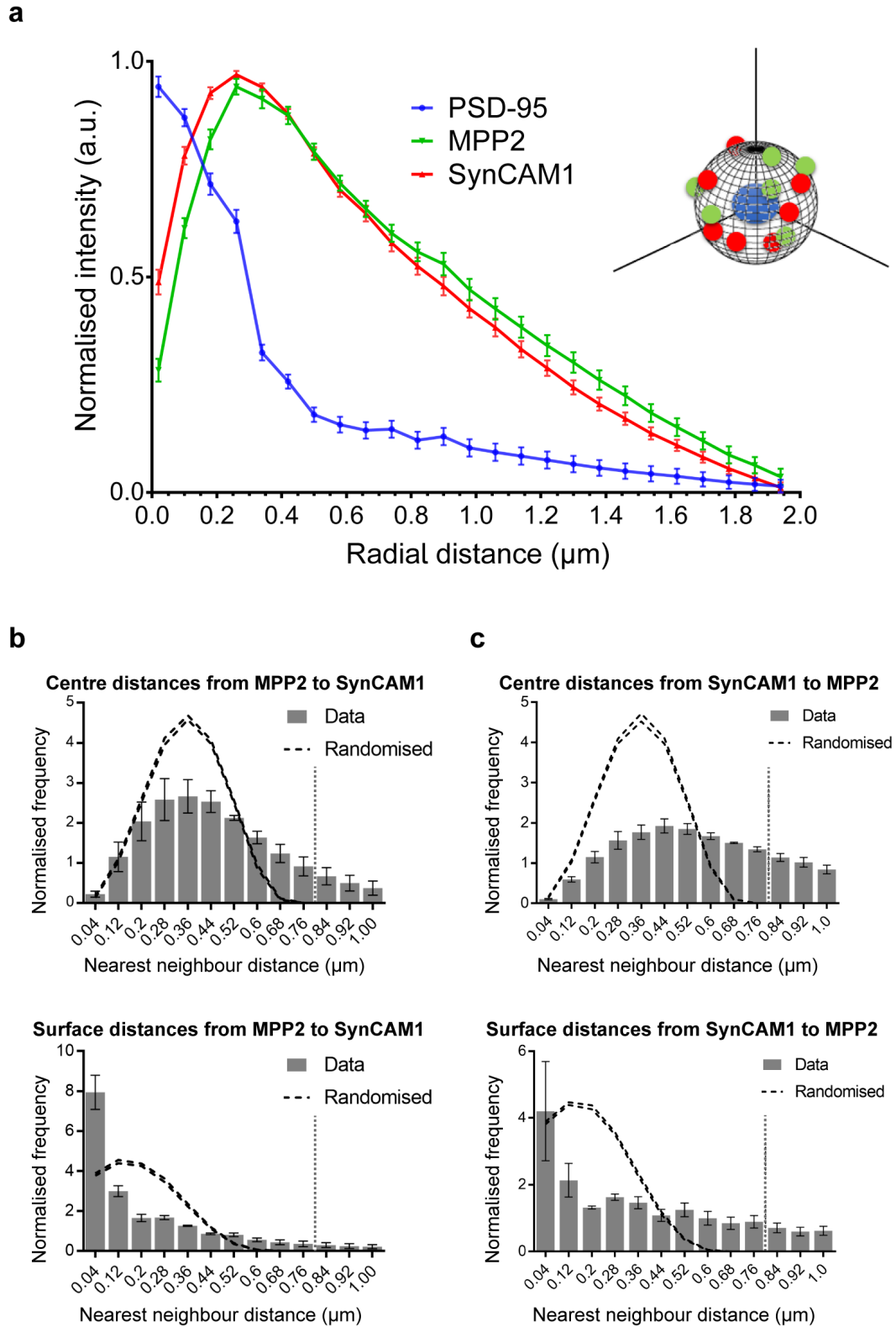


**Figure 16: Quantitative analysis of MPP2 and SynCAM1 positioning at the PSD periphery.**

a) 3D radial intensity profiles of PSD-95, MPP2 and SynCAM1 signals in relation to the centres of PSD-95 clusters. Plot shows averaged normalised mean  $\pm$  SEM from three independent experiments ( $\sim 40,000$  synapses from 50 images). For details on the analysis, please see the Materials and Methods. Inlet illustrates that the geometrical centre of a PSD-95 cluster served as starting coordinate for the three-dimensional radial profile analysis. b,c) Nearest neighbour

(NN) analysis of MPP2 and SynCAM1 protein clusters after 3D segmentation. b) NN distances from MPP2 to the nearest SynCAM1 cluster were calculated between cluster centres (top) and cluster surfaces (bottom). Dashed lines represent the upper and lower envelopes of complete spatial randomness (CSR). CSR was calculated by randomly distributing MPP2 within the volume and SynCAM1 on the surface of spheres of 0.8  $\mu\text{m}$  diameter as indicated by the grey dotted line (mean  $\pm$  SEM, 95% confidence interval, 10 simulations per synapse,  $N = 3$  independent experiments,  $\sim 40,000$  synapses from 50 images). c) NN analysis in the reverse direction. These figures have been published as preprint (Schmerl et al., 2020).

### **3.2.4.3 Clusters of MPP2 and SynCAM1 are distinctly localised to the PSD periphery**

Quantitative analysis of super-resolution imaging data has validated that MPP2 and SynCAM1 are positioned likewise at the PSD border. However, the 3D radial profile analysis does not provide information whether clusters of these two proteins overlap and co-localise significantly or whether they are organised rather adjacent to each other, as suggested by the super-resolution imaging data.

To address this question, in collaboration with Dr. Niclas Gimber (AG Schmoranzner) and the Advanced Medical Bioimaging Core Facility at Charité - Universitätsmedizin Berlin, a nearest neighbour (NN) analysis was performed, which interrogates nanoscale distances between any cluster of the three proteins of interest to the closest neighbouring protein cluster. Given, that PSD-95, MPP2 and SynCAM1 were observed in a tight arrangement, this analysis was performed in two modes, assessing distances from centre-to-centre as well as from surface-to-surface for each three-dimensional object.

Having established with diverse imaging strategies and analyses that PSD-95-labelled PSDs are surrounded by smaller clusters of SynCAM1 and MPP2, the next important question to ask was how clusters of SynCAM1 and MPP2 relate to each other. Hence, NN analysis was applied to investigate the interconnection of SynCAM1 and MPP2 regarding their centre-to-centre and surface-to-surface cluster distances. In line with the previously presented data, NN distances between centres of MPP2 and SynCAM1 clusters are mostly 200 nm - 500 nm (Figure 16b, top). These distances are well above the resolution limit offered by SIM and therefore further support that MPP2 and SynCAM1 are distinctly localised around the PSD. The reversely directed analysis (Figure 16c, top) reveals roughly the same distribution of NN distances; however, it is slightly broader, likely due to the broader distribution on SynCAM1 being less restricted to dendritic spines compared to MPP2. Moreover, taking the extracted cluster volumes into account (see again Figure 15b), it is apparent that the average centre-to-centre NN distances correspond to the sum of both proteins' average cluster radii.

Analysis of the NN distances between MPP2 and SynCAM1 cluster surfaces pro-

vides further evidence that the two proteins are positioned juxtaposed at the PSD periphery. Most cluster surfaces are at a distance of less than 100 nm (Figure 16c, bottom). Again, analysing the reverse direction (measuring from a given SynCAM1 to the nearest MPP2 cluster) indicates a slightly broader distribution of NN distances (Figure 15c, bottom), likely reflecting the differences in distribution of the two proteins within the dendrite.

### **3.3 Interactions of the MPP2 SH3GK tandem domain**

#### **3.3.1 Differential interactomes of MPP2 and PSD-95**

A combined super-resolution imaging approach allowed to demonstrate a distinct localisation of clusters of MPP2 and PSD-95 in relation to PSD centres, where PSD-95 is a central element while MPP2 and its PDZ domain ligand, the transmembrane cell adhesion molecule SynCAM1, are located to the edge of the PSD. This arrangement suggests that further differences in the interaction specificities of MPP2 and PSD-95 must exist to realise their different positioning. One obvious aspect here are the different interaction specificities of the MPP2 and PSD-95 PDZ domains: MPP2 binds to the C-termini of peripheral transmembrane proteins such as SynCAM1 as opposed to central synaptic proteins like Stargazin which is a PSD-95 ligand.

In addition to the typical PDZ domain as part of the characteristic ‘MAGUK core’, PSD-95 and MPP2 contain an SH3GK tandem domain at their C-terminus (Figure 17a), which also mediates the proteins’ scaffolding function (McGee et al., 2001). Interestingly, the MAGUK protein GK domain is an inactive guanylate kinase and no longer shows classical GTP/GMP binding activity, but instead has developed into an important protein interaction domain (Zhu et al., 2011). The SH3 and GK domains of MAGUKS have been found to be engaged in an intramolecular interaction, which is well characterised and moreover involved in the formation and regulation of multi-protein complexes (Zeng et al., 2018; Rademacher et al., 2019). Several specific interaction partners for the SHGK module of PSD-95 have been identified and characterised, however, no specific binders to this region of MPP2 have been described yet.

Taking advantage of a comparative and quantitative proteomics approach, in collaboration with Dr. Benno Kuroopka from the Protein Biochemistry Research Group (AG Freund) at Freie Universität Berlin, putative differences among the interactomes of MPP2 and PSD-95 were analysed in order to evaluate the hypothesis that these proteins orchestrate different protein complexes. Such differences in turn may be responsible for the distinct sub-synaptic protein localisations observed for these proteins.

The SHGK modules of MPP2 and PSD-95 were fused to an N-terminal GST-tag and expressed in bacteria. In a GST pull-down from a crude brain synaptosome preparation, interacting proteins were eluted from the beads and separated by SDS PAGE. Subsequently, proteins were subjected to tryptic in-gel digestions and thus enzymatic  $^{16}\text{O}/^{18}\text{O}$ -labelling and relative quantification by nanoLC-MS/MS analysis. This experiment was performed in two replicates with switched labels (in replicate A, MPP2 interacting proteins were labelled with the  $^{16}\text{O}$  isotope and PSD-95 interactors with  $^{18}\text{O}$ ; vice versa in replicate B, see also Figure 17b for experimental design overview), and in total 188 proteins were reproducibly identified and quantified, i.e. were found in both replicates and passed a threshold of at least two peptides and a geometric standard deviation  $<2$ . Of these proteins, 83% have been previously identified in postsynaptic density preparations from human and/or murine tissue (Bayes et al., 2012), what emphasises the validity of this approach.

Figure 17c shows all 188 proteins plotted according to their enrichment normalised to GST in the first (Figure 17c, X-axis) and second (Figure 17c, Y-axis) replicate; proteins that are either background (not entirely washed off the beads) or not specifically enriched in the GST-MPP2- nor GST-PSD-95 SH3GK pull-down score at ratios around  $\sim 1$ . In contrast, proteins in the first quadrant were enriched upon pull-down of GST-PSD-95-SH3GK, and proteins enriched in the third quadrant with the GST-MPP2 SH3GK pull-down (Figure 17c).

The facts that proteins in the first quadrant include well-established PSD-95 interacting proteins like Map1a, MeCP2, CaMKII and Fxr1 (see Figure 17c), together with the absence of classical PDZ domain ligands (like e.g. NMDA receptor subunits or SynCAM1 as MPP2 PDZ ligand, one would not expect as the MAGUK PDZ domain was purposefully not included) further support the reliability and specificity of this proteomics approach.

Quite interestingly, several of the proteins identified in the MPP2-SH3GK pull-down can be assigned to certain superordinate groups: proteins that are associated with guanine-nucleotides (e.g. GTPB1, GTP binding protein; AGAP2, ARF-GAP with GTPase; Arhgef2, ANK repeat and PH domain-containing protein 2, GEF, Rho/Rac Guanine Nucleotide Exchange Factor 2; Gnao1, guanine nucleotide-binding protein G(o) subunit alpha 1 and FARP1, FERM, ARH/RhoGEF and Pleckstrin Domain Protein 1) and cytoskeleton-associated and/or regulatory proteins (e.g. band 4.1-like protein; Septin-7 and -11, which are also GTPases; MAP4, microtubule-associated protein 4; MTAP2, microtubule-associated protein; multiple tubulin isoforms; Mark-1 and -2, microtubule-affinity regulating serine/threonine-protein kinase; DCKL1 and -2, doublecortin-like ki-

nase, serine/threonine-protein kinase). For more information see source data in Schmerl et al. (2020).

Importantly, this proteomics approach also identifies protein complex members which are only indirectly associated with MPP2, thus individual interactions need further targeted validation. Nonetheless, functional clustering of these identified proteins adds to the idea that MPP2 functions as a connector of membrane-bound cell adhesion factors to cytoskeleton elements, suggesting an important role in synaptic structure dynamics.

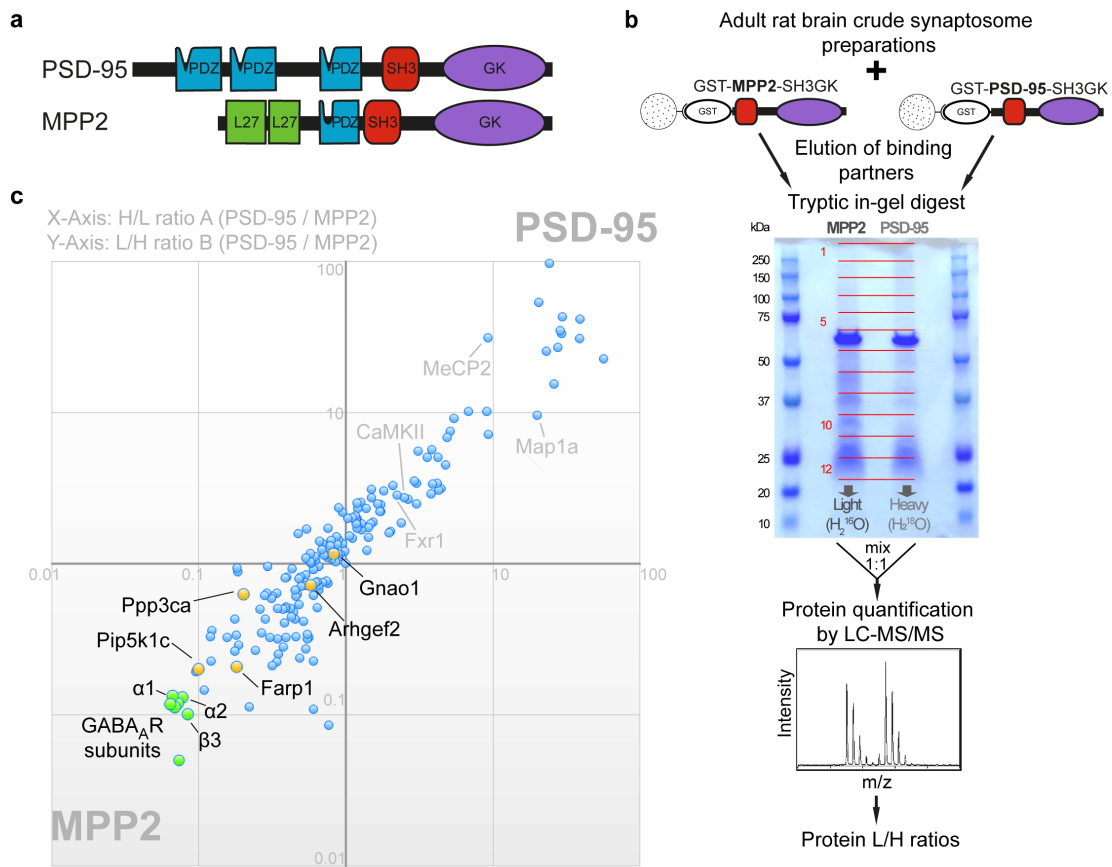


**Figure 17: Identification of interactors that differentially bind to the C-terminal SH3GK modules of MPP2 and PSD-95.**

a) Schematic domain structures of PSD-95 and MPP2 drawn to scale and aligned by their central PDZ domain. Both proteins contain two N-terminal domains (PDZ1+PDZ2 for PSD-95 and two L27 domains for MPP2) in addition to the C-terminal ‘MAGUK core’ domains PDZ-SH3-GK. Note the differences in the length of the ‘linker’ between PDZ and SH3 domain and of the ‘hook’ between SH3 and GK domains. b) Schematic representation of the quantitative LC-MS/MS experiment using  $^{16}\text{O}/^{18}\text{O}$ -labelling to identify differential interactors from adult rat brain crude synaptosomal preparations by GST pull-down of bacterially expressed GST-MPP2-SH3GK or GST-PSD-95-SH3GK. c) GST pull-downs were performed in duplicates with inverted labelling and 188 interacting proteins were identified and quantified by mass spectrometry passing the threshold settings. PSD-95 / MPP2 protein ratios from both replicates A and B (normalised to the ratio of GST) are plotted against each other. Proteins in the first quadrant indicate preferential enrichment to PSD-95 (ratios  $\gg 1$ ), while proteins in the third quadrant indicate preferential enrichment to MPP2 (ratios  $\ll 1$ ). Proteins with ratios of  $\sim 1$  show no preferential binding, and thus reflect equal binding to both baits or background proteins that were not fully removed by the washing steps. Selected novel potential interaction partners were validated by

co-IP (yellow, see also Figure 19). The most significantly enriched proteins to the GST-SH3GK construct of MPP2 (green cluster) are seven different GABA<sub>A</sub> receptor subunits, of which  $\alpha$ 1,  $\alpha$ 2 and  $\beta$ 3 have been validated for direct interaction with MPP2 (see also Figure 20). This data was generated by Dr. Nils Rademacher and Dr. Benno Kuroepka and is shown with permission. For further detail also see Table 3.2 and Source Data in Schmerl et al. (2020). This figure and legend have been published as preprint (Schmerl et al., 2020).

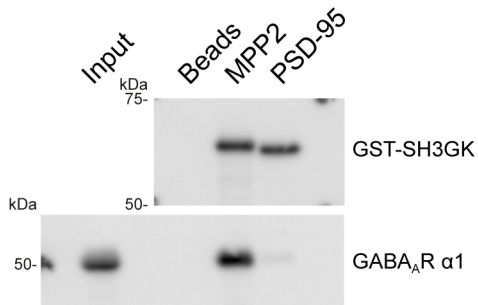


**Figure 18: GABA<sub>A</sub> R  $\alpha$ 1 differentially binds with higher affinity to MPP2 than PSD-95.**

Bacterially expressed GST-MPP2-SH3GK and GST-PSD-95-SH3GK were incubated with crude brain synaptosome preparations. After GST pull-down, compared to bead control, GABA<sub>A</sub> R  $\alpha$ 1 was efficiently enriched in the GST-MPP2-SH3GK pull-down, as detected by Western blot with  $\alpha$ GABA<sub>A</sub> R  $\alpha$ 1 and  $\alpha$ GST antibodies. This data was generated by Dr. Nils Rademacher and is shown with permission.

supports the validity of this approach to investigate differential interactomes of structurally related synaptic proteins.

### 3.3.2 Novel specific interactors for the MPP2 SH3GK tandem domain

Given the validity of these qualitative and quantitative mass spectrometry data regarding PSD-95-SH3GK interacting proteins, the consistently enriched proteins in the MPP2 pull-down comprise putative novel synaptic and specific interactors for the MPP2 SH3GK tandem domain. Moreover, most proteins enriched in the MPP2 pull-down have indeed been reported in postsynaptic density preparations before (Bayes et al., 2012), further supporting the idea that MPP2 is a scaffold protein with an important role at synapses.

The next aim was to validate several of these potential novel interactions to gain further insight into the protein complex composition that is associated with MPP2 scaffolds. Multiple proteins across the whole range of enrichment with MPP2

Unexpectedly, a cluster of seven different GABA<sub>A</sub> receptor subunits constituted the proteins that were most efficiently enriched with the SH3GK tandem domain of MPP2. A representative GABA<sub>A</sub> receptor subunit was selected to confirm the differential affinity of the newly identified interaction partners.

In comparative GST pull-down experiments from crude synaptosome preparations with GST-MPP2-SH3GK and GST-PSD-95-SH3GK, respectively, the endogenous GABA<sub>A</sub> R  $\alpha$ 1 subunit was identified in the MPP2 SH3GK pull-down, but not that of PSD-95 (Figure 18a). This result not only validates one of the putative novel interactors for the SH3GK module of MPP2, but also

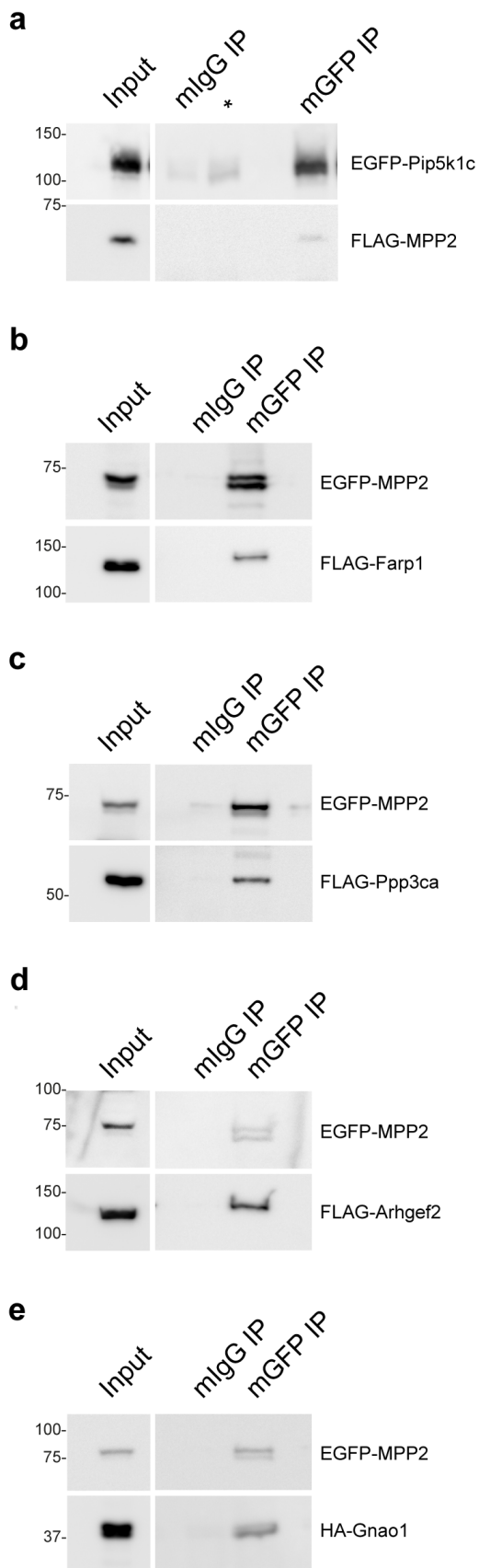


**Figure 19: Validation of novel interaction partners by co-IP.**

a) EGFP-tagged Pip5k1c was co-expressed with FLAG-tagged MPP2 in HEK293T cells. EGFP-Pip5k1c was precipitated with  $\alpha$ GFP antibody or normal mouse IgG as negative control and analysed by Western blot with  $\alpha$ FLAG and  $\alpha$ GFP antibodies. An additional IgG control lane is marked with an asterisk.

b) FLAG-tagged Farp1 was overexpressed together with EGFP-tagged MPP2 and co-purifies with  $\alpha$ GFP pull-down, as opposed to normal mouse IgG as negative control. Co-IP was detected by Western blot probing with  $\alpha$ FLAG and  $\alpha$ GFP antibodies.

c) Co-purification of FLAG-tagged Ppp3ca (a Calcineurin subunit) overexpressed together with EGFP-MPP2 after  $\alpha$ GFP pull-down or normal mouse IgG as negative control, detected by Western blot with  $\alpha$ FLAG and  $\alpha$ GFP antibodies.

d) Co-IP of FLAG-tagged Arhgef2 together with EGFP-MPP2 after pull-down with  $\alpha$ GFP antibody or IgG control, as detected by Western blot using  $\alpha$ FLAG and  $\alpha$ GFP antibodies.

e) HA-tagged Gnao1 was overexpressed together with EGFP-tagged MPP2 in HEK293T cells. Upon pull-down with Ms  $\alpha$ GFP antibody or normal mouse IgG, Gnao1 co-purification and GFP pull-down control were detected by Western blot with  $\alpha$ HA and  $\alpha$ GFP antibodies.

(protein ratios towards 0 being the most significant enriched with MPP2, while ratios  $\sim 1$  suggest no preferential binding with MPP2 or PSD-95) were selected for further study. Upon co-expression with EGFP-MPP2 in heterologous cells and immunoprecipitation experiments, several proteins were successfully co-purified and thus multiple direct interactions were confirmed (see Figure 19 and Table 3.2 for overview). These comprised membrane-associated synaptic proteins like Farp1 and Pip5k1c and proteins involved in synaptic signalling cascades like Ppp3ca (a Calcineurin subunit), the highly abundant brain membrane protein Gnao1 and Arhgef2 (J. Wang et al., 2003; Kang et al., 2009; Danti et al., 2017). Together with previous experiments related to different research projects, where no interaction e.g. between Arhgef2 and PSD-95 could be shown (Dr. Nils Rademacher, personal communication), these data provide valuable insight how the MPP2 and PSD-95 interactomes relate to each other. In addition to the validated interactions summarised in Table 3.2, also other potential interactions were tested, e.g. Mark1 and Clasp2, however, a direct interaction could not be demonstrated with initial co-immunoprecipitation experiments (data not shown) and was not further explored. This could be attributed to the fact that in such proteomics approaches protein complexes rather than only individual isolated interactions partners are being identified.

Of particular interest, not only Ppp3ca (a subunit of the calcium-dependent, calmodulin-stimulated protein phosphatase Calcineurin), which is known to influence GABA<sub>A</sub> receptor-mediated signalling, was enriched in the MPP2-SH3GK pull-down and confirmed to directly interact with MPP2. Most importantly, the proteins enriched with the highest protein ratios (all below 0.13 in both replicates) comprise a cluster of GABA<sub>A</sub> receptor subunits (Figure 17c, green cluster).

**Table 3.2: Overview of validated novel interaction partners for MPP2**

For co-immunoprecipitation data please see Figure 19 and Figure 20.

Name	Uniprot Accession ID	Description	Remarks
GABA <sub>A</sub> R $\beta$ 3	GBRB3_RAT	Gamma-aminobutyric acid receptor subunit beta-3	Representative brain expressed GABA <sub>A</sub> receptor subunit from the $\beta$ family
GABA <sub>A</sub> R $\alpha$ 1	GBRA1_RAT	Gamma-aminobutyric acid receptor subunit alpha-1	Predominant GABA <sub>A</sub> receptor subunit in the brain
GABA <sub>A</sub> R $\alpha$ 2	GBRA2_RAT	Gamma-aminobutyric acid receptor subunit alpha-2	Common GABA <sub>A</sub> receptor subunit in multiple brain tissues
Pip5k1c	PI51C_RAT	Phosphatidylinositol 4-phosphate 5-kinase type-1 gamma	Binds to FERM domains, activated by Rho / Rho GEF signalling
Farp1	FARP1_RAT	FERM, ARHGEF and pleckstrin domain-containing protein 1	SynCAM interactor
Ppp3ca	PP2BA_RAT	Serine/threonine-protein phosphatase 2B catalytic subunit alpha isoform	Calcineurin subunit and known GABA <sub>A</sub> R interactor
Arhgef2	ARHG2_RAT	Rho guanine nucleotide exchange factor 2	Interacts with AMPA receptors
Gnao1	GNAO_RAT	Guanine nucleotide-binding protein G(o) subunit alpha	Transducer in transmembrane signalling systems

### 3.4 MPP2 interacts with GABA<sub>A</sub> receptors at excitatory synapses

#### 3.4.1 MPP2 binds multiple GABA<sub>A</sub>R subunits

Unexpectedly, the proteins most significantly enriched in the GST-MPP2-SH3GK pull-down made up a group of seven different  $\gamma$ -aminobutyric acid (GABA) type A receptor subunits (highlighted in green in Figure 17c; see also Table 3.2). These seven subunits, namely  $\alpha 1$ ,  $\alpha 2$ ,  $\alpha 4$ ,  $\beta 1$ ,  $\beta 2$ ,  $\beta 3$ , and  $\delta$ , together are able to form functional GABA<sub>A</sub> receptors, which are typically composed of hetero-pentameric combinations of these subunits (Barrera et al., 2008; Patel et al., 2014). The subunit composition of GABA<sub>A</sub> receptors has been demonstrated to vary between receptors at different location in neurons (H. Shen et al., 2010) and influence receptor kinetics (Chang et al., 1996).

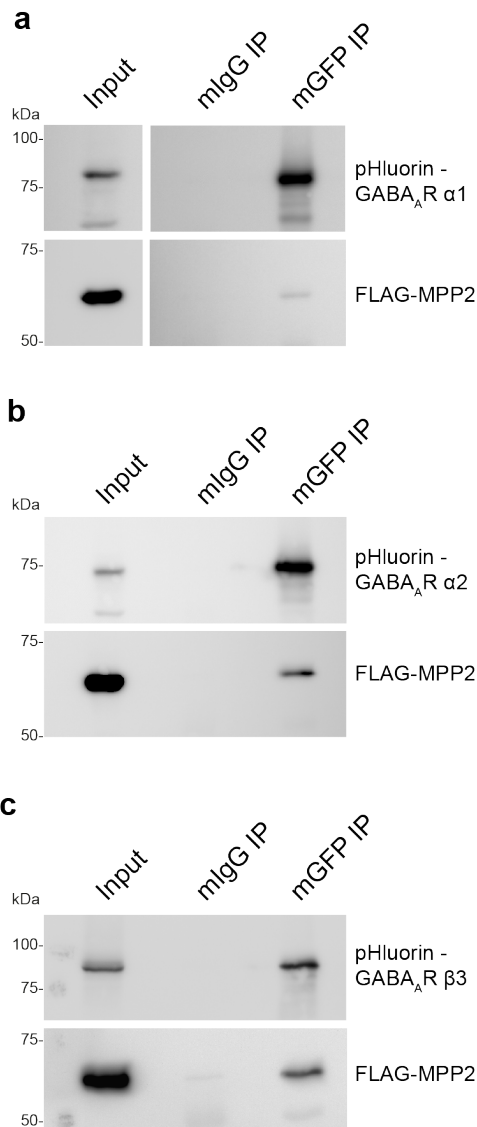


**Figure 20: Multiple GABA<sub>A</sub> receptor subunits directly interact with MPP2.**

GABA<sub>A</sub> receptor subunit constructs with an N-terminal pFluorin were acquired from addgene and expressed in CHL V79 cells together with N-terminally FLAG-tagged MPP2. Pull-down of a) GABA<sub>A</sub>R  $\alpha 1$  b) GABA<sub>A</sub>R  $\alpha 2$  and c) GABA<sub>A</sub>R  $\beta 3$  with  $\alpha$ GFP or normal mouse IgG resulted in co-precipitation of FLAG-MPP2 as detected by Western blot with  $\alpha$ FLAG-HRP and  $\alpha$ GFP antibodies. This data as shown was generated by Dr. Stella-Amrei Kunde (a,b) and Judith von Sivers (c) and is shown with permission.

The fact, that multiple subunits have been highly enriched (more than seven-fold) and identified in a quantitative and comparative mass spectrometry assay investigating interacting protein complexes associated with the MPP2 SH3GK module strongly suggests a potential for MPP2 to interact with functional GABA<sub>A</sub> receptors. This is particularly interesting, as GABA<sub>A</sub>Rs as mediators of inhibitory signalling are not typically present at high levels at postsynaptic sites of excitatory glutamatergic synapses, where MPP2 has been described (Rademacher\*, Schmerl\*, et al., 2016; G. Kim et al., 2016).

Next, N-terminal pHluorin-tagged expression constructs of the GABA<sub>A</sub> receptor subunits  $\alpha$ 1,  $\alpha$ 2 and  $\beta$ 3 were acquired and overexpressed together with FLAG-tagged full-length MPP2 in heterologous cells. Following immunoprecipitation of the GABA<sub>A</sub>R subunits using  $\alpha$ GFP antibodies, MPP2 was successfully co-purified in all experiments (Figure 20). Together these data strongly support the idea that MPP2 truly interacts with GABA<sub>A</sub> receptors and thus may serve as a mediator between excitatory and inhibitory signalling at dendritic spines.

### **3.4.2 MPP2 co-localises with GABA<sub>A</sub>Rs at excitatory synapses**

Typically, GABA<sub>A</sub> receptors are studied for their important function at inhibitory synapses, which most often are located to the dendritic shaft (rather than dendritic spines) and where Gephyrin provides the inhibitory postsynaptic scaffold (Tyagarajan and Fritschy, 2014), comparable to PSD-95 at glutamatergic synapses.

Thus, to further support the previous data acquired in vitro, clearly demonstrating a preferential binding of GABA<sub>A</sub> receptor subunits to the SH3GK module of MPP2, the endogenous protein localisations were investigated. Mature (DIV 21) cultured primary hippocampal neurons were fixed and immunostained for GABA<sub>A</sub>R  $\alpha$ 1 and MPP2, together with the neuronal dendritic marker MAP2, as well as the well-established excitatory postsynaptic density marker Homer1 (Figure 21) and analysed by confocal microscopy.

In line with previous experiments, MPP2 (Figure 21a-c, cyan) was observed enriched at dendritic spines, marked by Homer1 (Figure 21a-c, yellow), which are positioned exclusively along MAP2-positive dendritic branches (Figure 21a-c, grey). Quite interestingly, punctate GABA<sub>A</sub>R  $\alpha$ 1 signal (Figure 21a-c, magenta) was observed not only distributed along the dendritic branches marked by MAP2, where expected, but also occasionally located at dendritic spines positive for Homer1, where the GABA<sub>A</sub>R  $\alpha$ 1 staining co-localises with MPP2 (Figure 21c).

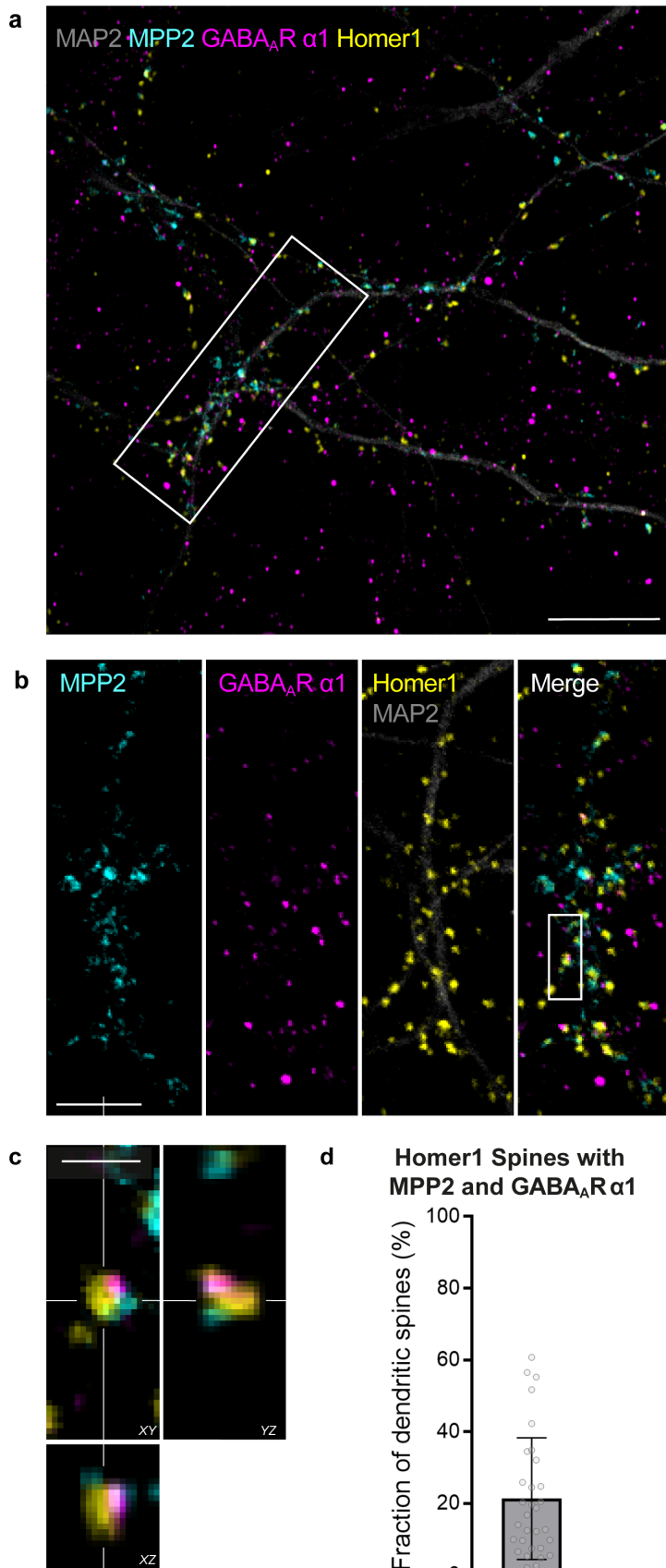


**Figure 21: GABA<sub>A</sub>R α1 co-localises with MPP2 in a subset of dendritic spines.**

a) Primary E18 rat hippocampal neurons were fixed at DIV 21 and immunostained for the endogenous proteins MAP2 (microtubule-associated protein 2), MPP2, GABA<sub>A</sub>R α1 and Homer1 using respective primary and Alexa fluorophore-coupled secondary antibodies, and visualised by confocal microscopy. Box in this maximum projected overview indicates location of detail image in b. Scale bar = 10 μm. b) Maximum projection composite of four-colour confocal immunofluorescence image of a primary to secondary dendrite branch point of a mature (DIV 21) hippocampal neuron. MPP2 is located in the majority of dendritic spines marked with Homer1, while GABA<sub>A</sub>R α1 co-localises with a subset of these spines. Additionally, solely GABA<sub>A</sub>R α1 positive puncta likely represent inhibitory synapses at the dendrite. Box indicates location of detail image in c. Scale bar = 5 μm. c) Enlarged single-plane image with corresponding orthogonal views of a dendritic spine exhibiting immunofluorescence staining for Homer1, MPP2 and GABA<sub>A</sub>R α1. Scale bar = 1 μm. d) Quantification of the fraction of excitatory synapses marked by Homer1, which also show MPP2 and GABA<sub>A</sub>R α1 immunofluorescence. Please see Material and Methods for details. Mean ± SD; n = 31 images of N = 4 independent experiments.

Given that this observed co-localisation applies only to a subset of dendritic spines, a confocal microscopy-based quantification approach aimed to quantify the prevalence of this co-localisation at primary to secondary dendrite branch points in mature cultured hippocampal neurons. A sequence of background filtering and thresholding algorithms was applied to segment dendritic spines, marked by Homer1 signal, as well as MPP2 and GABA<sub>A</sub>R  $\alpha$ 1 puncta, allowing for co-localisation analysis. Segmented spines were tested whether MPP2 and GABA<sub>A</sub>R  $\alpha$ 1 puncta were present within a 1  $\mu$ m diameter around the segmentation centre, what accounts to a dendritic spine head diameter (Adrian et al., 2017). Following this approach, the prevalence of those three proteins of interest co-localising at dendritic spines was accounted to a subset of  $\sim$ 20% of all segmented Homer1-positive dendritic spines (Figure 21d; Mean  $\pm$  SD; Median = 16.7%). This co-localisation was not restricted to the  $\alpha$ 1 subunit, but observed likewise for the representative beta subunit GABA<sub>A</sub>R  $\beta$ 1 (Figure 22a, cyan), which was also found at some Homer1-positive spines (Figure 22a, yellow) with MPP2 expression (Figure 22a, magenta).

GABA<sub>A</sub> receptors are typically associated with inhibitory synapses, which mostly reside on the dendritic shaft and are organised by Gephyrin as the main scaffold protein (Craig et al., 1996; Tretter et al., 2008; Petrini et al., 2014). In this thesis and other studies MPP2 was consistently found at PSDs of excitatory synapses (Rademacher\*, Schmerl\*, et al., 2016; G. Kim et al., 2016). To approach the question whether MPP2 might also be present at inhibitory synapses, dissociated cultures of rat hippocampal neurons were fixed at DIV 21 and subjected to immunostaining and analysis by confocal microscopy (Figure 22b). Neurons were stained for the dendritic marker MAP2 (Figure 22b, grey), the excitatory postsynapse marker Homer1 (Figure 22b, yellow), MPP2 (Figure 22b, magenta) and the inhibitory synaptic scaffold protein Gephyrin (Figure 22b, cyan). As expected, the observed Gephyrin and Homer1 puncta along the dendrite were hardly overlapping with each other. Further, while almost all Homer1-positive spines also exhibit MPP2 signal, the protein does not seem to be enriched at Gephyrin-positive sites, likely representing inhibitory synapses (Figure 22biii). Although this analysis does not rule out that MPP2 might be present at inhibitory synapses at very low levels, difficult to detect with a confocal microscopy approach, no obvious co-localisation of MPP2 and Gephyrin was observed. This further supports the idea that MPP2 is associated with inhibitory receptor subunits that are localised at excitatory synapses.

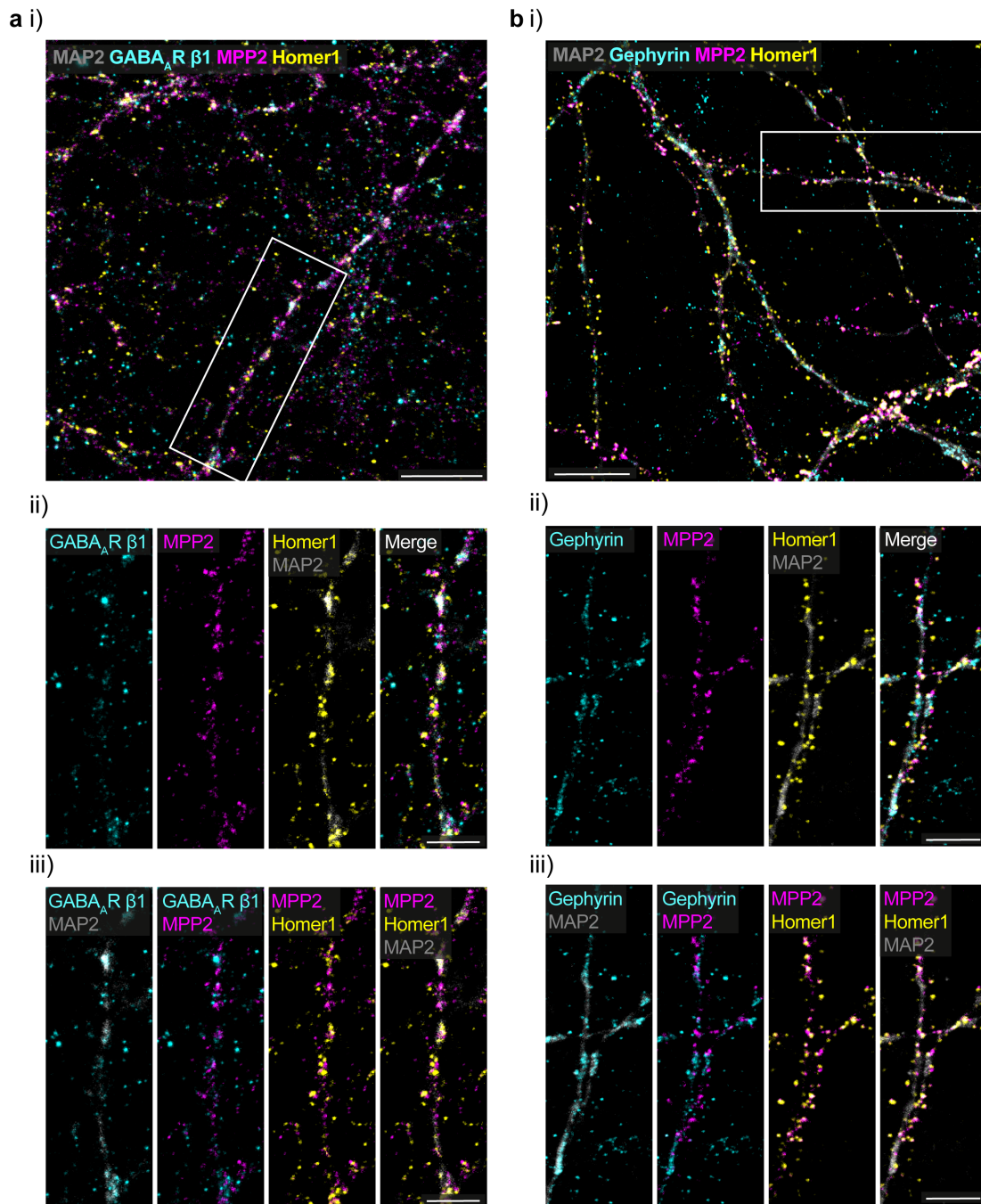


**Figure 22: Endogenous MPP2 co-localises with GABA<sub>A</sub> receptors, but not at inhibitory synapses.**

ai) Fixed DIV 21 hippocampal neurons were stained for endogenous MAP2 (grey), GABA<sub>A</sub> R β1 (cyan), MPP2 (magenta) and Homer1 as PSD marker (yellow). White box indicates detail view in ii and iii. aii) Detail view on a secondary dendrite segment. Endogenous GABA<sub>A</sub> R β1 (cyan), MPP2 (magenta) and Homer1 (yellow) occur as punctate structures along the dendrite (MAP2, grey). aiii) GABA<sub>A</sub> R β1 puncta (cyan) co-localise with a sub-set of dendritic spines marked with MPP2 (magenta) and Homer1 (yellow). GABA<sub>A</sub> R β1 puncta located to the dendrite, which do not overlap with MPP2 and Homer1, likely represent inhibitory synapses. bi) Fixed DIV 21 hippocampal neurons were stained for endogenous MAP2 (grey), Gephyrin (cyan), MPP2 (magenta) and Homer1 as PSD marker (yellow). White box indicates detail view in ii and iii. bii) Detail view on a secondary dendrite segment. Endogenous Gephyrin (cyan), MPP2 (magenta) and Homer1 (yellow) occur as punctate structures along the dendrite (MAP2, grey). biii) Gephyrin puncta (cyan) do not significantly overlap with dendritic spines marked with MPP2 (magenta) and Homer1 (yellow). Scale bars: overview = 10 μm; detail = 5 μm.

### 3.4.3 MPP2 and GABA<sub>A</sub>Rs co-localise at the PSD periphery

Given the previously described tight association of MPP2 and its PDZ domain ligand SynCAM1 at the periphery of the postsynaptic density (see again Figures 14, 15 and 16), it was of particular interest to examine the sub-synaptic localisation of MPP2 together with GABA<sub>A</sub> receptors. Taking advantage of triple-colour super-resolution *d*STORM imaging, the position of GABA<sub>A</sub>R  $\alpha$ 1 in relation to the PSD-peripheral MPP2 was explored in collaboration with Dr. Niclas Gimber (AG Schmoranzler) and the Advanced Medical BioImaging Core Facility at Charité - Universitätsmedizin Berlin. DIV 21 cultured primary hippocampal neurons were stained for endogenous MPP2, GABA<sub>A</sub>R  $\alpha$ 1 and Homer1 and imaged utilising a spectral de-mixing (SD) *d*STORM approach in combination with successively recorded ‘conventional’ *d*STORM imaging. Spectral de-mixing provides the great advantage that two channels are imaged simultaneously with the same camera, resulting in localisations inherently free of registration errors. While, MPP2 (CF 680) and GABA<sub>A</sub>R  $\alpha$ 1 (Alexa Fluor 647) were imaged in spectral de-mixing mode, Homer1 was subsequently imaged in ‘conventional’ *d*STORM mode and aligned manually, according to fiducial beads.

Again, using this imaging strategy, nanoclusters of MPP2 protein (Figure 23a, cyan) were observed in a bracelet-like arrangement surrounding postsynaptic densities as marked by Homer1 staining (Figure 23a, yellow) confirming the observations described previously with related methods. Most importantly, at the same synapses that exhibit these MPP2 bracelets, also clusters of GABA<sub>A</sub>R  $\alpha$ 1 (Figure 23a, magenta) were found in tight association with MPP2.

A quantitative analysis of the triple-colour *d*STORM data provides additional detail; automated image segmentation and analysis, utilising the DBSCAN clustering algorithm, provides further information on the observed protein clusters. Interestingly, MPP2 clusters are slightly larger (longest axis diameters of 30-60 nm; Figure 23b, cyan) than GABA<sub>A</sub>R  $\alpha$ 1 clusters (20-40 nm in diameter; see Figure 23b, magenta).

For a more detailed description of the spatial relationship between MPP2 and GABA<sub>A</sub>R  $\alpha$ 1 clusters, a nearest neighbour (NN) analysis was performed, which interrogates the distances between centres of MPP2 clusters to the nearest GABA<sub>A</sub>R  $\alpha$ 1 cluster at nanoscale. As shown in Figure 23c, the NN analysis reveals that centre-to-centre distances peak at approximately 10 nm. This is particularly interesting, as this is well below the cluster size and beyond the resolution provided by the utilised *d*STORM system. The control NN analysis of randomly distributed protein clusters (Figure 23c, dashed line) further supports that clusters of MPP2 and GABA<sub>A</sub>R  $\alpha$ 1 are highly overlapping at the periph-

ery of the postsynaptic density. This observation is particularly interesting, as investigations at super-resolution regarding MPP2 and its PDZ domain ligand SynCAM1 demonstrated a tight, but adjacent positioning of these interaction partners, whereas MPP2 and its SH3GK domain interactor GABA<sub>A</sub>R  $\alpha$ 1 overlap significantly.

In summary, these imaging and co-localisation studies suggest a close association between MPP2 and GABA<sub>A</sub> receptors at the periphery of PSDs of glutamatergic synapses and together with the presented in vitro data, further support the hypothesis that MPP2 may be involved in recruiting and anchoring GABA<sub>A</sub> receptors to these spines and thus influence synaptic function and transmission.

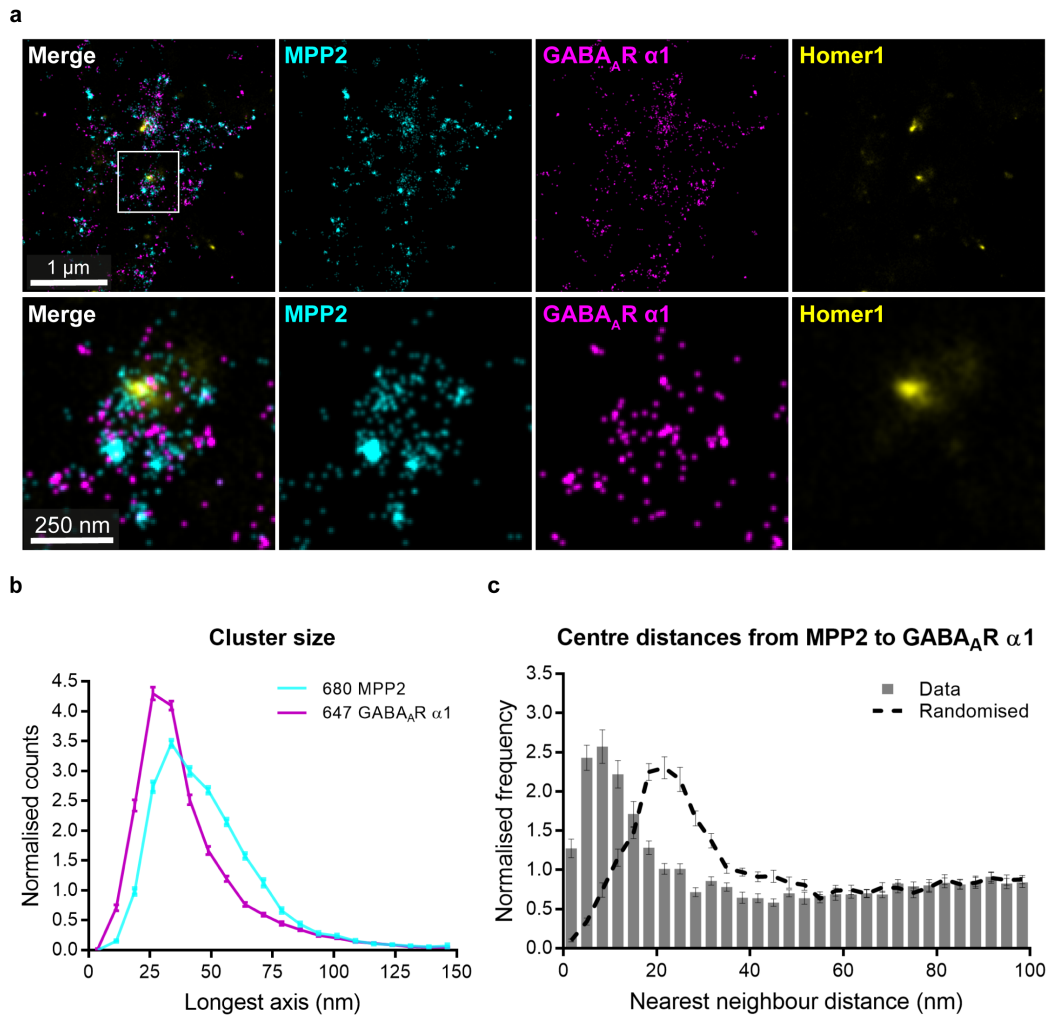


**Figure 23: MPP2 and GABA<sub>A</sub>R α1 form highly overlapping nanoclusters.**

Mature (DIV 21) primary rat hippocampal neurons were immunostained for endogenous MPP2 (cyan, second column), GABA<sub>A</sub>R α1 (magenta, third column) and the PSD marker Homer1 (yellow, fourth column) and subjected to triple-colour *d*STORM imaging. **a**) Overview of a dendritic segment (upper row). White box indicates location of detail image below. Zooming onto an individual synapse expressing Homer1, MPP2 and GABA<sub>A</sub>R α1 (lower row) reveals a close association between clusters of MPP2 and GABA<sub>A</sub>R α1 and the bracelet-like arrangements of MPP2 surrounding a centrally positioned Homer1 cluster. Scale bars: overview = 1 µm; detail = 250 nm. **b**) Histograms illustrating the distribution of nano-cluster sizes (longest axis) for MPP2 (cyan) and GABA<sub>A</sub>R α1 (magenta). Clusters were detected via DBSCAN. Mean ± SEM; n = 26 images from N = 3 independent experiments. **c**) Nearest Neighbour (NN) analysis of MPP2 and GABA<sub>A</sub>R α1 protein clusters after DBSCAN. NN distances were calculated from the cluster centres. Closest GABA<sub>A</sub>R α1 to MPP2 were analysed (grey bars). Dashed lines represent the random control by toroidal shift. Note the close association of both clusters (~10 nm distance between both centres), which is below the cluster sizes (20-40 and 30-60 nm, see **b**) and shifted after randomisation. Mean ± SEM; n = 26 images from N = 3 independent experiments.

## 4 Discussion

The present study describes the role of a member of the MPP family, which is mainly known for its important function at epithelial cell-cell contact sites, for the first time at synapses.

Major findings of this dissertation include the description of the membrane-associated guanylate kinase (MAGUK) family protein MPP2 as member of receptor-associated protein complexes at postsynaptic sites. MPP2 is linked to AMPA receptors, which are crucial for glutamatergic synaptic function, via several interactions with critical AMPA receptor complex proteins like PSD-95. Moreover, MPP2 is engaged as a synaptic scaffold protein by interacting with established scaffolding molecules like Lin7 and GKAP.

With their characteristic PDZ domain, many MAGUK proteins interact with the C-terminus of transmembrane proteins. To explore potential interaction partners of MPP2, a yeast-two-hybrid screen was conducted that used the PSG ‘MAGUK core’ domains of MPP2 as bait. With this strategy, multiple transmembrane cell adhesion proteins were found that were potentially interacting with their carboxyterminus. Interestingly, the important synapse formation-inducing and synapse-stabilising transmembrane cell adhesion molecule SynCAM1 was identified as a ligand to the PDZ domain of the postsynaptic scaffold proteins MPP2. Despite SynCAM proteins being present at both, pre- and postsynaptic sites, mainly presynaptic interactors for SynCAM1 have been described. Thus, this thesis identified MPP2 as the first postsynaptic PDZ domain-mediated interaction partner for the SynCAM1 C-terminus.

Applying diverse imaging strategies, the sub-synaptic positioning of MPP2 was localised to the periphery of the postsynaptic density (PSD) where it may be involved in mediating PSD size and stability together with SynCAM1.

Due to the distinct localisations of the two structurally very similar scaffold proteins PSD-95 and MPP2, a comparative and quantitative mass spectrometry assay was performed to gain insight into the different interactions that caused this differential localisation or are influenced by it. Differential analysis of the interactomes organised by PSD-95 and MPP2 revealed distinct roles of the two proteins in organising diverging protein complexes. Several new and specific interaction partners for the SH3GK module of MPP2 have been identified and validated, including membrane-associated proteins like Pip5k1c and proteins important for the regulation of synaptic signalling like Ppp3ca and Arhgef2.

Surprisingly, multiple GABA<sub>A</sub> receptor subunits were specifically enriched with an MPP2 pull-down and direct interactions could be confirmed for the GABA<sub>A</sub>R subunits  $\alpha 1$ ,  $\alpha 2$  and  $\beta 3$ . Subsequent imaging studies confirmed the co-localisation

of MPP2 and GABA<sub>A</sub>Rs at a subset of glutamatergic synapses and helped to determine the prevalence thereof. Moreover, super-resolution analysis confirmed a highly overlapping positioning of MPP2 and GABA<sub>A</sub>R  $\alpha$ 1 at the periphery of postsynaptic densities. These findings are new and unexpected and suggest that MPP2 may indeed serve as a physical and functional link between excitatory glutamatergic synaptic function and GABA<sub>A</sub> receptors, which mediate inhibitory signalling.

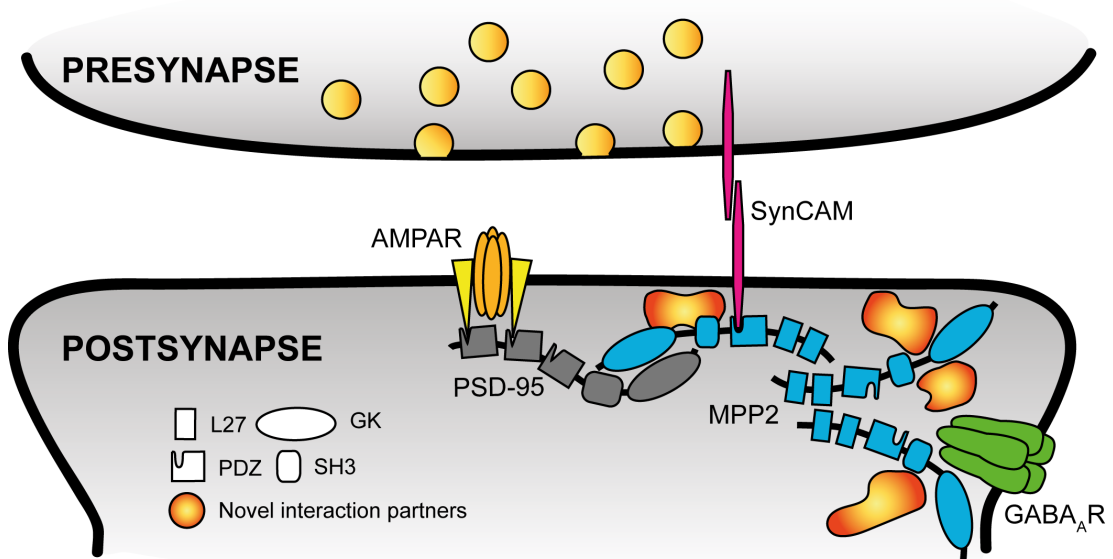


**Figure 24: Graphical summary of MPP2 and novel interaction partners at glutamatergic synapses.**

The data presented in this thesis indicate an important role of MPP2 (blue) in the sub-synaptic compartmentalisation of dendritic spines by connecting central components of AMPA receptor (orange) complexes, like TARPs (yellow) and PSD-95 (grey) not only to cell adhesion molecules like SynCAM proteins (magenta) and other scaffold and regulatory proteins (like the novel interaction partners PIP5k1c or Ppp3ca), but most importantly inhibitory GABA<sub>A</sub> receptors (green). For MAGUK proteins, the individual domain structure is indicated. This figure has been published as preprint (Schmerl et al., 2020).

#### 4.1 MPP2 is a novel component of postsynaptic protein complexes

PSD-95 family proteins are well established modulators of synaptic function and compose the prototypical synaptic MAGUK scaffold proteins (for review see Won et al., 2017). In contrast, membrane protein, palmitoylated (MPP) family proteins are well known regulators of epithelial cell polarity, especially MPP5 (also known as Pals1, a homologue of the well-characterised *Drosophila* protein *stardust* (std) (Bachmann et al., 2001). Interestingly, although a lot of literature is available on the role of MPP family proteins at cell-cell junctions, they have not been investigated in synapses, despite the fact that they resemble the classical MAGUK PSD-95 family protein structure in that they carry the PSG core

domain accompanied by two N-terminal protein interaction domains.

A first indication of a potential relevance of MPP family proteins at synapses prior to this dissertation was provided by Bachmann et al. (2010) at the *Drosophila* neuromuscular junction, followed by high-throughput mass spectrometry analysis results of glutamate receptor protein complexes (Schwenk et al., 2012; Shanks et al., 2012). Since these studies focussed on the diversity of AMPA receptor interactomes and associated protein complex composition, the role of MPP proteins was not discussed in detail. During the course of the present work, in which the relationship between MPP2 and AMPA receptor complexes was explored (Rademacher\*, Schmerl\*, et al., 2016), another group examined the function of MPP2 in neurons, after using a proteomic approach that highlighted an interaction between MPP2 and small conductance Ca<sup>2+</sup>-activated SK2 containing potassium channels (G. Kim et al., 2016). These SK2 containing channels are closely associated with NMDA type glutamate receptors, hence this study also suggests an important role of MPP2 at synapses. Together with other studies, this thesis provides the first evidence that MPP2 is a postsynaptic scaffold protein that is associated with glutamatergic excitatory transmission and therefore relevant for neuronal function.

## **4.2 Linking peripheral and central structural elements of the postsynapse**

PSD-95 family proteins have long been studied for their importance in excitatory transmission in that they are critical for proper receptor localisation and anchoring at synaptic membranes. Moreover, alterations can have detrimental effects on AMPAR mediated transmission and long term potentiation (Stein et al., 2003; Elias et al., 2006). Recent advances in super-resolution imaging have provided further evidence on how delicate and localised this functional regulation is: PSD-95 as well as glutamate receptors are organised in sub-synaptic clusters or nanodomains (MacGillavry et al., 2013; Nair et al., 2013), that may be individually regulated (for reviews see MacGillavry et al., 2011; Biederer et al., 2017; Scheefhals and MacGillavry, 2018; X. Yang and Specht, 2019).

Scaffold proteins like PSD-95 and MPP2 are perfectly suited for a central role in such an arrangement. Their domain structure, in particular the ‘MAGUK core’ PDZ-SH3-GK domain (PSG), facilitates homomultimerisation as well as complex formation with related MAGUKs (Zhu et al., 2011; Rademacher\*, Schmerl\*, et al., 2016; G. Kim et al., 2016) and further allows to incorporate other cytosolic proteins into these complexes. This is realised via their various protein-protein interaction domains, such as the L27 or additional PDZ domains of MPP2 and PSD-95, respectively (for review see Funke et al., 2005; Ye et al., 2017). The PDZ domain, however, is critical for the membrane association, as it typically binds

to transmembrane proteins, most significantly receptor subunits and auxiliary proteins (Kornau et al., 1995; Elias et al., 2006; Opazo et al., 2012).

In this regard, MPP2 poses a new kind of synaptic MAGUK scaffold protein, as it shares the domain structure with PSD-95 family proteins, but does not directly interact with glutamate receptors or their auxiliary subunits; hence is not a central element of such glutamate receptor complexes. However, the present work demonstrates that the MPP2 PDZ domain binds to multiple synaptic transmembrane proteins that are relevant for trans-cellular adhesion and signalling, foremost SynCAM1.

SynCAM1, which is also known as TSLC1, CADM1 or Nectin-like 2 in different cellular contexts, has been described as an important cell-cell adhesion factor (Masuda et al., 2002; Yageta et al., 2002; Masuda et al., 2005; Ito et al., 2011). SynCAM proteins have a large extracellular domain that contains immunoglobulin-like loops, which facilitate cis-dimerisation prior to interacting with SynCAM dimers in trans (Fogel et al., 2007), thereby bridging the extracellular space, forming the cell-cell contact and initiating downstream signalling (for review see Biederer and Stagi, 2008). In neuronal cells, SynCAM family molecules are known for their ability to induce synapse formation (Biederer et al., 2002), maintain synaptic stability (Doengi et al., 2016; Korber and Stein, 2016) and regulate memory formation (Robbins et al., 2010).

In epithelial and cancerous tissues, an interaction of different SynCAM family proteins with several MPP family members has already been described (Fukuhara et al., 2003; Sakurai-Yageta et al., 2009; Murakami et al., 2014). However, at synapses, where different SynCAM proteins are found at postsynaptic and presynaptic sites (Fogel et al., 2007), PDZ domain-mediated interactions have been described mainly with the presynaptic protein CASK (Biederer et al., 2002; Hsueh, 2006), a protein that is structurally similar to MPP2.

Nonetheless, SynCAM proteins play an important role also at postsynaptic sites: Using super-resolution imaging techniques, SynCAM1 was demonstrated to form clusters located to the edge of the postsynaptic density, and it was implicated in maintaining and regulating the PSD size and integrity (Perez de Arce et al., 2015). Of particular interest, SynCAM1 does not interact with postsynaptic PSD-95 family proteins (Biederer et al., 2002; Fujita et al., 2012), but instead, as found in the present thesis, interacts with MPP2 at postsynaptic sites.

Taking advantage of different super-resolution imaging approaches, the present work demonstrates a positioning of MPP2 at the edge of postsynaptic densities. Immunogold labelling experiments by G. Kim et al. (2016) have also suggested a rather peripheral positioning of MPP2 at synapses. Moreover, the arrangement of almost alternating MPP2 and SynCAM1 clusters at the PSD border further

advances the idea that MPP2 serves to moderate the functional interplay of peripheral SynCAM1 and PSD-95 as central PSD scaffold, two proteins that do not directly interact with each other. The fact that MPP2 as well as SynCAM1 were observed in sub-synaptic clusters is also in line with the idea that the interplay of synaptic nanodomains regulates synaptic transmission. Similar to PSD-95 and glutamate receptor nanodomains, the sub-synaptic clusters of MPP2 (and SynCAM1) may allow for dynamic structural changes, which may not only facilitate development but also enable and regulate synaptic plasticity at a mature state as implicated for PSD-95 nanodomains (Nair et al., 2013).

### **4.3 MPP2 is engaged in regulatory interaction networks**

MPP2 and PSD-95 are two proteins with a striking similarity in their domain structures and their common presence at synaptic sites (Rademacher\*, Schmerl\*, et al., 2016; G. Kim et al., 2016), suggesting similar roles in related aspects of synaptic structure and function. Despite their structural resemblance, there clearly exist very different interaction specificities between MPP and PSD-95 family proteins (G. Kim et al., 2016; Gavarini et al., 2006). Using a yeast two hybrid screen and a qualitative and quantitative proteomics approach, this thesis provides lists of potential interaction partners of the C-terminal domains of MPP2. Although the scope of the present thesis did not allow closely addressing and confirming every potential interaction partner, evaluation of the identified interactomes suggests that MPP2 is involved in established postsynaptic protein interaction and signalling networks that provide links between transmembrane proteins, channels and receptors to cytoskeleton elements and their regulators.

Although no direct binding between MPP2 and glutamate receptors was found, indirect associations are likely. The newly identified MPP2 PDZ domain ligand SynCAM1 has been proposed to recruit NMDA receptors to synaptic membranes (Hoy et al., 2009). In addition to SynCAM1 binding, this thesis demonstrates a direct interaction between MPP2 and Farp1, another membrane-associated protein that was found to bind to SynCAM via FERM domain interactions (Cheadle and Biederer, 2012). Whether SynCAM1 and Farp1 binding to MPP2 might compete was not assessed, but given that the domains mediating these interactions are different (PDZ for SynCAM1 and SH3GK for Farp1 binding), these interactions must not be exclusive, but could rather form a membrane-associated protein complex. Moreover, this potential MPP2-SynCAM1-Farp1 complex might be further stabilised by protein 4.1. The membrane protein-associated protein band 4.1 has been shown to be involved in AMPAR surface expression (L. Shen et al., 2000), and was further identified in the proteomics investigation as an interactor of MPP2. Interestingly, both, SynCAM1 and Farp1 also interact with protein 4.1

via a FERM domain interaction (Kuo et al., 2018). These FERM domains have been named amongst others after protein 4.1 and are found also e.g. at the N-terminus of MPP1, where it is involved in linking cytoskeleton elements with the cell membrane in a group of peripheral membrane proteins (Chishti et al., 1998). Indeed, several MPP family proteins have already been shown to interact with 4.1, which might be stabilising interactions between MPP proteins and transmembrane proteins (Sakurai-Yageta et al., 2009). Further, these complexes are associated with filamentous actin in HEK293 cells (Sakurai-Yageta et al., 2009; Sakurai-Yageta et al., 2015), thus providing a direct link to the cytoskeleton.

The idea that MPP2 at synapses connects transmembrane proteins with cytoskeletal components is further supported by multiple proteins identified in the Y2H and proteomic screens, conducted during the course of this thesis. Another interesting potential interaction partner, which was found in the Y2H as well as the proteomics experiments were multiple members of the Septin protein family. Septins are GTPases that are able to form filamentous structures (for reviews see Kinoshita, 2003; M. S. Kim et al., 2012) and have been described to form a diffusion barrier at the dendritic spine neck (Ewers et al., 2014).

GTP-binding proteins, as well as GTPases, GEFs and GAPs are important regulators of dendritic spine actin cytoskeleton elements (for reviews see Spence and Soderling, 2015; Hotulainen and Hoogenraad, 2010), and therefore identification of several proteins belonging to these groups associating with MPP2, together with multiple cytoskeleton components like MAP4 and several tubulin chain proteins, further supports the idea that MPP2 is involved in spine dynamics and plasticity processes by connecting central synaptic elements with deeper components of dendritic spines.

#### **4.4 MPP2 links elements of excitatory and inhibitory transmission**

Despite the striking structural similarity between the SH3GK module of MPP2 and PSD-95, the proteomics results presented in this thesis suggest that the respective associated synaptic protein complexes consist of distinct membrane and cytosolic proteins.

Unexpectedly, among the identified and validated novel interaction partners for the MPP2 SH3GK module, multiple different GABA<sub>A</sub> receptor subunits and additional signalling molecules, which are already well established for their role in the regulation of inhibitory signalling processes, were highly enriched. As SH3GK modules of synaptic MAGUK proteins are not known to bind with high affinity to GABA<sub>A</sub> receptors, this association seems to be MPP2 specific.

Remarkably, the seven GABA<sub>A</sub> receptor subunits that were identified represent more than one third of all known subunits (Sigel and Steinmann, 2012) and

contained the representative  $\alpha 1$  and  $\beta 1$  subunits (McKernan and Whiting, 1996; Nusser et al., 1996), as well as the more rare  $\delta$  subunit (Fritschy and Mohler, 1995; Barrera et al., 2008). In co-immunoprecipitation experiments, a direct interaction of MPP2 with the GABA<sub>A</sub>R subunits  $\alpha 1$ ,  $\alpha 2$  and  $\beta 3$  could be confirmed. While most studies on GABA<sub>A</sub> receptor function are based on analysis of inhibitory synapses (for reviews see Higley, 2014; Tyagarajan and Fritschy, 2014; Boivin and Nedivi, 2018; Chiu et al., 2019), the results presented in this thesis suggest a mode of integration of GABA<sub>A</sub>Rs at excitatory synapses.

MPP2 was shown to co-localise with several GABA<sub>A</sub>R subunits at glutamatergic synapses of cultured primary hippocampal neurons. Moreover, MPP2 nanoclusters are positioned highly overlapping with GABA<sub>A</sub>R  $\alpha 1$  clusters at the periphery of the postsynaptic density. At inhibitory synapses, scaffold proteins and receptors have been reported to cluster to sub-synaptic nanodomains, which are dynamic and regulated in an activity-dependent manner (Specht et al., 2013; Pennacchietti et al., 2017; Crosby et al., 2019), similar to sub-synaptic nanodomains at excitatory synapses formed by AMPARs and PSD-95 (MacGillavry et al., 2013; Nair et al., 2013). Interestingly, the super-resolution imaging of GABA<sub>A</sub>R clusters that were co-localising with MPP2 revealed small cluster sizes, which might represent relatively few receptor molecules that are specifically associated with excitatory synapses, rather than actual inhibitory synapses. Although a certain fraction of dendritic spines receives inputs via excitatory as well as inhibitory synapses (J. L. Chen et al., 2012), the absence of the typical inhibitory synapse marker and scaffold protein Gephyrin at MPP2- and GABA<sub>A</sub>R-positive spines observed in the present work, suggest that the GABA<sub>A</sub> receptors might represent a population independent from inhibitory synapses. Indeed, a peri-synaptic localisation of GABA<sub>A</sub> receptors has been observed at even better resolution (using electron microscopy) in cortical neurons (Kubota et al., 2007), where the GABA<sub>A</sub> receptor subunit expression and composition seem to be developmentally regulated (H. Shen et al., 2010).

Another potential explanation for GABA<sub>A</sub> receptors positioned at glutamatergic dendritic spines is provided by several studies investigating changes in GABA<sub>A</sub> receptor mobility by trapping of receptors at glutamatergic synapses, following desensitisation, in order to regulate inhibitory synaptic transmission (de Luca et al., 2017). Interestingly, another MPP family protein, MPP3, was found to prevent serotonin receptor desensitisation in cortical neurons (Gavarini et al., 2006). The link between MPP2 and GABA<sub>A</sub>Rs observed here might reflect a similar functional dynamic.

With recent developments in optogenetic tools and advances in imaging technology, the regulatory influence of GABA<sub>A</sub> receptors on excitatory transmission, e.g. via effects on Ca<sup>2+</sup> influx (J. L. Chen et al., 2012), has become a topic receiv-

ing increasing attention (for reviews see Higley, 2014; Boivin and Nedivi, 2018). Several studies have conversely linked NMDAR-mediated activity with inhibitory synaptic plasticity (Lu et al., 2000; Marsden et al., 2007). Clearly, this dynamic interplay involves further regulation of  $\text{Ca}^{2+}$  influx at dendritic spines. In this regard, it is especially important and interesting that, in addition to  $\text{GABA}_A$  receptors, the calcium- and calmodulin-dependent serine/threonine protein phosphatase (Calcineurin) subunit Ppp3ca was identified and validated as a novel interacting protein of the MPP2 SH3GK module. It not only interacts directly with  $\text{GABA}_A$  receptors (J. Wang et al., 2003; Bannai et al., 2009; Bannai et al., 2015), but has also been shown to influence NMDAR signalling-mediated effects on inhibitory synaptic plasticity (Lu et al., 2000; Marsden et al., 2010).

Interestingly, the only other study investigating MPP2 in neuronal cells beside this dissertation (G. Kim et al., 2016), provides further context for this potential relationship between MPP2 scaffolds and  $\text{Ca}^{2+}$  signalling-mediated regulation of synaptic function. The authors reported defects in LTP formation after MPP2 knock-down, which caused loss of SK2-containing channel activity that modulates postsynaptic plasticity in response to NMDAR mediated influx of  $\text{Ca}^{2+}$  (G. Kim et al., 2016). Investigations in erythrocyte membranes on a protein complex consisting of MPP1, protein band 4.1 and glycoporphin C, which is influenced by Calmodulin (Nunomura et al., 2000), additionally support the idea that MPP2-mediated protein complex function might be associated with  $\text{Ca}^{2+}$  signalling.

## 5 Conclusion and Outlook

While the functional role of the newly described MPP2  $\text{GABA}_A$ R protein complex still needs intense investigation, this thesis provides novel detail on how the regulated crosstalk between glutamatergic synapses and associated inhibitory synapses is organised. To coordinate such dynamic interplay, local compartmentalisation is indispensable. A synaptic scaffold protein like MPP2, which is demonstrated here to interact with a variety of synaptic transmembrane, scaffold and regulatory proteins, may be perfectly suited to contribute to these dynamics (see Figure 24). It provides a physical link between central elements of glutamatergic synapses and more peripheral structural and regulatory elements. Thus, it may play an important role in balancing excitatory and inhibitory synaptic transmission, which is essential for proper neuronal circuit function. Further, MPP2 provides a molecular connection to deeper synaptic structural and regulatory proteins as well as elements of the cytoskeleton, suggesting an important role in the functional and structural plasticity in response to synaptic activity.

Given that MPP2 is expressed in most dendritic spines, of which only a frac-

tion contains GABA<sub>A</sub> receptors, it is possible that the interactomes and MPP2-associated protein complexes differ in composition, thus functional role and regulation. In that regard, it would be important to analyse the co-occurrence of the novel MPP2 interaction partners that have been described in the present study. A broad, e.g. proteomics approach, would not allow distinguishing between MPP2-associated proteins in distinct sub-sets of dendritic spines. Potentially, the earlier presence of MPP2 at mature synapses is necessary to provide the scaffold to recruit and anchor GABA<sub>A</sub>Rs, as these receptors have been shown to differ in expression and subunit composition upon maturation and activity (H. Shen et al., 2010). This thesis provides a first, however, admittedly rather static insight to this new protein complex. A precise analysis, e.g. of the subunit composition of GABA<sub>A</sub>Rs interacting with MPP2 and whether this is subject to change upon maturation and activity, would pose an interesting, yet challenging future project.

Although this was not specifically addressed during this study, analysis of dendritic spines harbouring clusters of MPP2 together with GABA<sub>A</sub> receptors suggest that mainly larger synapses belong to the respective sub-population of spines. Whether this is true could be determined with thorough analysis of spine morphology in culture, or even in brain slices. Especially in light of the connections between MPP2 and cytoskeletal elements, it would be interesting to pursue the idea that the morphology of this sub-set of spines is modified in response to activity (Spence and Soderling, 2015).

A general difficulty for the more detailed investigation of the MPP2 GABA<sub>A</sub>R protein complex and its importance, as well as regulation, is posed by the fact that only a sub-population of dendritic spines has been found to harbour both proteins at considerable amounts. This likewise poses a challenge for investigating the functional consequences of manipulating MPP2 expression. More targeted approaches, e.g. live-cell imaging with single particle tracking of GABA<sub>A</sub> receptor trapping (de Luca et al., 2017) or combining molecule uncaging and calcium-imaging (Marlin and Carter, 2014), might be required to monitor the specific effects of manipulating MPP2 levels in spines.

PSD-95 family proteins are redundant, and assessing the functional effects of PSD-95 knock-out/-down, studies haven proven difficult due to compensation by related proteins (Elias et al., 2006). It is conceivable that MPP family proteins might be likewise redundant, as also other MPP family proteins have been reported in neuronal tissue (Jing-Ping et al., 2005; Dudok et al., 2013b). Despite efficiently abolishing the expression of MPP2 in cultured primary neurons, using lenti virus-mediated expression of shRNA (see also appendix, page 140), no striking effects on the gross morphology of neurons or expression levels of the main interacting proteins identified in this study were observed. While alterations

regarding PSD-95 family proteins have been demonstrated to significantly influence AMPA receptor-mediated transmission (El-Husseini et al., 2000a; Schnell et al., 2002; Stein et al., 2003) and surface localisation and anchoring (Schnell et al., 2002; Elias et al., 2008), it is unlikely that acute manipulations of MPP2 would have comparable effects, because it is not directly interacting with glutamate receptor subunits or auxiliary subunits. Instead, an influence on those GABA<sub>A</sub> receptors that are associated with excitatory synapses and their contribution to synaptic transmission, might be expected. Indeed, in explorative experiments, only subtle changes in basic excitatory (miniature excitatory postsynaptic currents, mEPSCs) upon knock-down of MPP2 and, more importantly, inhibitory (miniature inhibitory postsynaptic currents, mIPSCs) transmission properties upon overexpression were observed, which is in line with an interaction of MPP2 with a specific subset of GABA<sub>A</sub> receptors.

A certain disadvantage in working with primary neurons is that the variability in dissociated hippocampal cultures is high and the role of MPP2 in synaptic function seems to be more subtle. Therefore, monitoring the consequences of MPP2 alterations or loss requires more sophisticated approaches, which allow a targeted investigation of the respective sub-set of synapses. Knock-down of endogenous MPP2 in primary hippocampal cultures did not result in severe functional effects on AMPA receptor-mediated transmission. However, this approach does not allow monitoring effects on plasticity of the system, especially regarding the novel connection MPP2 poses to GABA<sub>A</sub> receptors. To gain insight into synaptic plasticity and local regulation of transmission, electrophysiological assessment of dissociated neurons, as used in the present work is not optimal and analyses in another system might be necessary. Acute and cultured slices have proven a relatively convenient tool in investigating synaptic networks and function. Taking advantage of virus-mediated gene delivery, MPP2 expression could be abolished and/or the protein replaced with a knock-down-resistant targeted mutation construct *in vivo*. Subsequent comparison of infected and neighbouring uninfected neurons, which are still integrated into the local circuits, would allow monitoring and challenging the system at a different level as it is possible in dissociated cultures. The additional combination with e.g. GABA uncaging, optogenetic tools and single-particle tracking of GABA<sub>A</sub> receptors (Marlin and Carter, 2014; de Luca et al., 2017) is an exciting future project that would provide a mechanistic understanding of the influence of this MPP2-GABA<sub>A</sub>R interaction on network activity balance and synaptic plasticity.

## References

- Aartsen, W. M., A. Kantardzhieva, J. Klooster, A. G. van Rossum, S. A. van de Pavert, I. Versteeg, B. N. Cardozo, F. Tonagel, S. C. Beck, N. Tanimoto, M. W. Seeliger, and J. Wijnholds (2006). „Mpp4 recruits Psd95 and Veli3 towards the photoreceptor synapse“. In: *Hum Mol Genet* 15(8), pp. 1291–302. DOI: 10.1093/hmg/dd1047.
- Adrian, M., R. Kusters, C. Storm, C. C. Hoogenraad, and L. C. Kapitein (2017). „Probing the Interplay between Dendritic Spine Morphology and Membrane-Bound Diffusion“. In: *Biophys J* 113(10), pp. 2261–2270. DOI: 10.1016/j.bpj.2017.06.048.
- Aigouy, B. and V. Mirouse (2013). „ScientiFig: a tool to build publication-ready scientific figures“. In: *Nat Methods* 10(11), p. 1048. DOI: 10.1038/nmeth.2692.
- Alloisio, N., N. Dalla Venezia, A. Rana, K. Andrabi, P. Texier, F. Gilsanz, J. P. Cartron, J. Delaunay, and A. H. Chishti (1993). „Evidence that red blood cell protein p55 may participate in the skeleton-membrane linkage that involves protein 4.1 and glycoporphin C“. In: *Blood* 82(4), pp. 1323–1327. DOI: 10.1182/blood.V82.4.1323.bloodjournal18241323.
- Assemat, E., E. Bazellieres, E. Pallesi-Pocachard, A. Le Bivic, and D. Massey-Harroche (2008). „Polarity complex proteins“. In: *Biochim Biophys Acta* 1778(3), pp. 614–30. DOI: 10.1016/j.bbamem.2007.08.029.
- Bachmann, A., O. Kobler, R. J. Kittel, C. Wichmann, J. Sierralta, S. J. Sigrist, E. D. Gundelfinger, E. Knust, and U. Thomas (2010). „A perisynaptic menage a trois between Dlg, DLin-7, and Metro controls proper organization of Drosophila synaptic junctions“. In: *J Neurosci* 30(17), pp. 5811–24. DOI: 10.1523/JNEUROSCI.0778-10.2010.
- Bachmann, A., M. Schneider, E. Theilenberg, F. Grawe, and E. Knust (2001). „Drosophila Stardust is a partner of Crumbs in the control of epithelial cell polarity“. In: *Nature* 414(6864), pp. 638–643. DOI: DOI10.1038/414638a.
- Ball, G., J. Demmerle, R. Kaufmann, I. Davis, I. M. Dobbie, and L. Schermelleh (2015). „SIMcheck: a Toolbox for Successful Super-resolution Structured Illumination Microscopy“. In: *Sci Rep* 5, p. 15915. DOI: 10.1038/srep15915.
- Bannai, H., S. Levi, C. Schweizer, T. Inoue, T. Launey, V. Racine, J. B. Sibarita, K. Mikoshiba, and A. Triller (2009). „Activity-dependent tuning of inhibitory neurotransmission based on GABAAR diffusion dynamics“. In: *Neuron* 62(5), pp. 670–82. DOI: 10.1016/j.neuron.2009.04.023.
- Bannai, H., F. Niwa, M. W. Sherwood, A. N. Shrivastava, M. Arizono, A. Miyamoto, K. Sugiura, S. Levi, A. Triller, and K. Mikoshiba (2015). „Bidirectional Control of Synaptic GABAAR Clustering by Glutamate and Calcium“. In: *Cell Rep* 13(12), pp. 2768–80. DOI: 10.1016/j.celrep.2015.12.002.
- Barrera, N. P., J. Betts, H. You, R. M. Henderson, I. L. Martin, S. M. Dunn, and J. M. Edwardson (2008). „Atomic force microscopy reveals the stoichiometry and subunit arrangement of the alpha4beta3delta GABA(A) receptor“. In: *Mol Pharmacol* 73(3), pp. 960–7. DOI: 10.1124/mol.107.042481.

- Bats, C., L. Groc, and D. Choquet (2007). „The interaction between Stargazin and PSD-95 regulates AMPA receptor surface trafficking“. In: *Neuron* 53(5), pp. 719–34. DOI: 10.1016/j.neuron.2007.01.030.
- Baumgartner, M., A. Weiss, T. Fritzius, J. Heinrich, and K. Moelling (2009). „The PDZ protein MPP2 interacts with c-Src in epithelial cells“. In: *Exp Cell Res* 315(17), pp. 2888–98. DOI: 10.1016/j.yexcr.2009.07.028.
- Bayes, A., M. O. Collins, M. D. Croning, L. N. van de Lagemaat, J. S. Choudhary, and S. G. Grant (2012). „Comparative study of human and mouse postsynaptic proteomes finds high compositional conservation and abundance differences for key synaptic proteins“. In: *PLoS One* 7(10), e46683. DOI: 10.1371/journal.pone.0046683.
- Berry, K. P. and E. Nedivi (2017). „Spine Dynamics: Are They All the Same?“ In: *Neuron* 96(1), pp. 43–55. DOI: 10.1016/j.neuron.2017.08.008.
- Biederer, T., P. S. Kaeser, and T. A. Blanpied (2017). „Transcellular Nanoalignment of Synaptic Function“. In: *Neuron* 96(3), pp. 680–696. DOI: 10.1016/j.neuron.2017.10.006.
- Biederer, T., Y. Sara, M. Mozhayeva, D. Atasoy, X. Liu, E. T. Kavalali, and T. C. Südhof (2002). „SynCAM, a synaptic adhesion molecule that drives synapse assembly“. In: *Science* 297(5586), pp. 1525–31. DOI: 10.1126/science.1072356.
- Biederer, T. and M. Stagi (2008). „Signaling by synaptogenic molecules“. In: *Curr Opin Neurobiol* 18(3), pp. 261–9. DOI: 10.1016/j.conb.2008.07.014.
- Biernatowska, A., J. Podkalicka, M. Majkowski, A. Hryniewicz-Jankowska, K. Augoff, K. Kozak, J. Korzeniewski, and A. F. Sikorski (2013). „The role of MPP1/p55 and its palmitoylation in resting state raft organization in HEL cells“. In: *Biochim Biophys Acta* 1833(8), pp. 1876–84. DOI: 10.1016/j.bbamcr.2013.03.009.
- Bohl, J., N. Brimer, C. Lyons, and S. B. Vande Pol (2007). „The stardust family protein MPP7 forms a tripartite complex with LIN7 and DLG1 that regulates the stability and localization of DLG1 to cell junctions“. In: *J Biol Chem* 282(13), pp. 9392–400. DOI: 10.1074/jbc.M610002200.
- Boivin, J. R. and E. Nedivi (2018). „Functional implications of inhibitory synapse placement on signal processing in pyramidal neuron dendrites“. In: *Curr Opin Neurobiol* 51, pp. 16–22. DOI: 10.1016/j.conb.2018.01.013.
- Borovac, J., M. Bosch, and K. Okamoto (2018). „Regulation of actin dynamics during structural plasticity of dendritic spines: Signaling messengers and actin-binding proteins“. In: *Mol Cell Neurosci* 91, pp. 122–130. DOI: 10.1016/j.mcn.2018.07.001.
- Butz, S., M. Okamoto, and T. C. Südhof (1998). „A Tripartite Protein Complex with the Potential to Couple Synaptic Vesicle Exocytosis to Cell Adhesion in Brain“. In: *Cell* 94(6), pp. 773–782. DOI: 10.1016/s0092-8674(00)81736-5.
- Cai, C., H. Li, C. Rivera, and K. Keinänen (2006). „Interaction between SAP97 and PSD-95, two Maguk proteins involved in synaptic trafficking of AMPA receptors“. In: *J Biol Chem* 281(7), pp. 4267–73. DOI: 10.1074/jbc.M505886200.
- Cai, T., J. Xiao, Z. F. Wang, Q. Liu, H. Wu, and Y. Z. Qiu (2013). „Identification of Differentially Coexpressed Genes in Gonadotrope Tumors and Normal Pituitary

- Using Bioinformatics Methods“. In: *Pathol Oncol Res*. DOI: 10.1007/s12253-013-9706-1.
- Cavallaro, U. and E. Dejana (2011). „Adhesion molecule signalling: not always a sticky business“. In: *Nat Rev Mol Cell Biol* 12(3), pp. 189–97. DOI: 10.1038/nrm3068.
- Chang, Y., R. Wang, S. Barot, and D. S. Weiss (1996). „Stoichiometry of a Recombinant GABAARceptor“. In: *The Journal of Neuroscience* 16(17), pp. 5415–5424. DOI: 10.1523/jneurosci.16-17-05415.1996.
- Cheadle, L. and T. Biederer (2012). „The novel synaptogenic protein Farp1 links postsynaptic cytoskeletal dynamics and transsynaptic organization“. In: *J Cell Biol* 199(6), pp. 985–1001. DOI: 10.1083/jcb.201205041.
- Chen, J. L., K. L. Villa, J. W. Cha, P. T. So, Y. Kubota, and E. Nedivi (2012). „Clustered dynamics of inhibitory synapses and dendritic spines in the adult neocortex“. In: *Neuron* 74(2), pp. 361–73. DOI: 10.1016/j.neuron.2012.02.030.
- Chen, L., D. M. Chetkovich, R. S. Petralia, N. T. Sweeney, Y. Kawasaki, R. J. Wenthold, D. S. Brecht, and R. A. Nicoll (2000). „Stargazin regulates synaptic targeting of AMPA receptors by two distinct mechanisms“. In: *Nature* 408(6815), pp. 936–43. DOI: 10.1038/35050030.
- Chen, X., L. Vinade, R. D. Leapman, J. D. Petersen, T. Nakagawa, T. M. Phillips, M. Sheng, and T. S. Reese (2005). „Mass of the postsynaptic density and enumeration of three key molecules“. In: *Proc Natl Acad Sci U S A* 102(32), pp. 11551–6. DOI: 10.1073/pnas.0505359102.
- Chetkovich, D. M., R. C. Bunn, S.-H. Kuo, Y. Kawasaki, M. Kohwi, and D. S. Brecht (2002). „Postsynaptic Targeting of Alternative Postsynaptic Density-95 Isoforms by Distinct Mechanisms“. In: *The Journal of Neuroscience* 22(15), pp. 6415–6425. DOI: 10.1523/jneurosci.22-15-06415.2002.
- Chishti, A. H., A. C. Kim, S. M. Marfatia, M. Lutchman, M. Hanspal, H. Jindal, S. C. Liu, P. S. Low, G. A. Rouleau, N. Mohandas, J. A. Chasis, J. G. Conboy, P. Gascard, Y. Takakuwa, S. C. Huang, J. Benz E. J., A. Bretscher, R. G. Fehon, J. F. Gusella, V. Ramesh, F. Solomon, V. T. Marchesi, S. Tsukita, S. Tsukita, K. B. Hoover, and et al. (1998). „The FERM domain: a unique module involved in the linkage of cytoplasmic proteins to the membrane“. In: *Trends Biochem Sci* 23(8), pp. 281–2. DOI: 10.1016/s0968-0004(98)01237-7.
- Chiu, C. Q., A. Barberis, and M. J. Higley (2019). „Preserving the balance: diverse forms of long-term GABAergic synaptic plasticity“. In: *Nat Rev Neurosci* 20(5), pp. 272–281. DOI: 10.1038/s41583-019-0141-5.
- Choquet, D. and A. Triller (2013). „The dynamic synapse“. In: *Neuron* 80(3), pp. 691–703. DOI: 10.1016/j.neuron.2013.10.013.
- Chubykin, A. A., D. Atasoy, M. R. Etherton, N. Brose, E. T. Kavalali, J. R. Gibson, and T. C. Sudhof (2007). „Activity-dependent validation of excitatory versus inhibitory synapses by neuroligin-1 versus neuroligin-2“. In: *Neuron* 54(6), pp. 919–31. DOI: 10.1016/j.neuron.2007.05.029.

- Coley, A. A. and W. J. Gao (2018). „PSD95: A synaptic protein implicated in schizophrenia or autism?“ In: *Prog Neuropsychopharmacol Biol Psychiatry* 82, pp. 187–194. DOI: 10.1016/j.pnpbp.2017.11.016.
- Craig, A. M., G. Banker, W. Chang, M. E. McGrath, and A. S. Serpinskaya (1996). „Clustering of Gephyrin at GABAergic but Not Glutamatergic Synapses in Cultured Rat Hippocampal Neurons“. In: *The Journal of Neuroscience* 16(10), pp. 3166–3177. DOI: 10.1523/jneurosci.16-10-03166.1996.
- Crosby, K. C., S. E. Gookin, J. D. Garcia, K. M. Hahm, M. L. Dell’Acqua, and K. R. Smith (2019). „Nanoscale Subsynaptic Domains Underlie the Organization of the Inhibitory Synapse“. In: *Cell Rep* 26(12), 3284–3297 e3. DOI: 10.1016/j.celrep.2019.02.070.
- Dakoji, S., S. Tomita, S. Karimzadegan, R. A. Nicoll, and D. S. Brecht (2003). „Interaction of transmembrane AMPA receptor regulatory proteins with multiple membrane associated guanylate kinases“. In: *Neuropharmacology* 45(6), pp. 849–856. DOI: 10.1016/s0028-3908(03)00267-3.
- Dalva, M. B., A. C. McClelland, and M. S. Kayser (2007). „Cell adhesion molecules: signalling functions at the synapse“. In: *Nat Rev Neurosci* 8(3), pp. 206–20. DOI: 10.1038/nrn2075.
- Dani, A., B. Huang, J. Bergan, C. Dulac, and X. Zhuang (2010). „Superresolution imaging of chemical synapses in the brain“. In: *Neuron* 68(5), pp. 843–56. DOI: 10.1016/j.neuron.2010.11.021.
- Danti, F. R., S. Galosi, M. Romani, M. Montomoli, K. J. Carss, F. L. Raymond, E. Parrini, C. Bianchini, T. McShane, R. C. Dale, S. S. Mohammad, U. Shah, N. Mahant, J. Ng, A. McTague, R. Samanta, G. Vadlamani, E. M. Valente, V. Leuzzi, M. A. Kurian, and R. Guerrini (2017). „GNAO1 encephalopathy: Broadening the phenotype and evaluating treatment and outcome“. In: *Neurol Genet* 3(2), e143. DOI: 10.1212/NXG.0000000000000143.
- De Luca, E., T. Ravasenga, E. M. Petrini, A. Polenghi, T. Nieus, S. Guazzi, and A. Barberis (2017). „Inter-Synaptic Lateral Diffusion of GABAA Receptors Shapes Inhibitory Synaptic Currents“. In: *Neuron* 95(1), 63–69.e5. DOI: 10.1016/j.neuron.2017.06.022.
- Di Paolo, G., L. Pellegrini, K. Letinic, G. Cestra, R. Zoncu, S. Voronov, S. H. Chang, J. Guo, M. R. Wenk, and P. De Camilli (2002). „Recruitment and regulation of phosphatidylinositol phosphate kinase type 1 gamma by the FERM domain of talin“. In: *Nature* 420(6911), pp. 85–89. DOI: 10.1038/nature01147.
- Doengi, M., A. J. Krupp, N. Korber, and V. Stein (2016). „SynCAM 1 improves survival of adult-born neurons by accelerating synapse maturation“. In: *Hippocampus* 26(3), pp. 319–28. DOI: 10.1002/hipo.22524.
- Dudak, A., J. Kim, B. Cheong, H. J. Federoff, and S. T. Lim (2011). „Membrane palmitoylated proteins regulate trafficking and processing of nectins“. In: *Eur J Cell Biol* 90(5), pp. 365–75. DOI: 10.1016/j.ejcb.2011.01.004.

- Dudok, J. J., A. S. Sanz, D. M. Lundvig, V. Sothilingam, M. G. Garrido, J. Klooster, M. W. Seeliger, and J. Wijnholds (2013a). „MPP3 regulates levels of PALS1 and adhesion between photoreceptors and Muller cells“. In: *Glia* 61(10), pp. 1629–44. DOI: 10.1002/glia.22545.
- Dudok, J. J., A. S. Sanz, D. M. Lundvig, and J. Wijnholds (2013b). „MPP3 is required for maintenance of the apical junctional complex, neuronal migration, and stratification in the developing cortex“. In: *J Neurosci* 33(19), pp. 8518–27. DOI: 10.1523/JNEUROSCI.5627-12.2013.
- Elias, G. M., L. A. Elias, P. F. Apostolides, A. R. Kriegstein, and R. A. Nicoll (2008). „Differential trafficking of AMPA and NMDA receptors by SAP102 and PSD-95 underlies synapse development“. In: *Proc Natl Acad Sci U S A* 105(52), pp. 20953–8. DOI: 10.1073/pnas.0811025106.
- Elias, G. M., L. Funke, V. Stein, S. G. Grant, D. S. Bredt, and R. A. Nicoll (2006). „Synapse-specific and developmentally regulated targeting of AMPA receptors by a family of MAGUK scaffolding proteins“. In: *Neuron* 52(2), pp. 307–20. DOI: 10.1016/j.neuron.2006.09.012.
- Elias, G. M. and R. A. Nicoll (2007). „Synaptic trafficking of glutamate receptors by MAGUK scaffolding proteins“. In: *Trends Cell Biol* 17(7), pp. 343–52. DOI: 10.1016/j.tcb.2007.07.005.
- Ernst, A., B. A. Appleton, Y. Ivarsson, Y. Zhang, D. Gfeller, C. Wiesmann, and S. S. Sidhu (2014). „A structural portrait of the PDZ domain family“. In: *J Mol Biol* 426(21), pp. 3509–19. DOI: 10.1016/j.jmb.2014.08.012.
- Ewers, H., T. Tada, J. D. Petersen, B. Racz, M. Sheng, and D. Choquet (2014). „A Septin-Dependent Diffusion Barrier at Dendritic Spine Necks“. In: *PLoS One* 9(12), e113916. DOI: 10.1371/journal.pone.0113916.
- Fanning, A. S. and J. M. Anderson (2009). „Zonula occludens-1 and -2 are cytosolic scaffolds that regulate the assembly of cellular junctions“. In: *Ann N Y Acad Sci* 1165, pp. 113–20. DOI: 10.1111/j.1749-6632.2009.04440.x.
- Feng, W., J. F. Long, J. S. Fan, T. Suetake, and M. Zhang (2004). „The tetrameric L27 domain complex as an organization platform for supramolecular assemblies“. In: *Nat Struct Mol Biol* 11(5), pp. 475–80. DOI: 10.1038/nsmb751.
- Feng, W., J. F. Long, and M. Zhang (2005). „A unified assembly mode revealed by the structures of tetrameric L27 domain complexes formed by mLin-2/mLin-7 and Patj/Pals1 scaffold proteins“. In: *Proc Natl Acad Sci U S A* 102(19), pp. 6861–6. DOI: 10.1073/pnas.0409346102.
- Feng, X., K. Chen, S. Ye, H. Wang, G. Wei, W. Tan, S. Cheng, Y. Zhang, S. Liu, and Y. Zhou (2012). „MPP3 inactivation by promoter CpG islands hypermethylation in colorectal carcinogenesis“. In: *Cancer Biomark* 11(2-3), pp. 99–106. DOI: 10.3233/CBM-2012-0264.
- Fogel, A. I., M. R. Akins, A. J. Krupp, M. Stagi, V. Stein, and T. Biederer (2007). „SynCAMs organize synapses through heterophilic adhesion“. In: *J Neurosci* 27(46), pp. 12516–30. DOI: 10.1523/JNEUROSCI.2739-07.2007.

- Fogg, V. C., C. J. Liu, and B. Margolis (2005). „Multiple regions of Crumbs3 are required for tight junction formation in MCF10A cells“. In: *J Cell Sci* 118(Pt 13), pp. 2859–69. DOI: 10.1242/jcs.02412.
- Friedman, J. I., T. Vrijenhoek, S. Markx, I. M. Janssen, W. A. van der Vliet, B. H. Faas, N. V. Knoers, W. Cahn, R. S. Kahn, L. Edelmann, K. L. Davis, J. M. Silverman, H. G. Brunner, A. G. van Kessel, C. Wijmenga, R. A. Ophoff, and J. A. Veltman (2008). „CNTNAP2 gene dosage variation is associated with schizophrenia and epilepsy“. In: *Mol Psychiatry* 13(3), pp. 261–6. DOI: 10.1038/sj.mp.4002049.
- Fritschy, J. M. and H. Mohler (1995). „GABAA-receptor heterogeneity in the adult rat brain: differential regional and cellular distribution of seven major subunits“. In: *J Comp Neurol* 359(1), pp. 154–94. DOI: 10.1002/cne.903590111.
- Fujita, E., Y. Tanabe, B. A. Imhof, M. Y. Momoi, and T. Momoi (2012). „A complex of synaptic adhesion molecule CADM1, a molecule related to autism spectrum disorder, with MUPP1 in the cerebellum“. In: *J Neurochem* 123(5), pp. 886–94. DOI: 10.1111/jnc.12022.
- Fukuhara, H., M. Masuda, M. Yageta, T. Fukami, M. Kuramochi, T. Maruyama, T. Kitamura, and Y. Murakami (2003). „Association of a lung tumor suppressor TSLC1 with MPP3, a human homologue of Drosophila tumor suppressor Dlg“. In: *Oncogene* 22(40), pp. 6160–5. DOI: 10.1038/sj.onc.1206744.
- Funke, L., S. Dakoji, and D. S. Brecht (2005). „Membrane-associated guanylate kinases regulate adhesion and plasticity at cell junctions“. In: *Annu Rev Biochem* 74, pp. 219–45. DOI: 10.1146/annurev.biochem.74.082803.133339.
- Futai, K., M. J. Kim, T. Hashikawa, P. Scheiffele, M. Sheng, and Y. Hayashi (2007). „Retrograde modulation of presynaptic release probability through signaling mediated by PSD-95-neuroigin“. In: *Nat Neurosci* 10(2), pp. 186–95. DOI: 10.1038/nn1837.
- Gavarini, S., C. Becamel, C. Altier, P. Lory, J. Poncet, J. Wijnholds, J. Bockaert, and P. Marin (2006). „Opposite effects of PSD-95 and MPP3 PDZ proteins on serotonin 5-hydroxytryptamine<sub>2C</sub> receptor desensitization and membrane stability“. In: *Mol Biol Cell* 17(11), pp. 4619–31. DOI: 10.1091/mbc.E06-03-0218.
- Gonzalez-Mariscal, L., A. Betanzos, and A. Avila-Flores (2000). „MAGUK proteins: structure and role in the tight junction“. In: *Semin Cell Dev Biol* 11(4), pp. 315–24. DOI: 10.1006/scdb.2000.0178.
- Good, M. C., J. G. Zalatan, and W. A. Lim (2011). „Scaffold proteins: hubs for controlling the flow of cellular information“. In: *Science* 332(6030), pp. 680–6. DOI: 10.1126/science.1198701.
- Gosens, I., A. I. den Hollander, F. P. Cremers, and R. Roepman (2008). „Composition and function of the Crumbs protein complex in the mammalian retina“. In: *Exp Eye Res* 86(5), pp. 713–26. DOI: 10.1016/j.exer.2008.02.005.
- Gosens, I., A. Sessa, A. I. den Hollander, S. J. Letteboer, V. Belloni, M. L. Arends, A. Le Bivic, F. P. Cremers, V. Broccoli, and R. Roepman (2007a). „FERM protein

- EPB41L5 is a novel member of the mammalian CRB-MPP5 polarity complex“. In: *Exp Cell Res* 313(19), pp. 3959–70. DOI: 10.1016/j.yexcr.2007.08.025.
- Gosens, I., E. van Wijk, F. F. Kersten, E. Krieger, B. van der Zwaag, T. Marker, S. J. Letteboer, S. Dusseljee, T. Peters, H. A. Spierenburg, I. M. Punte, U. Wolfrum, F. P. Cremers, H. Kremer, and R. Roepman (2007b). „MPP1 links the Usher protein network and the Crumbs protein complex in the retina“. In: *Hum Mol Genet* 16(16), pp. 1993–2003. DOI: 10.1093/hmg/ddm147.
- Guerreiro, A. S., S. Fattet, D. W. Kulesza, A. Atamer, A. N. Elsing, T. Shalaby, S. P. Jackson, S. M. Schoenwaelder, M. A. Grotzer, O. Delattre, and A. Arcaro (2011). „A sensitized RNA interference screen identifies a novel role for the PI3K p110gamma isoform in medulloblastoma cell proliferation and chemoresistance“. In: *Mol Cancer Res* 9(7), pp. 925–35. DOI: 10.1158/1541-7786.MCR-10-0200.
- Hauri, S., A. Wepf, A. van Drogen, M. Varjosalo, N. Tapon, R. Aebersold, and M. Gstaiger (2013). „Interaction proteome of human Hippo signaling: modular control of the co-activator YAP1“. In: *Mol Syst Biol* 9, p. 713. DOI: 10.1002/msb.201304750.
- Hayashi, M. K., C. Tang, C. Verpelli, R. Narayanan, M. H. Stearns, R. M. Xu, H. Li, C. Sala, and Y. Hayashi (2009). „The postsynaptic density proteins Homer and Shank form a polymeric network structure“. In: *Cell* 137(1), pp. 159–71. DOI: 10.1016/j.cell.2009.01.050.
- Herculano-Houzel, S. (2009). „The human brain in numbers: a linearly scaled-up primate brain“. In: *Front Hum Neurosci* 3, p. 31. DOI: 10.3389/neuro.09.031.2009.
- Higley, M. J. (2014). „Localized GABAergic inhibition of dendritic Ca(2+) signalling“. In: *Nat Rev Neurosci* 15(9), pp. 567–72. DOI: 10.1038/nrn3803.
- Horresh, I., S. Poliak, S. Grant, D. Brecht, M. N. Rasband, and E. Peles (2008). „Multiple molecular interactions determine the clustering of Caspr2 and Kv1 channels in myelinated axons“. In: *J Neurosci* 28(52), pp. 14213–22. DOI: 10.1523/JNEUROSCI.3398-08.2008.
- Hotulainen, P. and C. C. Hoogenraad (2010). „Actin in dendritic spines: connecting dynamics to function“. In: *J Cell Biol* 189(4), pp. 619–29. DOI: 10.1083/jcb.201003008.
- Hoy, J. L., J. R. Constable, S. Vicini, Z. Fu, and P. Washbourne (2009). „SynCAM1 recruits NMDA receptors via protein 4.1B“. In: *Mol Cell Neurosci* 42(4), pp. 466–83. DOI: 10.1016/j.mcn.2009.09.010.
- Hsueh, Y. P. (2006). „The role of the MAGUK protein CASK in neural development and synaptic function“. In: *Curr Med Chem* 13(16), pp. 1915–27. DOI: 10.2174/092986706777585040.
- Hurd, T. W., L. Gao, M. H. Roh, I. G. Macara, and B. Margolis (2003). „Direct interaction of two polarity complexes implicated in epithelial tight junction assembly“. In: *Nat Cell Biol* 5(2), pp. 137–42. DOI: 10.1038/ncb923.
- El-Husseini, A. E., E. Schnell, D. M. Chetkovich, R. A. Nicoll, and D. S. Brecht (2000a). „PSD-95 involvement in maturation of excitatory synapses“. In: *Science* 290(5495), pp. 1364–8. DOI: 10.1126/science.290.5495.1364.

- El-Husseini, A. E., J. R. Topinka, J. E. Lehrer-Graiwer, B. L. Firestein, S. E. Craven, C. Aoki, and D. S. Bredt (2000b). „Ion channel clustering by membrane-associated guanylate kinases. Differential regulation by N-terminal lipid and metal binding motifs“. In: *J Biol Chem* 275(31), pp. 23904–10. DOI: 10.1074/jbc.M909919199.
- Ibrahim, S. A., G. W. Yip, C. Stock, J. W. Pan, C. Neubauer, M. Poeter, D. Pujalis, C. Y. Koo, R. Kelsch, R. Schule, U. Rescher, L. Kiesel, and M. Gotte (2012). „Targeting of syndecan-1 by microRNA miR-10b promotes breast cancer cell motility and invasiveness via a Rho-GTPase- and E-cadherin-dependent mechanism“. In: *Int J Cancer* 131(6), E884–96. DOI: 10.1002/ijc.27629.
- Irie, M., Y. Hata, M. Takeuchi, K. Ichtchenko, A. Toyoda, K. Hirao, Y. Takai, T. W. Rosahl, and T. C. Sudhof (1997). „Binding of neuroligins to PSD-95“. In: *Science* 277(5331), pp. 1511–5.
- Ito, T., Y. Williams-Nate, M. Iwai, Y. Tsuboi, M. Hagiwara, A. Ito, M. Sakurai-Yageta, and Y. Murakami (2011). „Transcriptional regulation of the CADM1 gene by retinoic acid during the neural differentiation of murine embryonal carcinoma P19 cells“. In: *Genes Cells* 16(7), pp. 791–802. DOI: 10.1111/j.1365-2443.2011.01525.x.
- Ivanova, M. E., G. C. Fletcher, N. O'Reilly, A. G. Purkiss, B. J. Thompson, and N. Q. McDonald (2015). „Structures of the human Pals1 PDZ domain with and without ligand suggest gated access of Crb to the PDZ peptide-binding groove“. In: *Acta Crystallogr D Biol Crystallogr* 71(Pt 3), pp. 555–64. DOI: 10.1107/S139900471402776X.
- Jacob, T. C., Y. D. Bogdanov, C. Magnus, R. S. Saliba, J. T. Kittler, P. G. Haydon, and S. J. Moss (2005). „Gephyrin regulates the cell surface dynamics of synaptic GABA<sub>A</sub> receptors“. In: *J Neurosci* 25(45), pp. 10469–78. DOI: 10.1523/JNEUROSCI.2267-05.2005.
- Jamain, S., K. Radyushkin, K. Hammerschmidt, S. Granon, S. Boretius, F. Varoqueaux, N. Ramanantsoa, J. Gallego, A. Ronnenberg, D. Winter, J. Frahm, J. Fischer, T. Bourgeron, H. Ehrenreich, and N. Brose (2008). „Reduced social interaction and ultrasonic communication in a mouse model of monogenic heritable autism“. In: *Proc Natl Acad Sci U S A* 105(5), pp. 1710–5. DOI: 10.1073/pnas.0711555105.
- Jing-Ping, Z., Q. B. Tian, H. Sakagami, H. Kondo, S. Endo, and T. Suzuki (2005). „p55 protein is a member of PSD scaffold proteins in the rat brain and interacts with various PSD proteins“. In: *Brain Res Mol Brain Res* 135(1-2), pp. 204–16. DOI: 10.1016/j.molbrainres.2004.12.023.
- Kamberov, E., O. Makarova, M. Roh, A. Liu, D. Karnak, S. Straight, and B. Margolis (2000). „Molecular cloning and characterization of Pals, proteins associated with mLin-7“. In: *J Biol Chem* 275(15), pp. 11425–31. DOI: 10.1074/jbc.275.15.11425.
- Kamijo, A., Y. Saitoh, N. Ohno, S. Ohno, and N. Terada (2015). „Immunohistochemical study of the membrane skeletal protein, membrane protein palmitoylated 6 (MPP6), in the mouse small intestine“. In: *Histochem Cell Biol*. DOI: 10.1007/s00418-015-1374-7.

- Kang, M. G., Y. Guo, and R. L. Huganir (2009). „AMPA receptor and GEF-H1/Lfc complex regulates dendritic spine development through RhoA signaling cascade“. In: *Proc Natl Acad Sci U S A* 106(9), pp. 3549–54. DOI: 10.1073/pnas.0812861106.
- Kantardzhieva, A., S. Alexeeva, I. Versteeg, and J. Wijnholds (2006). „MPP3 is recruited to the MPP5 protein scaffold at the retinal outer limiting membrane“. In: *FEBS J* 273(6), pp. 1152–65. DOI: 10.1111/j.1742-4658.2006.05140.x.
- Kantardzhieva, A., I. Gosens, S. Alexeeva, I. M. Punte, I. Versteeg, E. Krieger, C. A. Neefjes-Mol, A. I. den Hollander, S. J. Letteboer, J. Klooster, F. P. Cremers, R. Roepman, and J. Wijnholds (2005). „MPP5 recruits MPP4 to the CRB1 complex in photoreceptors“. In: *Invest Ophthalmol Vis Sci* 46(6), pp. 2192–201. DOI: 10.1167/iovs.04-1417.
- Karnak, D., S. Lee, and B. Margolis (2002). „Identification of multiple binding partners for the amino-terminal domain of synapse-associated protein 97“. In: *J Biol Chem* 277(48), pp. 46730–5. DOI: 10.1074/jbc.M208781200.
- Kasai, H., M. Fukuda, S. Watanabe, A. Hayashi-Takagi, and J. Noguchi (2010). „Structural dynamics of dendritic spines in memory and cognition“. In: *Trends Neurosci* 33(3), pp. 121–9. DOI: 10.1016/j.tins.2010.01.001.
- Kim, E., S. Naisbitt, Y. P. Hsueh, A. Rao, A. Rothschild, A. M. Craig, and M. Sheng (1997). „GKAP, a novel synaptic protein that interacts with the guanylate kinase-like domain of the PSD-95/SAP90 family of channel clustering molecules“. In: *Journal of Cell Biology* 136(3), pp. 669–678. DOI: DOI10.1083/jcb.136.3.669.
- Kim, E. and M. Sheng (2004). „PDZ domain proteins of synapses“. In: *Nat Rev Neurosci* 5(10), pp. 771–81. DOI: 10.1038/nrn1517.
- Kim, G., R. Lujan, J. Schwenk, M. H. Kelley, C. Aguado, M. Watanabe, B. Fakler, J. Maylie, and J. P. Adelman (2016). „Membrane palmitoylated protein 2 is a synaptic scaffold protein required for synaptic SK2-containing channel function“. In: *Elife* 5. DOI: 10.7554/eLife.12637.
- Kim, M. S., C. D. Froese, H. Xie, and W. S. Trimble (2012). „Uncovering principles that control septin-septin interactions“. In: *J Biol Chem* 287(36), pp. 30406–13. DOI: 10.1074/jbc.M112.387464.
- Kim, S., M. K. Lehtinen, A. Sessa, M. W. Zappaterra, S. H. Cho, D. Gonzalez, B. Boggan, C. A. Austin, J. Wijnholds, M. J. Gambello, J. Malicki, A. S. LaMantia, V. Broccoli, and C. A. Walsh (2010). „The apical complex couples cell fate and cell survival to cerebral cortical development“. In: *Neuron* 66(1), pp. 69–84. DOI: 10.1016/j.neuron.2010.03.019.
- Kinoshita, M. (2003). „Assembly of mammalian septins“. In: *J Biochem* 134(4), pp. 491–6. DOI: 10.1093/jb/mvg182.
- Korber, N. and V. Stein (2016). „In vivo imaging demonstrates dendritic spine stabilization by SynCAM 1“. In: *Sci Rep* 6, p. 24241. DOI: 10.1038/srep24241.
- Kornau, H. C., L. T. Schenker, M. B. Kennedy, and P. H. Seeburg (1995). „Domain interaction between NMDA receptor subunits and the postsynaptic density protein PSD-95“. In: *Science* 269(5231), pp. 1737–40. DOI: 10.1126/science.7569905.

- Kristiansen, T. Z., H. C. Harsha, M. Grønberg, A. Maitra, and A. Pandey (2008). „Differential Membrane Proteomics Using<sup>18</sup>O-Labeling To Identify Biomarkers for Cholangiocarcinoma“. In: *Journal of Proteome Research* 7(11), pp. 4670–4677. DOI: 10.1021/pr800215n.
- Kubota, Y., S. Hatada, S. Kondo, F. Karube, and Y. Kawaguchi (2007). „Neocortical inhibitory terminals innervate dendritic spines targeted by thalamocortical afferents“. In: *J Neurosci* 27(5), pp. 1139–50. DOI: 10.1523/JNEUROSCI.3846-06.2007.
- Kuo, Y. C., X. He, A. J. Coleman, Y. J. Chen, P. Dasari, J. Liou, T. Biederer, and X. Zhang (2018). „Structural analyses of FERM domain-mediated membrane localization of FARP1“. In: *Sci Rep* 8(1), p. 10477. DOI: 10.1038/s41598-018-28692-4.
- Lach, A., M. Grzybek, E. Heger, J. Korycka, M. Wolny, J. Kubiak, A. Kolondra, D. M. Boguslawska, K. Augoff, M. Majkowski, J. Podkalicka, J. Kaczor, A. Stefanko, K. Kuliczowski, and A. F. Sikorski (2012). „Palmitoylation of MPP1 (membrane-palmitoylated protein 1)/p55 is crucial for lateral membrane organization in erythroid cells“. In: *J Biol Chem* 287(23), pp. 18974–84. DOI: 10.1074/jbc.M111.332981.
- Lampe, A., G. Tadeus, and J. Schmoranzer (2015). „Spectral demixing avoids registration errors and reduces noise in multicolor localization-based super-resolution microscopy“. In: *Methods Appl Fluoresc* 3(3), p. 034006. DOI: 10.1088/2050-6120/3/3/034006.
- Lange, S., M. Sylvester, M. Schumann, C. Freund, and E. Krause (2010). „Identification of phosphorylation-dependent interaction partners of the adapter protein ADAP using quantitative mass spectrometry: SILAC vs (<sup>18</sup>O)-labeling“. In: *J Proteome Res* 9(8), pp. 4113–22. DOI: 10.1021/pr1003054.
- Lee, H. J. and J. J. Zheng (2010). „PDZ domains and their binding partners: structure, specificity, and modification“. In: *Cell Commun Signal* 8, p. 8. DOI: 10.1186/1478-811X-8-8.
- Lee, H. K. (2006). „Synaptic plasticity and phosphorylation“. In: *Pharmacol Ther* 112(3), pp. 810–32. DOI: 10.1016/j.pharmthera.2006.06.003.
- Lehmann, M., G. Lichtner, H. Klenz, and J. Schmoranzer (2016). „Novel organic dyes for multicolor localization-based super-resolution microscopy“. In: *J Biophotonics* 9(1-2), pp. 161–70. DOI: 10.1002/jbio.201500119.
- Leonoudakis, D., L. R. Conti, S. Anderson, C. M. Radeke, L. M. McGuire, M. E. Adams, S. C. Froehner, J. R. Yates, and C. A. Vandenberg (2004a). „Protein trafficking and anchoring complexes revealed by proteomic analysis of inward rectifier potassium channel (Kir2.x)-associated proteins“. In: *J Biol Chem* 279(21), pp. 22331–46. DOI: 10.1074/jbc.M400285200.
- Leonoudakis, D., L. R. Conti, C. M. Radeke, L. M. McGuire, and C. A. Vandenberg (2004b). „A multiprotein trafficking complex composed of SAP97, CASK, Veli, and Mint1 is associated with inward rectifier Kir2 potassium channels“. In: *J Biol Chem* 279(18), pp. 19051–63. DOI: 10.1074/jbc.M400284200.

- Li, Y., D. Karnak, B. Demeler, B. Margolis, and A. Lavie (2004). „Structural basis for L27 domain-mediated assembly of signaling and cell polarity complexes“. In: *EMBO J* 23(14), pp. 2723–33. DOI: 10.1038/sj.emboj.7600294.
- Li, Y., Z. Wei, Y. Yan, Q. Wan, Q. Du, and M. Zhang (2014). „Structure of Crumbs tail in complex with the PALS1 PDZ-SH3-GK tandem reveals a highly specific assembly mechanism for the apical Crumbs complex“. In: *Proc Natl Acad Sci U S A*. DOI: 10.1073/pnas.1416515111.
- Lisman, J. (2017). „Glutamatergic synapses are structurally and biochemically complex because of multiple plasticity processes: long-term potentiation, long-term depression, short-term potentiation and scaling“. In: *Philos Trans R Soc Lond B Biol Sci* 372(1715). DOI: 10.1098/rstb.2016.0260.
- Lu, Y. M., I. M. Mansuy, E. R. Kandel, and J. Roder (2000). „Calcineurin-Mediated LTD of GABAergic Inhibition Underlies the Increased Excitability of CA1 Neurons Associated with LTP“. In: *Neuron* 26(1), pp. 197–205. DOI: 10.1016/S0896-6273(00)81150-2.
- Lue, R. A., S. M. Marfatia, D. Branton, and A. H. Chishti (1994). „Cloning and characterization of hdlg: the human homologue of the Drosophila discs large tumor suppressor binds to protein 4.1“. In: *Proc Natl Acad Sci U S A* 91(21), pp. 9818–22. DOI: 10.1073/pnas.91.21.9818.
- Ma, H., H. Cai, Y. Zhang, J. Wu, X. Liu, J. Zuo, W. Jiang, G. Ji, Y. Zhang, C. Liu, W. Zhu, and L. Yu (2014). „Membrane palmitoylated protein 3 promotes hepatocellular carcinoma cell migration and invasion via up-regulating matrix metalloproteinase 1“. In: *Cancer Lett* 344(1), pp. 74–81. DOI: 10.1016/j.canlet.2013.10.017.
- MacGillavry, H. D., J. M. Kerr, and T. A. Blanpied (2011). „Lateral organization of the postsynaptic density“. In: *Mol Cell Neurosci* 48(4), pp. 321–31. DOI: 10.1016/j.mcn.2011.09.001.
- MacGillavry, H. D., Y. Song, S. Raghavachari, and T. A. Blanpied (2013). „Nanoscale scaffolding domains within the postsynaptic density concentrate synaptic AMPA receptors“. In: *Neuron* 78(4), pp. 615–22. DOI: 10.1016/j.neuron.2013.03.009.
- Makarova, O., M. H. Roh, C.-J. Liu, S. Laurinec, and B. Margolis (2002). „Mammalian Crumbs3 is a small transmembrane protein linked to protein associated with Lin-7 (Pals1)“. In: *Gene* 302, pp. 21–39. DOI: 10.1016/S0378-1119(02)01084-3.
- Malenka, R. C. and M. F. Bear (2004). „LTP and LTD: an embarrassment of riches“. In: *Neuron* 44(1), pp. 5–21. DOI: 10.1016/j.neuron.2004.09.012.
- Marfatia, S. M., R. A. Lue, D. Branton, and A. H. Chishti (1994). „In-Vitro Binding-Studies Suggest a Membrane-Associated Complex between Erythroid P55, Protein-4.1, and Glycophorin-C“. In: *Journal of Biological Chemistry* 269(12), pp. 8631–8634. DOI: 10.1016/S0021-9258(17)37012-6.
- Margolis, B. and J. P. Borg (2005). „Apicobasal polarity complexes“. In: *J Cell Sci* 118(Pt 22), pp. 5157–9. DOI: 10.1242/jcs.02597.

- Marlin, J. J. and A. G. Carter (2014). „GABA-A receptor inhibition of local calcium signaling in spines and dendrites“. In: *J Neurosci* 34(48), pp. 15898–911. DOI: 10.1523/JNEUROSCI.0869-13.2014.
- Marsden, K. C., J. B. Beattie, J. Friedenthal, and R. C. Carroll (2007). „NMDA receptor activation potentiates inhibitory transmission through GABA receptor-associated protein-dependent exocytosis of GABA(A) receptors“. In: *J Neurosci* 27(52), pp. 14326–37. DOI: 10.1523/JNEUROSCI.4433-07.2007.
- Marsden, K. C., A. Shemesh, K. U. Bayer, and R. C. Carroll (2010). „Selective translocation of Ca<sup>2+</sup>/calmodulin protein kinase IIalpha (CaMKIIalpha) to inhibitory synapses“. In: *Proc Natl Acad Sci U S A* 107(47), pp. 20559–64. DOI: 10.1073/pnas.1010346107.
- Masuda, M., S. Kikuchi, T. Maruyama, M. Sakurai-Yageta, Y. N. Williams, H. P. Ghosh, and Y. Murakami (2005). „Tumor suppressor in lung cancer (TSLC)1 suppresses epithelial cell scattering and tubulogenesis“. In: *J Biol Chem* 280(51), pp. 42164–71. DOI: 10.1074/jbc.M507136200.
- Masuda, M., M. Yageta, H. Fukuhara, M. Kuramochi, T. Maruyama, A. Nomoto, and Y. Murakami (2002). „The tumor suppressor protein TSLC1 is involved in cell-cell adhesion“. In: *J Biol Chem* 277(34), pp. 31014–9. DOI: 10.1074/jbc.M203620200.
- Mburu, P., Y. Kikkawa, S. Townsend, R. Romero, H. Yonekawa, and S. D. Brown (2006). „Whirlin complexes with p55 at the stereocilia tip during hair cell development“. In: *Proc Natl Acad Sci U S A* 103(29), pp. 10973–8. DOI: 10.1073/pnas.0600923103.
- McGee, A. W., S. R. Dakoji, O. Olsen, D. S. Bredt, W. A. Lim, and K. E. Prehoda (2001). „Structure of the SH3-guanylate kinase module from PSD-95 suggests a mechanism for regulated assembly of MAGUK scaffolding proteins“. In: *Mol Cell* 8(6), pp. 1291–301. DOI: Doi10.1016/S1097-2765(01)00411-7.
- McHugh, E. M., W. Zhu, S. Milgram, and S. Mager (2004). „The GABA transporter GAT1 and the MAGUK protein Pals1: interaction, uptake modulation, and coexpression in the brain“. In: *Mol Cell Neurosci* 26(3), pp. 406–17. DOI: 10.1016/j.mcn.2004.03.006.
- McKernan, R. M. and P. J. Whiting (1996). „Which GABAA-receptor subtypes really occur in the brain?“ In: *Trends in Neurosciences* 19(4), pp. 139–143. DOI: 10.1016/S0166-2236(96)80023-3.
- Michel, D., J.-P. Arsanto, D. Massey-Harroche, C. Béclin, J. Wijnholds, and A. Le Bivic (2005). „PATJ connects and stabilizes apical and lateral components of tight junctions in human intestinal cells“. In: *Journal of Cell Science* 118(17), pp. 4049–4057. DOI: 10.1242/jcs.02528.
- Milstein, A. D., W. Zhou, S. Karimzadegan, D. S. Bredt, and R. A. Nicoll (2007). „TARP subtypes differentially and dose-dependently control synaptic AMPA receptor gating“. In: *Neuron* 55(6), pp. 905–18. DOI: 10.1016/j.neuron.2007.08.022.
- Misawa, H., Y. Kawasaki, J. Mellor, N. Sweeney, K. Jo, R. A. Nicoll, and D. S. Bredt (2001). „Contrasting localizations of MALS/LIN-7 PDZ proteins in brain and molec-

- ular compensation in knockout mice“. In: *J Biol Chem* 276(12), pp. 9264–72. DOI: 10.1074/jbc.M009334200.
- Missler, M., T. C. Sudhof, and T. Biederer (2012). „Synaptic cell adhesion“. In: *Cold Spring Harb Perspect Biol* 4(4), a005694. DOI: 10.1101/cshperspect.a005694.
- Mizoguchi, A., H. Nakanishi, K. Kimura, K. Matsubara, K. Ozaki-Kuroda, T. Katata, T. Honda, Y. Kiyohara, K. Heo, M. Higashi, T. Tsutsumi, S. Sonoda, C. Ide, and Y. Takai (2002). „Nectin: an adhesion molecule involved in formation of synapses“. In: *J Cell Biol* 156(3), pp. 555–65. DOI: 10.1083/jcb.200103113.
- Momose, Y., T. Honda, M. Inagaki, K. Shimizu, K. Irie, H. Nakanishi, and Y. Takai (2002). „Role of the second immunoglobulin-like loop of nectin in cell-cell adhesion“. In: *Biochem Biophys Res Commun* 293(1), pp. 45–9. DOI: 10.1016/S0006-291X(02)00183-3.
- Mroczkowski, H. J., G. Arnold, F. X. Schneck, A. Rajkovic, and S. A. Yatsenko (2014). „Interstitial 10p11.23-p12.1 microdeletions associated with developmental delay, craniofacial abnormalities, and cryptorchidism“. In: *Am J Med Genet A* 164A(10), pp. 2623–6. DOI: 10.1002/ajmg.a.36627.
- Mukherjee, K., M. Sharma, H. Urlaub, G. P. Bourenkov, R. Jahn, T. C. Sudhof, and M. C. Wahl (2008). „CASK Functions as a Mg<sup>2+</sup>-independent neurexin kinase“. In: *Cell* 133(2), pp. 328–39. DOI: 10.1016/j.cell.2008.02.036.
- Murakami, S., M. Sakurai-Yageta, T. Maruyama, and Y. Murakami (2014). „Trans-homophilic interaction of CADM1 activates PI3K by forming a complex with MAGuK-family proteins MPP3 and Dlg“. In: *PLoS One* 9(2), e82894. DOI: 10.1371/journal.pone.0082894.
- Murata, Y. and M. Constantine-Paton (2013). „Postsynaptic density scaffold SAP102 regulates cortical synapse development through EphB and PAK signaling pathway“. In: *J Neurosci* 33(11), pp. 5040–52. DOI: 10.1523/JNEUROSCI.2896-12.2013.
- Nair, D., E. Hosy, J. D. Petersen, A. Constals, G. Giannone, D. Choquet, and J. B. Sibarita (2013). „Super-resolution imaging reveals that AMPA receptors inside synapses are dynamically organized in nanodomains regulated by PSD95“. In: *J Neurosci* 33(32), pp. 13204–24. DOI: 10.1523/JNEUROSCI.2381-12.2013.
- New, M., T. Van Acker, J. I. Sakamaki, M. Jiang, R. E. Saunders, J. Long, V. M. Wang, A. Behrens, J. Cerveira, P. Sudhakar, T. Korcsmaros, H. B. J. Jefferies, K. M. Ryan, M. Howell, and S. A. Tooze (2019). „MDH1 and MPP7 Regulate Autophagy in Pancreatic Ductal Adenocarcinoma“. In: *Cancer Res* 79(8), pp. 1884–1898. DOI: 10.1158/0008-5472.CAN-18-2553.
- Niswender, C. M. and P. J. Conn (2010). „Metabotropic glutamate receptors: physiology, pharmacology, and disease“. In: *Annu Rev Pharmacol Toxicol* 50, pp. 295–322. DOI: 10.1146/annurev.pharmtox.011008.145533.
- Nunomura, W., Y. Takakuwa, M. Parra, J. Conboy, and N. Mohandas (2000). „Regulation of protein 4.1R, p55, and glycophorin C ternary complex in human erythrocyte membrane“. In: *J Biol Chem* 275(32), pp. 24540–6. DOI: 10.1074/jbc.M002492200.

- Nusser, Z., W. Sieghart, D. Benke, J. M. Fritschy, and P. Somogyi (1996). „Differential synaptic localization of two major gamma-aminobutyric acid type A receptor alpha subunits on hippocampal pyramidal cells“. In: *Proc Natl Acad Sci U S A* 93(21), pp. 11939–44. DOI: 10.1073/pnas.93.21.11939.
- Olsen, O. and D. S. Bredt (2003). „Functional analysis of the nucleotide binding domain of membrane-associated guanylate kinases“. In: *J Biol Chem* 278(9), pp. 6873–8. DOI: 10.1074/jbc.M210165200.
- Opazo, P., M. Sainlos, and D. Choquet (2012). „Regulation of AMPA receptor surface diffusion by PSD-95 slots“. In: *Curr Opin Neurobiol* 22(3), pp. 453–60. DOI: 10.1016/j.conb.2011.10.010.
- Ovesny, M., P. Krizek, J. Borkovec, Z. Svindrych, and G. M. Hagen (2014). „Thunder-STORM: a comprehensive ImageJ plug-in for PALM and STORM data analysis and super-resolution imaging“. In: *Bioinformatics* 30(16), pp. 2389–90. DOI: 10.1093/bioinformatics/btu202.
- Park, J. Y., L. J. Hughes, U. Y. Moon, R. Park, S. B. Kim, K. Tran, J. S. Lee, S. H. Cho, and S. Kim (2015). „The apical complex protein Pals1 is required to maintain cerebellar progenitor cells in a proliferative state“. In: *Development* 143(1), pp. 133–146. DOI: 10.1242/dev.124180.
- Patel, B., M. Mortensen, and T. G. Smart (2014). „Stoichiometry of delta subunit containing GABA(A) receptors“. In: *Br J Pharmacol* 171(4), pp. 985–94. DOI: 10.1111/bph.12514.
- Pedregosa, F., G. Varoquaux, A. Gramfort, V. Michel, B. Thirion, O. Grisel, M. Blondel, P. Prettenhofer, R. Weiss, V. Dubourg, J. Vanderplas, A. Passos, D. Cournapeau, M. Brucher, M. Perrot, and É. Duchesnay (2011). „Scikit-learn: Machine Learning in Python“. In: *Journal of Machine Learning Research* 12(85), pp. 2825–30.
- Penagarikano, O., B. S. Abrahams, E. I. Herman, K. D. Winden, A. Gdalyahu, H. Dong, L. I. Sonnenblick, R. Gruver, J. Almajano, A. Bragin, P. Golshani, J. T. Trachtenberg, E. Peles, and D. H. Geschwind (2011). „Absence of CNTNAP2 leads to epilepsy, neuronal migration abnormalities, and core autism-related deficits“. In: *Cell* 147(1), pp. 235–46. DOI: 10.1016/j.cell.2011.08.040.
- Pennacchietti, F., S. Vascon, T. Nieuw, C. Rosillo, S. Das, S. K. Tyagarajan, A. Diaspro, A. Del Bue, E. M. Petrini, A. Barberis, and F. Cella Zancacchi (2017). „Nanoscale Molecular Reorganization of the Inhibitory Postsynaptic Density Is a Determinant of GABAergic Synaptic Potentiation“. In: *J Neurosci* 37(7), pp. 1747–1756. DOI: 10.1523/JNEUROSCI.0514-16.2016.
- Perez de Arce, K., N. Schrod, S. W. R. Metzbower, E. Allgeyer, G. K. Kong, A. H. Tang, A. J. Krupp, V. Stein, X. Liu, J. Bewersdorf, T. A. Blanpied, V. Lucic, and T. Biederer (2015). „Topographic Mapping of the Synaptic Cleft into Adhesive Nanodomains“. In: *Neuron* 88(6), pp. 1165–1172. DOI: 10.1016/j.neuron.2015.11.011.
- Petralia, R. S., N. Sans, Y. X. Wang, and R. J. Wenthold (2005). „Ontogeny of postsynaptic density proteins at glutamatergic synapses“. In: *Mol Cell Neurosci* 29(3), pp. 436–52. DOI: 10.1016/j.mcn.2005.03.013.

- Petrini, E. M., T. Ravasenga, T. J. Hausrat, G. Iurilli, U. Olcese, V. Racine, J. B. Sibarita, T. C. Jacob, S. J. Moss, F. Benfenati, P. Medini, M. Kneussel, and A. Barberis (2014). „Synaptic recruitment of gephyrin regulates surface GABAA receptor dynamics for the expression of inhibitory LTP“. In: *Nat Commun* 5, p. 3921. DOI: 10.1038/ncomms4921.
- Petrosky, K. Y., H. D. Ou, F. Lohr, V. Dotsch, and W. A. Lim (2005). „A general model for preferential hetero-oligomerization of LIN-2/7 domains: mechanism underlying directed assembly of supramolecular signaling complexes“. In: *J Biol Chem* 280(46), pp. 38528–36. DOI: 10.1074/jbc.M506536200.
- Rademacher, N., S. A. Kunde, V. M. Kalscheuer, and S. A. Shoichet (2013). „Synaptic MAGUK multimer formation is mediated by PDZ domains and promoted by ligand binding“. In: *Chem Biol* 20(8), pp. 1044–54. DOI: 10.1016/j.chembiol.2013.06.016.
- Rademacher, N., B. Kuroopka, S. A. Kunde, M. C. Wahl, C. Freund, and S. A. Shoichet (2019). „Intramolecular domain dynamics regulate synaptic MAGUK protein interactions“. In: *Elife* 8. DOI: 10.7554/eLife.41299.
- Rademacher\*, N., B. Schmerl\*, J. A. Lardong, M. C. Wahl, and S. A. Shoichet (2016). „MPP2 is a postsynaptic MAGUK scaffold protein that links SynCAM1 cell adhesion molecules to core components of the postsynaptic density“. In: *Sci Rep* 6, p. 35283. DOI: 10.1038/srep35283.
- Reese, M. L., S. Dakoji, D. S. Bredt, and V. Dotsch (2007). „The guanylate kinase domain of the MAGUK PSD-95 binds dynamically to a conserved motif in MAP1a“. In: *Nat Struct Mol Biol* 14(2), pp. 155–63. DOI: 10.1038/nsmb1195.
- Reiner, A. and J. Levitz (2018). „Glutamatergic Signaling in the Central Nervous System: Ionotropic and Metabotropic Receptors in Concert“. In: *Neuron* 98(6), pp. 1080–1098. DOI: 10.1016/j.neuron.2018.05.018.
- Robbins, E. M., A. J. Krupp, K. Perez de Arce, A. K. Ghosh, A. I. Fogel, A. Boucard, T. C. Sudhof, V. Stein, and T. Biederer (2010). „SynCAM 1 adhesion dynamically regulates synapse number and impacts plasticity and learning“. In: *Neuron* 68(5), pp. 894–906. DOI: 10.1016/j.neuron.2010.11.003.
- Roh, M. H., O. Makarova, C. J. Liu, K. Shin, S. Lee, S. Laurinec, M. Goyal, R. Wiggins, and B. Margolis (2002). „The Maguk protein, Pals1, functions as an adapter, linking mammalian homologues of Crumbs and Discs Lost“. In: *J Cell Biol* 157(1), pp. 161–72. DOI: 10.1083/jcb.200109010.
- Sakisaka, T. and Y. Takai (2004). „Biology and pathology of nectins and nectin-like molecules“. In: *Curr Opin Cell Biol* 16(5), pp. 513–21. DOI: 10.1016/j.ceb.2004.07.007.
- Sakurai-Yageta, M., T. Maruyama, T. Suzuki, K. Ichikawa, and Y. Murakami (2015). „Dynamic regulation of a cell adhesion protein complex including CADM1 by combinatorial analysis of FRAP with exponential curve-fitting“. In: *PLoS One* 10(3), e0116637. DOI: 10.1371/journal.pone.0116637.

- Sakurai-Yageta, M., M. Masuda, Y. Tsuboi, A. Ito, and Y. Murakami (2009). „Tumor suppressor CADM1 is involved in epithelial cell structure“. In: *Biochem Biophys Res Commun* 390(3), pp. 977–82. DOI: 10.1016/j.bbrc.2009.10.088.
- Scheefhals, N. and H. D. MacGillavry (2018). „Functional organization of postsynaptic glutamate receptors“. In: *Mol Cell Neurosci* 91, pp. 82–94. DOI: 10.1016/j.mcn.2018.05.002.
- Scheiffele, P., J. Fan, J. Choih, R. Fetter, and T. Serafini (2000). „Neuroigin Expressed in Nonneuronal Cells Triggers Presynaptic Development in Contacting Axons“. In: *Cell* 101(6), pp. 657–669. DOI: 10.1016/s0092-8674(00)80877-6.
- Schikorski, T. and C. F. Stevens (1997). „Quantitative Ultrastructural Analysis of Hippocampal Excitatory Synapses“. In: *The Journal of Neuroscience* 17(15), pp. 5858–5867. DOI: 10.1523/jneurosci.17-15-05858.1997.
- Schindelin, J., I. Arganda-Carreras, E. Frise, V. Kaynig, M. Longair, T. Pietzsch, S. Preibisch, C. Rueden, S. Saalfeld, B. Schmid, J. Y. Tinevez, D. J. White, V. Hartenstein, K. Eliceiri, P. Tomancak, and A. Cardona (2012). „Fiji: an open-source platform for biological-image analysis“. In: *Nat Methods* 9(7), pp. 676–82. DOI: 10.1038/nmeth.2019.
- Schmerl, B., N. Gimber, B. Kuroepka, J. Rentsch, S.-A. Kunde, H. Ewers, C. Freund, J. Schmoranzner, N. Rademacher\*, and S. Shoichet\* (2020). „The postsynaptic MAGUK scaffold protein MPP2 organises a distinct interactome that incorporates GABA<sub>A</sub> receptors at the periphery of excitatory synapses“. In: *bioRxiv*, p. 2020.05.29.123034. DOI: 10.1101/2020.05.29.123034.
- Schneider, C. A., W. S. Rasband, and K. W. Eliceiri (2012). „NIH Image to ImageJ: 25 years of image analysis“. In: *Nat Methods* 9(7), pp. 671–5. DOI: 10.1038/nmeth.2089.
- Schnell, E., M. Sizemore, S. Karimzadegan, L. Chen, D. S. Bredt, and R. A. Nicoll (2002). „Direct interactions between PSD-95 and stargazin control synaptic AMPA receptor number“. In: *Proc Natl Acad Sci U S A* 99(21), pp. 13902–7. DOI: 10.1073/pnas.172511199.
- Schwenk, J., N. Harmel, A. Brechet, G. Zolles, H. Berkefeld, C. S. Muller, W. Bildl, D. Baehrens, B. Huber, A. Kulik, N. Klocker, U. Schulte, and B. Fakler (2012). „High-resolution proteomics unravel architecture and molecular diversity of native AMPA receptor complexes“. In: *Neuron* 74(4), pp. 621–33. DOI: 10.1016/j.neuron.2012.03.034.
- Seo, P. S., B. J. Quinn, A. A. Khan, L. Zeng, C. G. Takoudis, T. Hanada, A. Bolis, A. Bolino, and A. H. Chishti (2009). „Identification of erythrocyte p55/MPP1 as a binding partner of NF2 tumor suppressor protein/Merlin“. In: *Exp Biol Med (Maywood)* 234(3), pp. 255–62. DOI: 10.3181/0809-RM-275.
- Shanks, N. F., J. N. Savas, T. Maruo, O. Cais, A. Hirao, S. Oe, A. Ghosh, Y. Noda, I. H. Greger, 3. Yates J. R., and T. Nakagawa (2012). „Differences in AMPA and kainate receptor interactomes facilitate identification of AMPA receptor auxiliary subunit GSG1L“. In: *Cell Rep* 1(6), pp. 590–8. DOI: 10.1016/j.celrep.2012.05.004.

- Shen, H., N. Sabaliauskas, A. Sherpa, A. A. Fenton, A. Stelzer, C. Aoki, and S. S. Smith (2010). „A critical role for alpha4betadelta GABAA receptors in shaping learning deficits at puberty in mice“. In: *Science* 327(5972), pp. 1515–8. DOI: 10.1126/science.1184245.
- Shen, L., F. Liang, L. D. Walensky, and R. L. Huganir (2000). „Regulation of AMPA receptor GluR1 subunit surface expression by a 4.1N-linked actin cytoskeletal association“. In: *J Neurosci* 20(21), pp. 7932–40. DOI: <https://doi.org/10.1523/JNEUROSCI.20-21-07932.2000>.
- Sheng, M. and C. C. Hoogenraad (2007). „The postsynaptic architecture of excitatory synapses: a more quantitative view“. In: *Annu Rev Biochem* 76, pp. 823–47. DOI: 10.1146/annurev.biochem.76.060805.160029.
- Shingai, T., W. Ikeda, S. Kakunaga, K. Morimoto, K. Takekuni, S. Itoh, K. Satoh, M. Takeuchi, T. Imai, M. Monden, and Y. Takai (2003). „Implications of nectin-like molecule-2/IGSF4/RA175/SgIGSF/TSLC1/SynCAM1 in cell-cell adhesion and transmembrane protein localization in epithelial cells“. In: *J Biol Chem* 278(37), pp. 35421–7. DOI: 10.1074/jbc.M305387200.
- Sigel, E. and M. E. Steinmann (2012). „Structure, function, and modulation of GABA(A) receptors“. In: *J Biol Chem* 287(48), pp. 40224–31. DOI: 10.1074/jbc.R112.386664.
- Smith, S. A., P. Holik, J. Stevens, S. Mazoyer, R. Melis, B. Williams, R. White, and H. Albertsen (1996). „Isolation of a gene (DLG3) encoding a second member of the discs-large family on chromosome 17q12-q21“. In: *Genomics* 31(2), pp. 145–50. DOI: 10.1006/geno.1996.0025.
- Songyang, Z., A. S. Fanning, C. Fu, J. Xu, S. M. Marfatia, A. H. Chishti, A. Crompton, A. C. Chan, J. M. Anderson, and L. C. Cantley (1997). „Recognition of unique carboxyl-terminal motifs by distinct PDZ domains“. In: *Science* 275(5296), pp. 73–7. DOI: 10.1126/science.275.5296.73.
- Specht, C. G., I. Izeddin, P. C. Rodriguez, M. El Beheiry, P. Rostaing, X. Darzacq, M. Dahan, and A. Triller (2013). „Quantitative nanoscopy of inhibitory synapses: counting gephyrin molecules and receptor binding sites“. In: *Neuron* 79(2), pp. 308–21. DOI: 10.1016/j.neuron.2013.05.013.
- Spence, E. F. and S. H. Soderling (2015). „Actin Out: Regulation of the Synaptic Cytoskeleton“. In: *J Biol Chem* 290(48), pp. 28613–22. DOI: 10.1074/jbc.R115.655118.
- Stein, V., D. R. House, D. S. Bredt, and R. A. Nicoll (2003). „Postsynaptic density-95 mimics and occludes hippocampal long-term potentiation and enhances long-term depression“. In: *J Neurosci* 23(13), pp. 5503–6. DOI: 10.1523/JNEUROSCI.23-13-05503.2003.
- Stohr, H., L. L. Molday, R. S. Molday, B. H. Weber, B. Biedermann, A. Reichenbach, and F. Kramer (2005). „Membrane-associated guanylate kinase proteins MPP4 and MPP5 associate with Veli3 at distinct intercellular junctions of the neurosensory retina“. In: *J Comp Neurol* 481(1), pp. 31–41. DOI: 10.1002/cne.20367.

- Straight, S. W., K. Shin, V. C. Fogg, S. Fan, C. J. Liu, M. Roh, and B. Margolis (2004). „Loss of PALS1 expression leads to tight junction and polarity defects“. In: *Mol Biol Cell* 15(4), pp. 1981–90. DOI: 10.1091/mbc.E03-08-0620.
- Straub, C. and S. Tomita (2012). „The regulation of glutamate receptor trafficking and function by TARPs and other transmembrane auxiliary subunits“. In: *Curr Opin Neurobiol* 22(3), pp. 488–95. DOI: 10.1016/j.conb.2011.09.005.
- Strauss, K. A., E. G. Puffenberger, M. J. Huentelman, S. Gottlieb, S. E. Dobrin, J. M. Parod, D. A. Stephan, and D. H. Morton (2006). „Recessive symptomatic focal epilepsy and mutant contactin-associated protein-like 2“. In: *N Engl J Med* 354(13), pp. 1370–7. DOI: 10.1056/NEJMoa052773.
- Stucke, V. M., E. Timmerman, J. Vandekerckhove, K. Gevaert, and A. Hall (2007). „The MAGUK protein MPP7 binds to the polarity protein hDlg1 and facilitates epithelial tight junction formation“. In: *Mol Biol Cell* 18(5), pp. 1744–55. DOI: 10.1091/mbc.E06-11-0980.
- Sudhof, T. C. (2008). „Neuroligins and neuroligins link synaptic function to cognitive disease“. In: *Nature* 455(7215), pp. 903–11. DOI: 10.1038/nature07456.
- Tabuchi, K., J. Blundell, M. R. Etherton, R. E. Hammer, X. Liu, C. M. Powell, and T. C. Sudhof (2007). „A neuroligin-3 mutation implicated in autism increases inhibitory synaptic transmission in mice“. In: *Science* 318(5847), pp. 71–6. DOI: 10.1126/science.1146221.
- Tadeus, G., A. Lampe, and J. Schmoranzler (2015). „SDmixer-a versatile software tool for spectral demixing of multicolor single molecule localization data“. In: *Methods Appl Fluoresc* 3(3), p. 037001. DOI: 10.1088/2050-6120/3/3/037001.
- Takeuchi, M. (1997). „SAPAPs. A Family of PSD-95/SAP90-associated proteins localized at postsynaptic density“. In: *Journal of Biological Chemistry* 272(18), pp. 11943–11951. DOI: 10.1074/jbc.272.18.11943.
- Tao-Cheng, J. H., Y. Yang, T. S. Reese, and A. Dosemeci (2015). „Differential distribution of Shank and GKAP at the postsynaptic density“. In: *PLoS One* 10(3), e0118750. DOI: 10.1371/journal.pone.0118750.
- Thompson, R. E., D. R. Larson, and W. W. Webb (2002). „Precise Nanometer Localization Analysis for Individual Fluorescent Probes“. In: *Biophysical Journal* 82(5), pp. 2775–2783. DOI: 10.1016/s0006-3495(02)75618-x.
- Tonikian, R., Y. Zhang, S. L. Sazinsky, B. Currell, J. H. Yeh, B. Reva, H. A. Held, B. A. Appleton, M. Evangelista, Y. Wu, X. Xin, A. C. Chan, S. Seshagiri, L. A. Lasky, C. Sander, C. Boone, G. D. Bader, and S. S. Sidhu (2008). „A specificity map for the PDZ domain family“. In: *PLoS Biol* 6(9), e239. DOI: 10.1371/journal.pbio.0060239.
- Tretter, V., T. C. Jacob, J. Mukherjee, J. M. Fritschy, M. N. Pangalos, and S. J. Moss (2008). „The clustering of GABA(A) receptor subtypes at inhibitory synapses is facilitated via the direct binding of receptor alpha 2 subunits to gephyrin“. In: *J Neurosci* 28(6), pp. 1356–65. DOI: 10.1523/JNEUROSCI.5050-07.2008.

- Tyagarajan, S. K. and J. M. Fritschy (2014). „Gephyrin: a master regulator of neuronal function?“ In: *Nat Rev Neurosci* 15(3), pp. 141–56. DOI: 10.1038/nrn3670.
- Ullrich, B., Y. A. Ushkaryov, and T. C. Sudhof (1995). „Cartography of Neurexins - More Than 1000 Isoforms Generated by Alternative Splicing and Expressed in Distinct Subsets of Neurons“. In: *Neuron* 14(3), pp. 497–507. DOI: Doi10.1016/0896-6273(95)90306-2.
- Varea, O., M. D. Martin-de-Saavedra, K. J. Kopeikina, B. Schurmann, H. J. Fleming, J. M. Fawcett-Patel, A. Bach, S. Jang, E. Peles, E. Kim, and P. Penzes (2015). „Synaptic abnormalities and cytoplasmic glutamate receptor aggregates in contactin associated protein-like 2/Caspr2 knockout neurons“. In: *Proceedings of the National Academy of Sciences of the United States of America* 112(19), pp. 6176–6181. DOI: 10.1073/pnas.1423205112.
- Varoqueaux, F., G. Aramuni, R. L. Rawson, R. Mohrmann, M. Missler, K. Gottmann, W. Zhang, T. C. Sudhof, and N. Brose (2006). „Neuroligins determine synapse maturation and function“. In: *Neuron* 51(6), pp. 741–54. DOI: 10.1016/j.neuron.2006.09.003.
- Wang, J., S. Liu, U. Haditsch, W. Tu, K. Cochrane, G. Ahmadian, L. Tran, J. Paw, Y. Wang, I. Mansuy, M. M. Salter, and Y. Lu (2003). „Interaction of Calcineurin and Type-A GABA Receptor 2Subunits Produces Long-Term Depression at CA1 Inhibitory Synapses“. In: *The Journal of Neuroscience* 23(3), pp. 826–836. DOI: 10.1523/jneurosci.23-03-00826.2003.
- Wang, Q., T. W. Hurd, and B. Margolis (2004). „Tight junction protein Par6 interacts with an evolutionarily conserved region in the amino terminus of PALS1/stardust“. In: *J Biol Chem* 279(29), pp. 30715–21. DOI: 10.1074/jbc.M401930200.
- Wei, Z., Y. Li, F. Ye, and M. Zhang (2015). „Structural basis for the phosphorylation-regulated interaction between the cytoplasmic tail of cell polarity protein Crumbs and the actin binding protein Moesin“. In: *J Biol Chem*. DOI: 10.1074/jbc.M115.643791.
- Wollmuth, L. P. and A. I. Sobolevsky (2004). „Structure and gating of the glutamate receptor ion channel“. In: *Trends Neurosci* 27(6), pp. 321–8. DOI: 10.1016/j.tins.2004.04.005.
- Won, S., J. M. Levy, R. A. Nicoll, and K. W. Roche (2017). „MAGUKs: multifaceted synaptic organizers“. In: *Curr Opin Neurobiol* 43, pp. 94–101. DOI: 10.1016/j.conb.2017.01.006.
- Woods, D. F. and P. J. Bryant (1991). „The Disks-Large Tumor Suppressor Gene of Drosophila Encodes a Guanylate Kinase Homolog Localized at Septate Junctions“. In: *Cell* 66(3), pp. 451–464. DOI: Doi10.1016/0092-8674(81)90009-X.
- Yageta, M., M. Kuramochi, M. Masuda, T. Fukami, H. Fukuhara, T. Maruyama, M. Shibuya, and Y. Murakami (2002). „Direct association of TSLC1 and DAL-1, two distinct tumor suppressor proteins in lung cancer“. In: *Cancer Research* 62(18), pp. 5129–5133.
- Yang, J., B. Pawlyk, X. H. Wen, M. Adamian, M. Soloviev, N. Michaud, Y. Zhao, M. A. Sandberg, C. L. Makino, and T. Li (2007). „Mpp4 is required for proper localization

- of plasma membrane calcium ATPases and maintenance of calcium homeostasis at the rod photoreceptor synaptic terminals“. In: *Hum Mol Genet* 16(9), pp. 1017–29. DOI: 10.1093/hmg/ddm047.
- Yang, X. and C. G. Specht (2019). „Subsynaptic Domains in Super-Resolution Microscopy: The Treachery of Images“. In: *Front Mol Neurosci* 12, p. 161. DOI: 10.3389/fnmol.2019.00161.
- Yang, X., X. Xie, L. Chen, H. Zhou, Z. Wang, W. Zhao, R. Tian, R. Zhang, C. Tian, J. Long, and Y. Shen (2010). „Structural basis for tandem L27 domain-mediated polymerization“. In: *FASEB J* 24(12), pp. 4806–15. DOI: 10.1096/fj.10-163857.
- Ye, F., M. Zeng, and M. Zhang (2017). „Mechanisms of MAGUK-mediated cellular junctional complex organization“. In: *Curr Opin Struct Biol* 48, pp. 6–15. DOI: 10.1016/j.sbi.2017.08.006.
- Yokoi, N., M. Fukata, and Y. Fukata (2012). „Synaptic plasticity regulated by protein-protein interactions and posttranslational modifications“. In: *Int Rev Cell Mol Biol* 297, pp. 1–43. DOI: 10.1016/B978-0-12-394308-8.00001-7.
- Yuste, R. and T. Bonhoeffer (2004). „Genesis of dendritic spines: insights from ultrastructural and imaging studies“. In: *Nat Rev Neurosci* 5(1), pp. 24–34. DOI: 10.1038/nrn1300.
- Zeng, M., F. Ye, J. Xu, and M. Zhang (2018). „PDZ Ligand Binding-Induced Conformational Coupling of the PDZ-SH3-GK Tandems in PSD-95 Family MAGUKs“. In: *J Mol Biol* 430(1), pp. 69–86. DOI: 10.1016/j.jmb.2017.11.003.
- Zhang, J., X. Yang, Y. Shen, and J. Long (2011). „Crystallization and preliminary X-ray data collection of the L27(PATJ)-(L27N,L27C)(Pals1)-L27(MALS) tripartite complex“. In: *Acta Crystallogr Sect F Struct Biol Cryst Commun* 67(Pt 11), pp. 1443–7. DOI: 10.1107/S174430911103689X.
- Zhu, J., Y. Shang, C. Xia, W. Wang, W. Wen, and M. Zhang (2011). „Guanylate kinase domains of the MAGUK family scaffold proteins as specific phospho-protein-binding modules“. In: *EMBO J* 30(24), pp. 4986–97. DOI: 10.1038/emboj.2011.428.
- Zhu, J., Y. Shang, and M. Zhang (2016). „Mechanistic basis of MAGUK-organized complexes in synaptic development and signalling“. In: *Nat Rev Neurosci* 17(4), pp. 209–23. DOI: 10.1038/nrn.2016.18.

## Appendix

### Validation of commercial antibodies

In order to visualise and purify endogenous MPP2, this study aiming to characterise MPP2 started with the acquisition and validation of commercially available antibodies, however, only few companies offered products targeting MPP2. Antibodies from two different companies were obtained: Abcam offered a mono- and a polyclonal antibody raised in rabbit (ab156874, with an undisclosed synthetic peptide corresponding to the human MPP2 amino acid sequence, and ab27290 against human MPP2 aa112-432, respectively) and a Sigma polyclonal antibody raised in mouse (SAB1400169, raised against full-length human MPP2).

The Abcam product data sheets included Western blot examples of different cell lysates (human cerebellum, T47-D and C6 and A549 cell lysates, respectively), showing a single band at a reasonable size above 50 kDa and below 72 kDa, corresponding to the expected molecular weight of ~64 kDa of human MPP2, based on its amino acid sequence. The Sigma antibody data sheet included Western blot examples of HEK293T cell lysates with and without overexpression of MPP2, showing a single band below 75 kDa, corresponding to the expected molecular weight of human MPP2. At the beginning of this project, none of the antibodies had been cited in publications.

To test these antibodies, an expression constructs of N-terminally FLAG-tagged full-length murine MPP2 was generated and overexpressed in CHL V79 cells. At first, the applicability of these antibodies was confirmed by Western blot analysis of whole cell lysates of untransfected CHL V79 cells and cells transiently expressing FLAG-tagged MPP2. Immunoblotting with the monoclonal rabbit antibody (ab156874) resulted in the detection of a double band at 50 kDa only in the untransfected cell lysates, whereas probing with the polyclonal rabbit antibody (ab27290) did not bind any protein in lysates of untransfected cells and clearly detected a single band at 64 kDa in lysates with overexpressed MPP2 (Figure A1a, top). Subsequent immunoblotting with  $\alpha$ FLAG antibody detects a band between 50 and 75 kDa, what corresponds to the expected molecular weight of murine MPP2 (Figure A1a, bottom), demonstrating that only the polyclonal rabbit antibody is suitable to detect MPP2 in Western blot.

Testing the polyclonal Sigma antibody similarly for Western application blot has demonstrated that it is indeed specific, however, at a low sensitivity (data not shown), resulting in a detection of MPP2 only at comparatively high protein amounts and a high antibody concentration.

Further, cells transiently transfected with EGFP-MPP2 were fixed and stained with either of the Abcam antibodies and Alexa Fluor 568-coupled  $\alpha$ Rabbit sec-

ondary antibody and DAPI as nuclear marker. Remarkably, the staining patterns of the two Abcam antibodies differed tremendously. Figure A1b shows a single-cell layer of cells (indicated by DAPI nuclear staining, blue), with a fraction of successfully transfected cells, which express EGFP-MPP2 (cyan). While the mono-clonal antibody (ab156874) seemed to unspecifically stain all cell membranes (Figure A1b, upper panel), the staining pattern of the polyclonal antibody (ab27290) entirely matches the signal of EGFP-MPP2 (Figure A1b, lower panel).

Moreover, when comparing the staining of the two Abcam antibodies on primary hippocampal neurons, tremendous differences in the structures stained were observed. The monoclonal antibody stained cytoskeleton-like structures across the whole neuron, while the polyclonal antibody specifically stained punctate structures along neuronal dendrites. This punctate staining pattern is in line with what was expected from a protein specifically enriched at synapses (Figure A1c). Lastly, the specificity of the polyclonal antibody among the MPP protein family was analysed by Western blot of whole cell lysates of CHL V79 cells that were transiently transfected with expression constructs of FLAG-tagged MPP1, MPP2, MPP3, MPP5 and MPP6, all of which have been implicated in studies involving neuronal tissues. Indeed, the polyclonal rabbit antibody specifically detects only overexpressed MPP2 and does not bind the other MPP proteins (Figure A1d). These validation experiments demonstrated that only two of the tested antibodies are specifically detecting overexpressed MPP2. Moreover, only the polyclonal antibody from Abcam is suitable for immunofluorescence and Western blot application and therefore used throughout the present study.

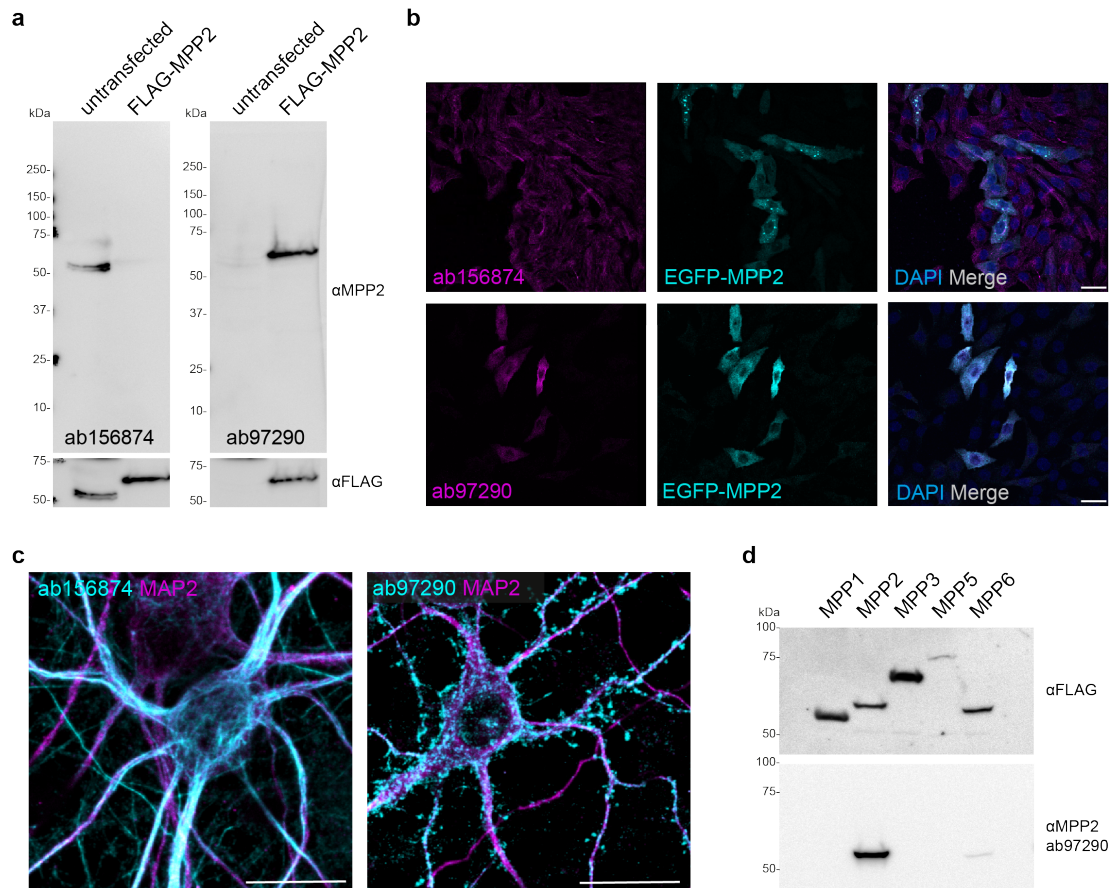


**Figure A1: Validation of commercially available antibodies targeting endogenous MPP2.**

a) Lysates of untransfected and FLAG MPP2 overexpressing CHL V79 cells were analysed by SDS PAGE and Western blot probed with a monoclonal (ab156874) or polyclonal (ab97290) rabbit antibody against MPP2. Control immunoblotting with αFLAG antibody revealed that the monoclonal antibody detects only unspecific protein bands. Note the re-emergence of the unspecific double band in the untransfected cell lysates. b) CHL V79 cell were transiently transfected with an EGFP MPP2 overexpression construct, fixed 24 hrs post-transfection and stained with αMPP2 antibodies and the nuclear marker DAPI. c) Primary hippocampal neurons were fixed at DIV 21 and stained for the dendritic marker MAP2 together with monoclonal (ab156874, left) or polyclonal (ab97290, right) rabbit αMPP2 antibody. d) CHL V79 cells were transiently transfected with expression constructs for FLAG-tagged MPP2, MPP3, MPP5 and MPP6, respectively, and lysates analysed by SDS PAGE and Western blot. Immunoblotting with polyclonal rabbit αMPP2 antibody (ab97290) detects only FLAG-MPP2 as demonstrated by αFLAG antibody control. Scale bars = 20 μm.

## **Knock-down of endogenous MPP2**

To study the relevance and function of a newly described protein in neurons, knock-out and knock-down strategies are a common approach to investigate the consequences of removing this protein. At the beginning of the present study, no published shRNA sequences or commercial kits to knock down MPP2 were available. Taking advantage of several freely available online tools for the computational prediction of suitable siRNA targets (see Material and Methods), candidate shRNA sequences specifically targeting rat MPP2, were selected and cloned into pSUPER RNAi vector. Indeed, one of the sequences was effective: Upon overexpression of MPP2 in CHL V79 cells together with the shRNA or control, expression of MPP2 was abolished (Figure A2a). Moreover, the specificity of this knock-down was validated by likewise co-expression with MPP1, MPP3, MPP5 and MPP6. Indeed, the expression of none of the other tested MPP family proteins was affected by the shRNA targeting MPP2 (Figure A2a). This sequence was then introduced into a lentiviral vector, provided by the Viral Core Facility (VCF, Charité - Universitätsmedizin Berlin), to knock-down endogenous MPP2 in primary hippocampal neurons. Indeed, this lentivirus-mediated knock-down was highly effective, as demonstrated by Western blot of lysates of mature primary neuron lysates that were infected at DIV 3 with either shRNA or control virus (Figure A2b).

Following the successful knock-down of endogenous MPP2 in cultured neurons, the expression of various synaptic proteins, like PSD-95 and AMPARs as well as MPP2 interaction partners like SynCAM1, was analysed by Western blot, but no obvious differences were observed (data not shown). Moreover, analyses of gross morphological features, such as dendrite branching or synapse density, also showed no striking differences (data not shown). This suggests that loss of MPP2 might be compensated (e.g. by another neuronal MPP protein like MPP6, which has already been described at the presynapse) and/or that the main function of MPP2 is not in establishing neuronal morphology, but probably a more subtle role in synaptic function and plasticity.

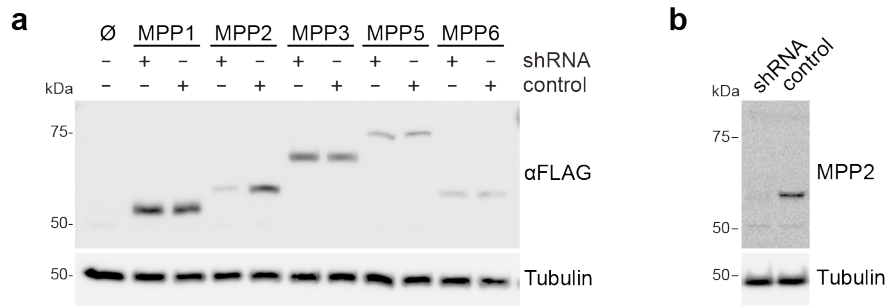


**Figure A2: Knock-down of endogenous MPP2.**

To facilitate knock-down of endogenous MPP2, several shRNA sequences were computationally predicted and cloned into pSUPER shRNAi plasmids and the most efficient sequence was further validated. a) Co-transfection of MPP1, MPP2, MPP3, MPP5 and MPP6 together with shRNA targeting MPP2 or control shRNA, respectively, leads to loss of expression of MPP2 together with shRNA, confirming efficacy and specificity of the selected shRNA sequence. b) The same sequence introduced to cultured hippocampal neurons at DIV 3 with lentivirus-mediated knock-down, successfully abolishes expression of endogenous MPP2 as demonstrated by Western blot analysis of whole cell lysates harvested at DIV 21 probed with  $\alpha$ MPP2 antibody.